POLITECNICO DI MILANO

School of Industrial and Information Engineering
Department of Mechanical

Master Degree in Mechanical Engineering

SEMI-ACTIVE AND FULL-ACTIVE CONTROL OF HUNTING VIBRATION IN A HIGH-SPEED RAILWAY BOGIE

Supervisor: Prof. Stefano Bruni
Assistant Supervisor: Dr. Egidio Di Gialleonardo

Candidate:

Lorenzo Di Pasquali Matricola 883546

Academic Year 2017 – 2018

Table of contents

List of Figures

List of Tables

Acknowledgments

I have to thank many people at the end of this adventure as a student at the Politecnico di Milano, which began more than five years ago.

First of all, I would like to thank Professor Bruni for giving me the opportunity to work on a very interesting project, allowing me to broaden my knowledge both theoretically and practically and for the huge revision work done on this thesis.

A sincere thanks go to Dr. Di Gialleonardo who followed me from the first to the last day of this thesis, sharing his knowledge and helping me at any time and for any problem, showing me a great availability and an extraordinary dedication to his work.

I would also like to thank Dr. Liu for his advices, especially on the part of numerical co-simulations, Dr. Bionda for the help and support on the experimental part and Dr. Bacci for having prepared the part linked to the electronics used in the laboratory tests.

Obviously, I thank my family, my dad and my mom, who made this graduation possible by supporting me in these five years of study which were not always easy. Thanks to my brother Alessandro for all the valuable advices and the help that he has given me over the years and to my sister Annalisa who, even though she has not really helped me, she has always supported and encouraged me. Thanks also to my grandfather Luciano who has always followed me and has been interested in my studies since I was a child.

A very special thank you is for my friend Melinda with whom I have shared every experience for the last 10 years of my life. Thank you for supporting me in all these years of high school and university. You have been and you are an example and an important reference point for me, the merit of this goal is also yours and I hope we will be able to celebrate it as soon as possible like we did for the bachelor.

I would like to thank Lorenzo, with whom I attended and shared all the courses and the efforts of this long experience from the first to the last day. Thanks, of course, to all the guys I have met over the years: Claudia, Pietro, Daniele, Massimo, Lorenzo, Carlo, Fabio, Matteo, Piergiorgio, Alessandro, Giovanni, Giuseppe, Luca, Giulia and all those who accompanied me so far.

Last, but not least, I thank all the guys and the people I met and who helped me grow during the Erasmus experience in the Czech Republic. In particular, I thank Giovanni with whom I shared many of the experiences made around Europe.

Finally, thanks to all of you who made this day possible. Thank you for helping, supporting and making me grow. I hope I can achieve other important goals in the future, and I hope to do it again with all of you.

Lorenzo

Ringraziamenti

Sono molte le persone che devo ringraziare a conclusione di questa avventura da studente al Politecnico di Milano iniziata ormai più di cinque anni fa.

Innanzitutto, vorrei ringraziare il Professor Bruni per avermi dato la possibilità di lavorare su un progetto molto interessante, permettendomi di ampliare le mie conoscenze sia a livello teorico che pratico e per il grandissimo lavoro di revisione fatto su questa tesi.

Un grazie sincero va al Dottor Di Gialleonardo che mi ha seguito dal primo all'ultimo giorno di questo percorso di tesi, trasmettendomi le sue conoscenze e aiutandomi in qualunque momento e per qualunque problema, mostrando una disponibilità e una dedizione straordinaria al suo lavoro.

Ringrazio anche il Dottor Liu per i sui consigli soprattutto sulla parte di co-simulazioni numeriche, il Dottor Bionda per l'aiuto e il supporto sulla parte sperimentale e la Dottoressa Bacci per aver preparato la parte legata all'elettronica usata nei tests di laboratorio.

Ovviamente ringrazio la mia famiglia, mio papà e mia mamma, che hanno reso possibile tutto questo sostenendomi in questi cinque anni di studio non sempre facili. Grazie a mio fratello Alessandro per tutti i consigli e gli aiuti preziosi che mi ha dato in questi anni e a mia sorella Annalisa che, anche se non mi ha proprio aiutato, mi ha comunque sempre sostenuto e incoraggiato. Grazie anche a mio nonno Luciano che mi ha sempre seguito e si è interessato al mio percorso di studi fin da quando ero piccolo.

Un grazie veramente speciale va alla mia amica Melinda con cui da quasi 10 anni ormai condivido ogni esperienza. Grazie per avermi supportato e sopportato in tutti questi anni tra liceo e università. Sei stata e sei esempio e punto di riferimento importante per me, il merito di questo traguardo è anche tuo e spero potremo festeggiarlo presto come abbiamo fatto per la triennale.

Un particolare grazie va a Lorenzo, con cui ho frequentato e condiviso tutti i corsi e le fatiche di questo lungo percorso dal primo all'ultimo giorno. Grazie ovviamente anche a tutti i ragazzi che ho conosciuto in questi anni: Claudia, Pietro, Daniele, Massimo, Lorenzo, Carlo, Fabio, Matteo, Piergiorgio, Alessandro, Giovanni, Giuseppe, Luca, Giulia e tutti quelli che mi hanno accompagnato fin qui.

Ultimo, ma non per importanza, ringrazio tutti i ragazzi e le persone che ho conosciuto e che mi hanno aiutato a crescere durante l'esperienza Erasmus in Repubblica Ceca. In particolare, ringrazio Giovanni con cui ho condiviso molte delle esperienze fatte in giro per l'Europa.

Insomma, grazie a tutti voi che avete reso possibile questo giorno. Grazie per avermi aiutato, sostenuto e fatto crescere. Spero di poter raggiungere altri traguardi importanti in futuro e spero di farlo ancora con tutti voi.

Lorenzo

Abstract

In the field of high-speed rail transport, the need to use suspensions with adjustable damping characteristics to increase passengers' comfort, reduce transmission of vibrations to the carbody and thus increase driving stability, has led to the introduction and development of semi-active and full-active suspensions.

The yaw damper is generally placed longitudinally between the bogie frame and the carbody and has the purpose of limiting the lateral oscillation motion of the bogie caused mainly by the conicity of the wheels rigidly connected to each other and which can lead to dynamic instability at high speeds. The passive hydraulic yaw damper is adapted through the introduction of an electronically controlled servo-valve which allows the oil to be regulated between the two damper chambers, thus adjusting the damping characteristic. A numerical model of semi-active and full-active yaw damper is introduced in Simulink together with the control logics used to regulate its characteristic. The multibody model of high-speed train is instead obtained through Simpack software. The control logics introduced for the yaw damper are then tested by numerical co-simulations showing an increase in driving stability both in the case of a semi-active and full-active solution.

The control logics for the semi-active damper were finally analyzed by laboratory tests, using a Hardware-in-the-Loop approach. The results of these tests show that the type of control logic adopted for controlling the semi-active damper plays a very important role in determining the stability of the vehicle.

Keywords: high-speed trains; yaw damper; hydraulic actuator; control logics; HIL tests

Sommario

Nell’ambito del trasporto ferroviario ad alta velocità la necessità di utilizzare sospensioni con caratteristiche smorzanti regolabili per aumentare il comfort dei passeggeri, diminuire la trasmissione di vibrazioni alla cassa e aumentare quindi la stabilità di marcia, ha portato all’introduzione e allo sviluppo di sospensioni semi-attive e attive.

Lo smorzatore anti-serpeggio è generalmente posto in maniera longitudinale tra carrello e cassa del veicolo e ha lo scopo di limitare il moto di oscillazione laterale del carrello causato principalmente dalla conicità delle ruote rigidamente connesse tra loro e che può portare a instabilità dinamica per elevate velocità di marcia. Lo smorzatore anti-serpeggio idraulico passivo viene adattato tramite l’introduzione di una servo-valvola controllata elettronicamente che permette di regolare il passaggio d’olio tra le due camere dello smorzatore, andando così a modificarne la caratteristica smorzante. Un modello numerico di smorzatore anti-serpeggio semi-attivo e attivo viene introdotto in Simulink insieme alle logiche di controllo usate per regolarne la caratteristica. Il modello multibody di treno ad alta velocità è invece ottenuto tramite software Simpack. Le logiche di controllo introdotte per lo smorzatore anti-serpeggio vengono quindi testate tramite co-simulazioni numeriche evidenziando un aumento della stabilità di marcia sia in caso di soluzione semi-attiva che attiva.

Le logiche di controllo per lo smorzatore semi-attivo sono state infine analizzate mediante prove di laboratorio, utilizzando un approccio Hardware-in-the-Loop. I risultati di queste prove evidenziano che il tipo di logica adottato per il controllo dello smorzatore semi-attivo assume un ruolo molto importante nel determinare la stabilità del veicolo.

Parole chiave: treni ad alta velocità; smorzatore anti-serpeggio; attuatore idraulico; logiche di controllo; banco HIL.

Chapter 1 Introduction

High-speed railways are facing an increasing demand to increase service speed, leading to the concept of “Very-High-Speed-Trains” (VHST), which means trains capable of running at speeds beyond 300 km/h. For instance, trains are already operated at speeds higher than 300 km/h in France and Japan [1-4], whilst in China the target speed for some lines is 380 km/h [5-7]. Raising service speed expands the range of distances in which VHST can provide a fast, efficient and seamless transportation means for passengers, winning the competition with airplanes and at the same time providing an energy efficient and environmentally friendly way of transporting people.

One of the major technical challenges with raising the service speed of VHST is to ensure vehicle stability at very high speed. Indeed, railway bogies travelling at high speed tend to exhibit a self-excited vibration consisting of a combination of lateral motion and yaw rotation. This phenomenon is known as ‘bogie hunting’ and is caused by the conicity of the wheels when the two wheels in a same wheelset are rigidly connected by a solid axle [8]. A vehicle exhibiting a large hunting motion with lateral wheelset/track relative displacements in the range of 6-8 mm is traditionally said to be ‘unstable’, despite the motion occurring in this case is a stable periodic motion. Apart from terminology issues, an ‘unstable’ running of the bogie means that large track shift forces are generated between the wheelsets and the track, with the possible risk that the unstable bogies will produce large permanent misalignment of the track in lateral direction, ultimately impairing or even endangering the circulation of next trains.

A well-established way to reduce bogie hunting and ensure vehicle ‘stability’ at speeds up to 300÷350 km/h is to use passive hydraulic yaw dampers. These dampers are mounted between the car body and the bogie frame on the side of the bogie and react to a yaw motion of the bogie relative to the car body, increasing the energy dissipation for this kind of motion and therefore counteracting the formation of a large hunting limit cycle. However, when attempting to further raise the speed of the train, the use of passive yaw dampers finds some limitations. First of all, it is not possible to simply increase the damping force of the yaw dampers, because this would produce large yaw torques applied on the bogie when the vehicle negotiates curve transitions, which might impair the steering capability of the vehicle and possibly lead to a derailment. Furthermore, the damping capability of hydraulic dampers becomes lower at increasing frequencies, due to the effect of internal flexibility and elastic deformation of the end mountings [9]. Finally, very large yaw dampers are difficult to accommodate on a bogie and their use may become critical in case of a failure, whilst the duplication of yaw dampers is unfavourable from a life cycle cost point of view.

An innovative solution to the problem described above is represented by the use of active or semi-active devices to replace passive yaw dampers. This enhanced solution allows to exploit at best the damping capability of the active or semi-active device, maximizing the part of the force generated by the device which is in counterphase to the yaw speed of the bogie frame (thus maximizing energy dissipation) at the same time reducing as much as possible the part of the force which is in phase with bogie displacement, as this component results in an unwanted elastic force effect [10]. An additional advantage of using an active yaw damper is that this device can be also used to help the vehicle running through curves.

In the past, the use of active yaw dampers, also known as “Secondary Yaw Control” (SYC) has been proposed with application to long-distance / high-speed trains [10-12] with a focus on raising the vehicle’s critical speed, but also for low speed railway cars [13] and freight locomotives [14]. The solution proposed for high-speed vehicle in [10, 11] was based on the use of an electromechanical actuator but had the drawback of being potentially sensitive to failures like jamming of the ball screw in the actuator, which might lead to blocking the rotation of the bogie relative to the car body, resulting in a high risk of derailment.

In this thesis, the active yaw damper concept is revisited for a VHST, considering however hydraulic actuation instead of electromechanical. The main advantage of this technology is that jamming of the actuator is impossible, facilitating the fail-safe design of the device. However, the pass-band of hydraulic actuators is highly depending on the performances of the hardware used (particularly proportional valves or servo-valves) and care must be paid to make sure that the component can provide the required performances in terms of maximum force and pass-band and also that it is capable of guaranteeing a safe running condition also in case of failure. Besides the full-active solution, the thesis also considers the case of a semi-active hydraulic yaw damper which, compared to a full-active solution, is easier to install on a vehicle due to the absence of bulky equipment such as the pumps and is also less expensive.

In the thesis a concept and preliminary dimensioning for one full-active and one semi-active yaw damper is developed and suitable control laws for both are defined. A multi-body model of a vehicle for a VHST train is built using software Simpack and numerical simulations are performed to assess the behavior of the vehicle with active and semi-active suspensions, considering as a reference the same vehicle equipped with a traditional passive yaw damper. The multi-body model incorporates a dynamic model of the semi-active or active actuator and is established using a co-simulation between Simulink and Simpack.

Finally, a Hardware-in-the-Loop (HIL) tests rig is designed, allowing to perform laboratory tests on passive, semi-active and full-active yaw dampers and to reproduce conditions close to the one of the real case of a vehicle running on the track, so that the effectiveness of the control strategies can be assessed using the real hardware. Results of test on a prototype semi-active damper (realized outside this thesis work) are reported and consideration about the suitability of different control strategies in relation to the pass band of the proportional valve in the damper are provided.

The thesis is structured as follows:

In Chapter 2 an overview of the state of the art in high-speed railway field is presented and discussed, with a focus on yaw damper technology and its benefits. The configurations and the technologies adopted for passive, semi-active and full-active devices are presented. Different actuator types with their specific characteristics, as well as advantages and disadvantages, are described. The main control strategies adopted for semi-active and full-active suspensions are introduced referring to previous studies that have covered these fields.

In Chapter 3 the yaw damper concept is introduced. The control logics of the semi-active and full-active yaw dampers are presented both from a qualitative and numerical point of view. In particular, for the semi-active case the Maximum Power Point Tracking (MPPT) and the sky-hook control logics are considered and analyzed, while for the full-active case the ideal reference damping force control logic is taken into account. Then, mathematical models are formulated for the semi-active and full-active yaw dampers and simplified models are derived to obtain models suitable for numerical simulations.

In Chapter 4 the Simpack multibody model of a single railway vehicle is introduced, considering three versions: with passive, with semi-active and with full-active yaw dampers. Then, different methods for stability assessment are presented also based on the EN 14363 Standard [15] . In the last part of the chapter, the stability assessment considering numerical multibody simulations for the passive, semi-active and full-active solution is performed, and the results are discussed.

In Chapter 5 the laboratory setup for HIL tests is presented and described. Since the multibody model defined in Simpack is too complex for real-time simulations a simplified model with only two degrees of freedom is developed and validated. Finally, the results of the HIL tests are shown and explained both for the MPPT and sky-hook control strategies.

Finally, Chapter 6 provides some conclusive remarks and outlines possible future extensions of this work.

Chapter 2 State of Art

The subject of railway vehicle dynamics has developed principally as mechanical engineering discipline, but an important technological change is starting to occur through the use of semi-active and active suspension concepts. In this chapter past investigations addressing the use of active and semi-active control in railway vehicle suspensions are reviewed. In the first part, the basics of semi-active and full-active suspensions are described. Then, the main actuator types will be introduced, describing for each one the principal pros and cons and the application fields. Finally, a large set of control strategy will be mentioned with some specific case of application and a few examples of active secondary suspensions will be considered.

2.1 Basics of semi-active and full-active suspensions

In the last decades, with the increase of railway vehicle speed, the mechanical vehicle's dynamic performance is negatively affected and for this reason suspensions and other components of the railway vehicle have to be modified in order to compensate for the deteriorated dynamic behavior. From the suspension point of view, improvement possibilities due to passive suspension technology will eventually reach a limit because of the mechanical limitation of the components. Therefore, semi-active and full-active suspension technology in railway vehicles are considered as a valid alternative solution for this issue, since they could be offer better possibilities of improving the vehicle's dynamic performance compared to the conventional passive solution. Although the term of "semi-active suspension" and "active suspension" are commonly taken to providing improved ride quality in fact, they are generic terms that define the use of actuators, sensors and electronic controllers to enhance and/or replace the spring and dampers that are the key constituents of a conventional, purely mechanical, "passive" suspension; as such they can be applied to any aspect of the vehicle's dynamic system [16].

Vehicle dynamicists have been aware of active suspensions for some time, with major reviews having been undertaken in 1975 so far they have only found substantial application in tilting trains, which can now be thought of an established suspension technology.

The concept of active technology in rail vehicles has been analyzed theoretically and experimentally since the 1970s [17-19], but until some years ago it has not yet made its convincing breakthrough in operational use (except for tilting train technology), as has been experienced in, for example aircraft and automotive industry. With reliability increase and cost decrease of active control technologies, these technologies become more and more common in personal cars. However, active control technology has not yet completely revolutionized the rail vehicles dynamic performance. The main reasons for the non-complete success of implementing and maintaining active technology in railway vehicles is the high cost and fault problems. Compared to the passive solution, the active suspension system must prove to be at least as reliable and safe as a passive suspension, in order to be considered as an option. However, if a concept can be found that simultaneously manages good performance and acceptable costs there is significant potential for future implementation [12].

Active control of the vehicle suspensions can be used to obtain levels of dynamic performance that are not possible with purely passive solutions, facilitating higher speed and/or reduced train track interaction. The general scheme of an active suspension is shown in diagrammatic form in Figure 2.1. The input/output relationship provided by the suspensions is not anymore dependent just by the value of masses, springs, dampers and the geometrical arrangement as in the passive case, but it also depends on control strategy and the sensors and actuator configurations. Moreover, with the active control introduction, it is possible to reach performances that are impossible, or at least very difficult, to reach with a passive suspension [12].

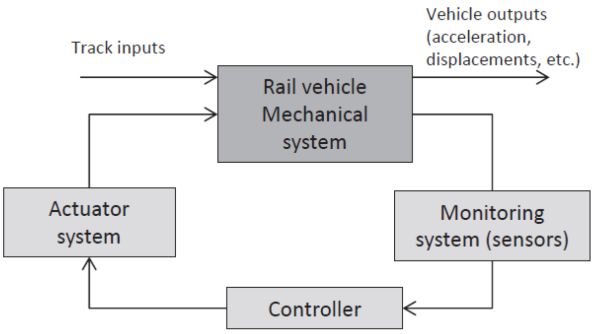

Figure 2.1 Generalized active suspension scheme [16].

The greatest benefits can be achieved by using fully-controllable actuators with their own power supply, such that the desired control action (usually a force) can be achieved irrespective of the movement of the actuator. Energy can flow from or to the power supply as required to implement the particular control law. This is known as a “full-active” suspension, but it is also possible to use a “semi-active” approach in which the characteristic of an otherwise passive suspension component can be rapidly varied under electronic control (Figure 2.2).

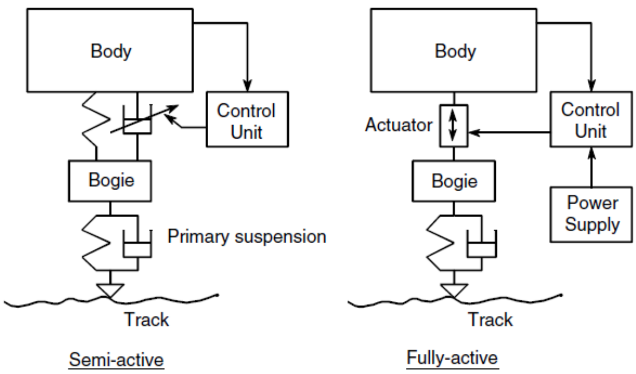

Figure 2.2 Semi- and full-active control [16].

The benefit of the semi-active approach compared with full active is one of simplicity, because a separate power supply for the actuator is not needed. The disadvantage of a semi-active damper is that the force remains dependent upon the speed of damper movement, which means that large forces cannot be produced when the speed is low, and, in particular, it cannot develop a positive force when the speed reverses because it is only possible to dissipate energy, while it is not possible to feed mechanical power to the vehicle’s motion. Figure 2.3 clarifies the limitation by showing areas on the force-velocity diagram that are available for a semi-active damper based upon its minimum and maximum levels, whereas an actuator in a full-active system can cover all four quadrants. This limitation upon controllability restricts the performance of a semi-active suspension to a significant degree [16].

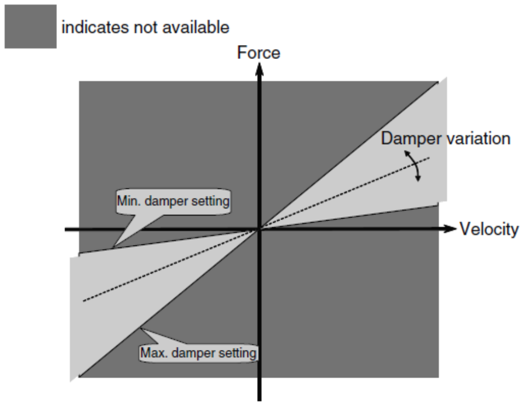

Figure 2.3 Force-velocity diagram for semi-active damper [16].

Halfway between passive and full-active suspensions, there are also semi-active and semi-passive controls [12]. Semi-active controls vary rapidly the characteristics of another-wise passive element on the basis of measurements of variables within the dynamic system. Semi-passive, adjustable passive and adaptive passive controls modify the characteristics on the basis of a variable that is not influenced by the dynamic system being controlled (*e.g.* as a function of the vehicle speed). Those alternatives are relatively simple to implement and less demanding in power consumptions, but the performance improvements are not as significant compared with what is possible with full active suspension [12].

Active control can be applied to any or all of the suspension degrees-of-freedom (in principle every rigid mode and all relevant flexible modes), but in practice, control is usually restricted to a subset. Most commonly, control is applied in the vertical, lateral or roll direction, depending principally upon where the actuators are fitted within the suspension and what sensors are being used to provide feedback signals. Generally, there would be minimal coupling from an active vertical suspension to either lateral or roll, but interactions between lateral and roll direction can be profound.

An interesting comparison between fully-active and semi-active suspension concepts has been performed by Ballo [20], however, applied to a quarter-car road vehicle. When analyzing the root mean square value of the sprung mass acceleration the semi-active suspension concept offers as good reduction as the fully-active, additionally, to much lower power consumption. In contrast, the root mean square value of the force transmitted to the roadway is significantly reduced with the fully-active system compared to the semi-active. It was also shown that the fully-active suspension concept offers possibilities of further increase of the effectiveness (however, at the expense of increased power consumption), whereas the semi-active concept is rather limited.

In general, in many observed studies [20-22], fully- and semi- active suspensions are being compared, with the results that fully-active actually offers better performance and ride comfort improvement. However, when it comes to implementing active suspension for operational use, the semi-active concept or passive concept are always chosen. The explanation, as mentioned before, is that fully-active suspension is more expensive, and the railway companies not yet fully believe in the system's reliability.

It is important to understand that the improved performance offered by an active suspension can be utilized from an operative point of view in different ways. The first option is simply to provide the passengers with a better ride quality, but if the ride quality is already good there is little justification for the extra cost of the active suspension. The second option is the possibility of running faster and using the improved performance to maintain an acceptable ride quality. The third option is to operate the train on a lower quality track, with the active suspension again being used to maintain acceptable ride quality: in this case, a significant savings in track maintenance, arising from not needing to achieve such a high track quality, can be used to justify the active suspension [12].

Active secondary suspension can be used in lateral and/or vertical directions and different actuator configurations are possible to use as illustrated in Figure 2.4. Actuators can be used to replace the passive suspensions as shown in Figure 2.4(a) and the suspension behavior will be completely controlled via active means. In practice, however, it is more beneficial that actuators are used in conjunction with passive components. When connected in parallel, as illustrated in Figure 2.4(b), the size of an actuator can be significantly reduced as the passive component will be largely responsible for providing a constant force to support the body mass of a vehicle in the vertical direction or quasi-static curving forces in lateral direction. On the other hand, fitting a spring in series with the actuator, as shown in Figure 2.4(c), helps with the high frequency problem caused by the lack of response in the actuator movement and control output at high frequency, and in practice a combination of parallel spring for load-carrying and series spring to help with the high frequency response is the most appropriate arrangement. The stiffness of the series spring depends upon the actuator technology: a relatively high value can be used for technologies such as hydraulics that have good high frequency performance, and softer value for the other technologies which means that achieving a high bandwidth is more problematic [16].

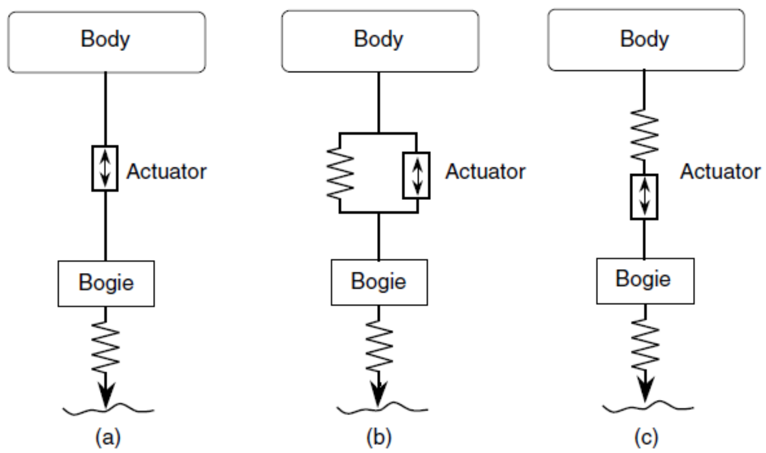

Figure 2.4 Active secondary suspension actuator configurations [16].

Active suspensions allow possible actuation principles in order to guarantee stability and steering of the vehicle. As Goodall *et al.* present in [23], with an actuator and a power supply, different configuration can be achieved to enhance the performance of the train. However, the Actuated Solid

Wheelset (ASW), Actuated Independently Rotating Wheels (AIRW), Directly Steered Wheels (DSW) and Driven Independently Rotating Wheels (DIRW) concepts require the complete redesign not only of the bogie but also of the entire vehicle. Instead with the Secondary Yaw Control (SYC) mode, the active device can be placed directly on the passive yaw damper position, reducing the redesign efforts.

A comparison between active and passive secondary yaw suspension is treated by Braghin, Bruni and Resta [11]. From their analysis it is possible to conclude that with the proposed active device based on an electro-mechanical actuator it is possible to significantly raise the critical speed of the vehicle and to negotiate the curves at higher values of cant deficiency. Reference [11] compared also the use of yaw actuation (actuators mounted in longitudinal direction) to the combined use of lateral and yaw actuation (actuators in lateral direction). It is demonstrated that the latter has a much higher potential for vehicle stabilization and may lead to use of small-scale actuators but has a negative effect on passenger’s comfort.

2.2 Actuator types

Active suspension and, to some extent, semi-active ones, rely the use of actuators. Several actuator types have been studied in the area of railway technology over the years. The following paragraph gives an overview of the different types, the concept of how they work and their advantages and disadvantages. The choice of the actuator is dependent on the trade-off between actuator performance and cost considerations. Ideal actuator behavior is often not possible to realize, since it would not be economically justified.

2.2.1 Electro-mechanical actuator

An electro-mechanical actuator is powered by an electrical motor (AC or DC), which is able to operate a mechanism (*e.g.* a ball screw or a four-bar linkage). An example is shown in Figure 2.5: in this case the rotational motion and torque of the screw is transformed into a translational motion, or force, which acts on the body that the actuator is mounted on [11]. Electro-mechanical actuators are in general less compact than other actuator types. In [19] it is stated that they can encounter problems with reliability and life of mechanical components.

The development of electro-mechanical actuators has been in progress during at least three decades. The performance of an electro-mechanical actuator in a rail vehicle was studied already in 1984 in England by Pollard and Simons [24]. Furthermore, experimental research in the late 1990s in France using electro-mechanical actuators has been described by Gautier, Quetin and Vincent [25]. The electro-mechanical actuator was chosen due to its low noise levels and compact design. Regarding the size of the actuators there is no full consensus in literature. In general, the choice of the size depends on the particular application it is used for. Lately, an electro-mechanical actuator with a roller screw has been analysed by Kjellqvist, Sadarangani and Östlund [26] making a suggestion on how to manage the design conflict between actuator size, temperature and dynamic properties.

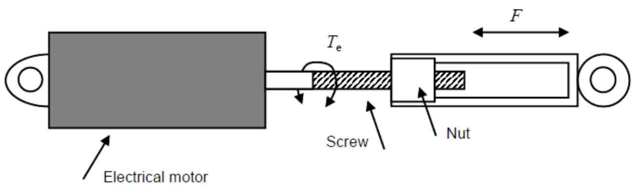

Figure 2.5 Principal function of an electro-mechanical actuator [26].

2.2.2 Electro-magnetic actuator

The electro-magnetic actuator consists of two pairs of electro-magnets mounted back to back operating in attraction mode. The magnets produce a force in both directions between two masses connected through the actuator, *e.g*. carbody and bogie.

The electro-magnetic actuator is often preferred because of its property of large frequency bandwidth. It is considered to show good frequency response up to 50 Hz. Since it does not contain any moving parts it is a robust and reliable device, described by Pollard [27]. However, it suffers from a relatively high unit size and weight, and can be difficult to fit in narrow places between two bodies of the vehicle. The effect of air gap variations between the magnets causes an unstable system, which can be mitigated with proper force feedback, according to Goodall, Pearson and Pratt [28].

2.2.3 Hydraulic actuator

There exist several variations of hydraulic actuators used in active railway technology, sometimes mentioned as servo-hydraulic and sometimes as electro-hydraulic. Accordingly, the use of these actuators in the literature is mostly referred to as just hydraulic. The general concept of hydraulic actuators is based on the idea that a control signal activates valves or a pump controlling the flow of the hydraulic fluid into and out from the actuator. With these mechanisms, a pressure difference appears between the two chambers of the actuator cylinder, which, in turn, gives rise to the actuator force. Figure 2.6 shows the basic principle of an electro-hydraulic actuator with a hydraulic-filled cylinder consisting of two chambers divided by a movable piston.

Generally, hydraulic actuators have a fast response time and they are able to maintain a demanded loading capacity indefinitely without excessive heat generation. However, hydraulic systems are highly non-linear and subject to parameter uncertainty, described by Niksefat and Sepehri [29]. Hydraulic actuators are compact and can easily be fitted in narrow spaces between carbody and bogie frame. Their cost-effectiveness makes them favorable to be implemented in vehicles for full-scale tests. An experimental analysis was performed by Shimamune and Tanifuji [30], who chose a hydraulic actuator before a pneumatic actuator instead of its ability to control in a frequency range up to about 10 Hz, compared to 2–3 Hz. The major disadvantage with hydraulic actuators is the risk of oil leakage. Furthermore, questions regarding maintainability and maintenance costs of hydraulic actuators can be raised [28].

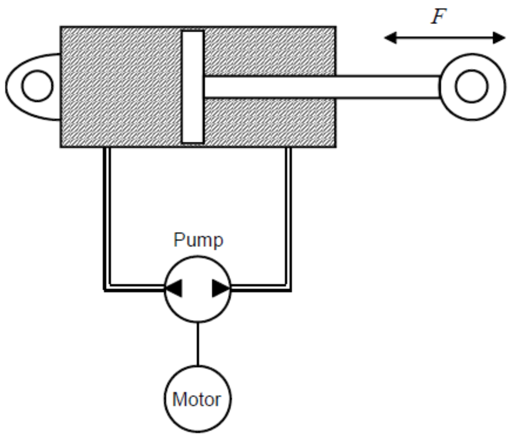

Figure 2.6 Principal function of an electro-hydraulic actuator [29].

2.2.4 Servo-pneumatic actuator

In an active servo-pneumatic system the air pressure is controlled, which gives rise to desired suspension characteristics. In vertical direction the air pressure in an already existing air spring system with fixed reservoir volume can be actively controlled by a reservoir with variable volume, as described by Pollard and Simons [24]. In lateral direction the pneumatic actuator can be of the same principle as a hydraulic actuator, but instead varying the air pressure by controlling the air flow into and out from the actuator cylinder.

The advantage with servo-pneumatic actuators is that they can be linked to already existing pneumatic systems of the vehicle (*e.g.* to air springs and the braking system). Components of the actuator are relatively cheap and there is no liquid that can leak. However, due to large air compressibility the controllable frequency bandwidth is restricted to 2–3 Hz, and the energy efficiency of the actuator is limited.

In an investigation performed in the mid-1990s by Sasaki, Kamoshita and Enomoto [31] servo-pneumatic actuators were tested on a roller rig in order to reduce vibrations in vertical, lateral and roll modes. Up to 50% reduction of these particular modes of vibration could be shown with the active system. Another Japanese study was performed at approximately the same time by Hirata, Koizumi and Takahashi [32], where an experimental rail vehicle was used. One of two passive lateral hydraulic dampers was replaced by a pneumatic actuator. With active suspension the lateral, yaw and roll motions caused by track irregularities could be reduced. However, these pneumatic actuators were rather weak compared to, for example hydraulic actuators. Nevertheless, lateral accelerations in the carbody could be reduced although vehicle speed was higher than in a passive suspension case.

2.2.5 Rheological semi-active damper

There are two types of rheological semi-active dampers, namely electro- and magneto-rheological (ER or MR). They are cylindrical dampers divided into two chambers by a movable piston. The chambers are entirely filled with a low-viscosity fluid containing fine electric or magnetic particles. The actuator is exposed to an electric or a magnetic field, by means of electrodes or electro-magnets, respectively. The viscosity of the fluid is varied according to the strength of the field applied to the actuator. Hence, the damping characteristics of the actuator are varied. The stronger the field, the larger the actuator force. The increase in viscosity can be as much as ten times higher with the MR fluid, according to Yao, Yap, Chen, Li and Yeo [33]. In Figure 2.7 a schematic picture of the electro-rheological concept is shown.

The ER and MR actuators are relatively cheap to manufacture and have low energy consumption. The response to the electric or magnetic field is fast, which enables a wide control bandwidth. The MR actuator has been analyzed in an experimental test rig by means of semi-active control in [33]. It was concluded that the MR actuator could generate damping forces in a very broad range under the influence of a magnetic field.

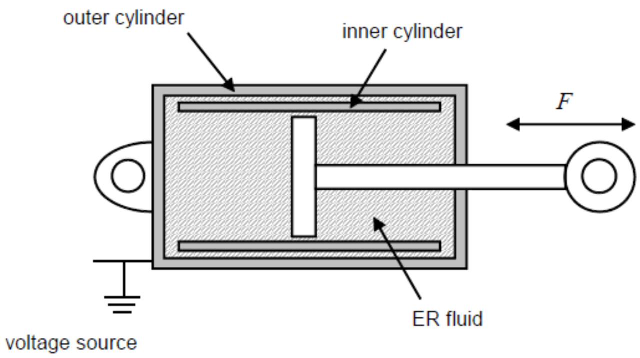

Figure 2.7 Principal function of an electro-rheological actuator [33].

2.3 Control strategies

In order to enable steering, guarantee stability and control of the actuators in a favorable way an appropriate control algorithm is needed. Several control strategies have been studied and implemented in the area of active technology within rail vehicles.

2.3.1 PID control

Classical loop-shaping with a proportional-integral-derivative controller (PID controller) is widely used in industrial control systems. The PID controller creates an input signal u to the system process by attempting to correct the error e between a demanded reference signal r and the actual output signal y (Figure 2.8):

$$e(t) = r(t) - y(t) \tag{2.1}$$

The PID controller is described as

$$u(t) = K_P e(t) + K_I \int_0^t e(s)ds + K_D \frac{d}{dt} e(t) \tag{2.2}$$

where K_P, K_I and K_D are controller coefficients for the proportional, integral and derivative parts, respectively. Appropriate design of the coefficients makes it possible to achieve a control system with desired performance characteristics. The PID algorithm is relatively simple and offers a robust performance. The largest challenge is to find the appropriate design of the control parameters [34]. Increased K_P, *i.e.* tuning of the proportional part, enables a faster controller, whereas an increased integral part, K_I, eliminates steady-state errors in the output signal. However, both K_P and K_I decrease the margins of stability, so by increasing the derivative part, K_D, possible instability can be suppressed.

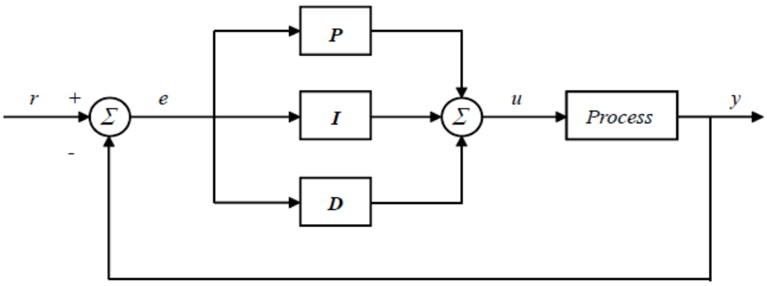

Figure 2.8 Block diagram for a *PID* controller.

2.3.2 Sky-hook damping

One of the most implemented control algorithms in the area of semi-active and active technology in trains is the so-called sky-hook damping. The name is based on the idea that the system is damped relative to a fictive sky reference point, instead of the ground (Figure 2.9).

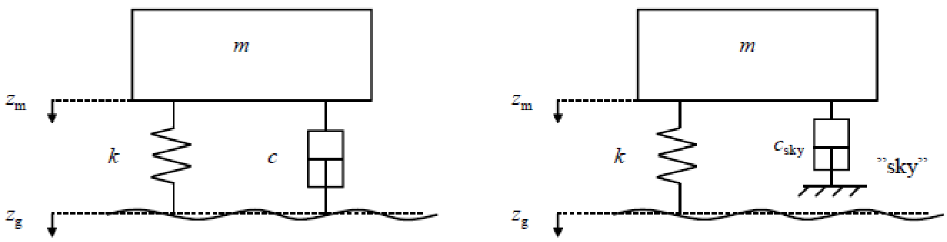

Figure 2.9 Difference between conventional suspension model and sky-hook damping suspension model [16].

The effective principle of absolute damping is depicted in Figure 2.10(a), where a damper is connected from the mass to the sky, hence the term ‘sky-hook’ damping. For practical implementations, the principle of the sky-hook damping can be realized by the arrangement shown in Figure 2.10(b). The feedback measurement is provided from a sensor mounted above the suspension on the body and the control demand is fed to the actuator which is placed between the vehicle body and the bogie. A comparison between the passive and the sky-hook damping of a simple (one-mass) system illustrates the potential advantages of the active concept very well. For a passive damper, a higher level of modal damping can only be achieved at the expense of increased suspension transmissibility at high frequencies, as shown in Figure 2.11. For the sky-hook damper, however, the high frequency responses are independent of the damping ratio, and the transmissibility is significantly lower than that of the passive damping at all frequencies concerned [16].

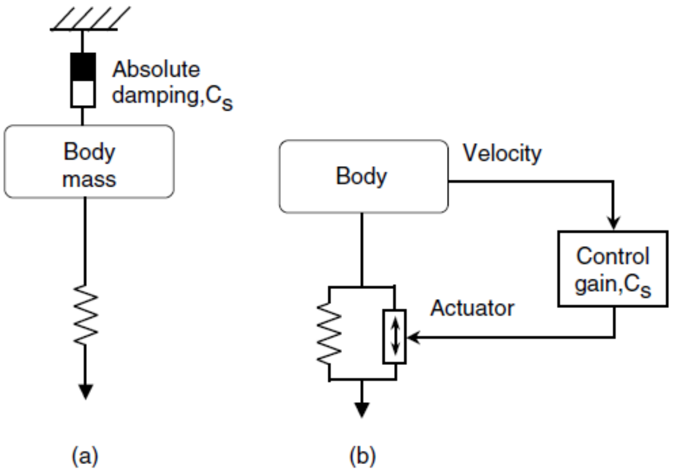

Figure 2.10 Sky-hook damping [16].

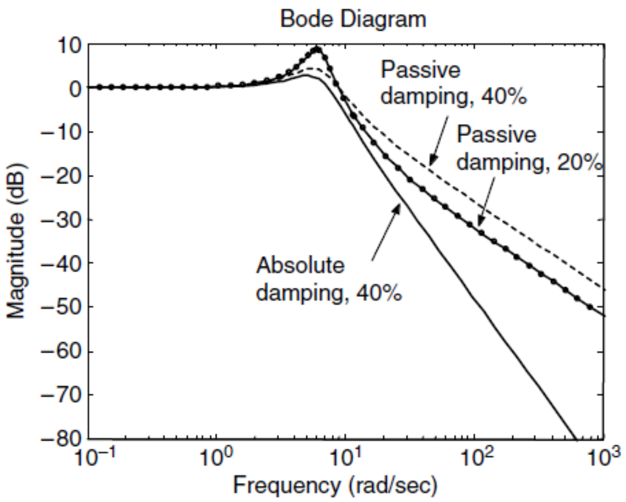

Figure 2.11 Comparison of passive and absolute damping [16].

The strategy of sky-hook damping was first introduced by Karnopp in the late 1970s and a comprehensive description was published in 1983 [35]. Thereafter, sky-hook damping has been thoroughly investigated and analyzed by various researchers throughout the years. Stribersky, Kienberger, Wagner and Müller [36] have shown by means of simulations that sky-hook damping significantly reduces resonance peaks and the root mean square of the acceleration, thus improving ride comfort, both vertically and laterally. Generally, sky-hook damping offers a great benefit on the ride quality in case of straight track, but at the same time it can be affected by some problems in curve or in correspondence of gradient variations of the track. A practical implementation of the sky-hook damping methodology is shown in the scheme in Figure 2.12. The absolute velocity signal that is required for sky-hook damping will usually be produced by integrating the signal from an accelerometer, and so, in practice, it will also be necessary to filter out the low frequency components in order to avoid problems with thermal drift in the accelerometer.

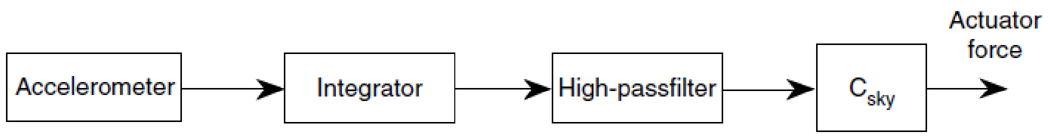

Figure 2.12 Practical implementation of sky-hook damping.

2.3.3 Maximum power point tracking control (MPPT)

The MPPT control logic was in origin developed to adjust the controller variables with the aim of maximizing the power generated in a production plant [37] but can also be applied to a mechanical system: the physical quantities that have to be optimized are included in the cost function J that is minimized by the algorithm. For a vehicle suspension, the cost function can be defined as a weighted sum of the root mean square values of signals representing the performances of the suspension and in some cases the intensity of the control force. An example of this control strategy was used by Chiarabaglio for semi-active secondary suspension in [38]. This control algorithm is very useful since it solves only one linear equation and so it does not consume much computational power. Moreover, it is easy to implement and can be used in analog or digital circuits.

2.3.4 Fuzzy control

The Fuzzy control algorithm is characterized by the presence of a look-up table obtained from experiments performed on the system. The look-up table links the computed errors with the control action, as shown in Figure 2.13. The feedback variables depend on the data set of experiments available. Moreover, this control logic can deal with nonlinear systems without introducing nonlinear control methods. The Fuzzy algorithm is a sort of 'discrete' controller since the damping characteristics are not continuously adjustable due to the discretization performed by the look-up table. Examples of Fuzzy control for vehicle suspensions are reported in [39-41].

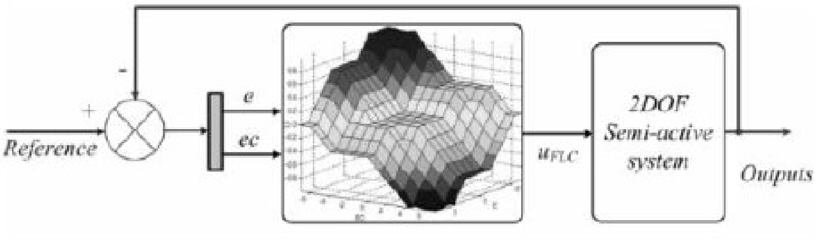

Figure 2.13 Fuzzy controller block diagram [16].

2.3.5 Low bandwidth control

Active secondary suspensions can also be used to provide a low bandwidth control, which is similar to tilting controls in that the action is intended to respond principally to the low frequency deterministic track inputs. In low bandwidth systems, there will be passive elements which dictate the fundamental dynamic response, and the function of the active element is associated with some low frequency activity. A particular use of the concept is for maintaining the average position of the suspension in the center of its working space, thereby minimizing contact with the mechanical limits of travel, and enabling the possibility of a softer spring to be used [42]. This is a powerful technique for the lateral suspensions because curving forces are large, and without centering action there may sometimes be significant reductions in ride quality whilst curving.

2.3.6 Modal control approach

For a conventional railway vehicle with two secondary suspensions between the body frame and the two bogies, it is possible to use local control for each suspension, *i.e.*, the measurement from the sensors mounted above either of the bogies is fed to the controller which controls the actuator on the same bogie. However, the tuning of control parameters may be problematic, as interactions between the two controllers via the vehicle body will be inevitable. To overcome this difficulty, a centralized controller for both suspensions may be used to enable independent control of the body modes. Figure 2.14 shows how the lateral and yaw modes of a vehicle body can be separately controlled by using active suspensions in the lateral direction, and a similar scheme can be applied to actuators in the vertical direction to control the bounce and pitch modes. The output measurements from the two bogies are decomposed to give feedback signals required by the lateral and yaw controllers, respectively, and the output signals from the two controllers are then recombined to control two actuators at the two bogies accordingly. In this way, it is possible to apply different levels of control, in particular to reduce the suspension frequency and add more damping to the yaw (or pitch) mode, which is less susceptible to the low frequency deterministic inputs [16].

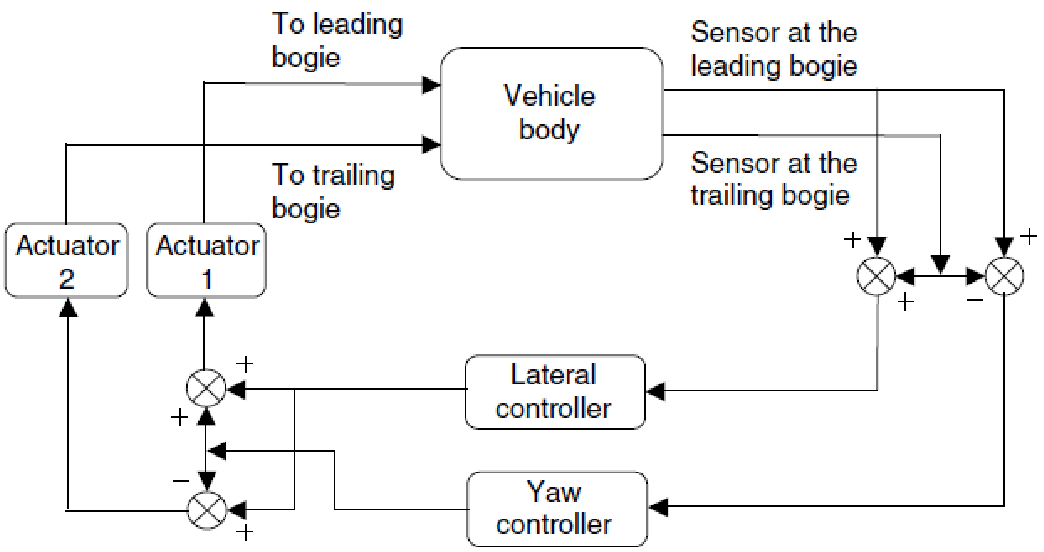

Figure 2.14 Modal control diagram [16].

2.3.7 H_∞ control

H_∞ control is a control methodology acting on the full state of the system. It is concerned with finding a controller K_C for the open-loop system G_0, such that the closed-loop system G_{ec} has good performance, stability and robustness. Figure 2.15 illustrates a typical configuration of a general control system. The closed-loop system G_{ec} is a transfer matrix from the external disturbance signal w to the error signal z. Moreover, the measurement signal y is used in K_C to calculate the control signal u. In order to achieve secured stability and robustness of the system the signal z should be minimized.

"H_∞ control theory" has been developed by Doyle *et al.*[43], Kimura *et al.* [44] and many other theorists and there have been some applications of H_∞ control theory to the control design of an automotive active suspension. Moran and Nagai [45] designed an H_∞ robust control system based on a half-car model, in order to achieve a reduction of the body acceleration and the steering stability, simultaneously. Yamashita *et al.* [46] designed an H_∞ control system based on a quarter-car model, for the purpose of attenuating the body acceleration in the range of human acceleration sensitivity. Hirata *et. al.* [32] applied H_∞ control theory to the control design of a railroad vehicle active suspension in order to reducing the resonance of each vibration appearing in a carbody.

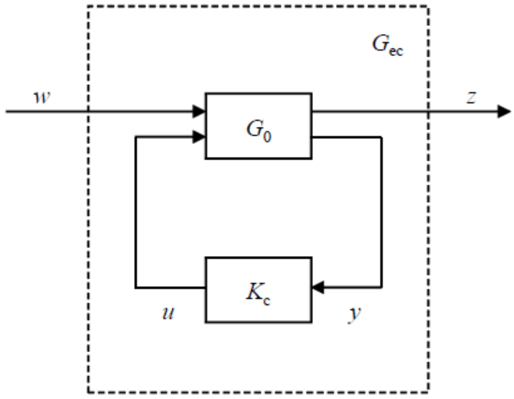

Figure 2.15 Typical configuration of a general control system.

2.3.8 LQ/LQG control

Another control theory that is concerned with state feedback is the so-called “Linear Quadratic” (LQ) control or extended to “Linear Quadratic Gaussian” (LQG) control. A dynamic system that is described through linear differential equations and a quadratic cost function that should be minimized is called an LQ problem. If normally distributed (Gaussian) disturbances are considered the control theory is extended to LQG, as described by Glad and Ljung [47].

A linear system can be described on state-space form,

$$\begin{cases} \dot{x}(t) = Ax(t) + Bu(t) + N\nu_1 \\ y(t) = Cx(t) + \nu_2 \end{cases} \tag{2.3}$$

where x is the system state vector, u is the control signal, y is the output signal and ν_1 and ν_2 are white noise intensity signals. A is the system matrix, B the input matrix, N the disturbance input matrix and C the output matrix. The quadratic cost function J that should be minimized is described as the sum of the quadratic norm of the control error e and the control signal u, respectively,

$$J = min\left(\|e\|_{Q_1}^2 + \|u\|_{Q_2}^2\right) = min \int e^T(t)Q_1e(t) + u^T(t)Q_2u(t)dt \tag{2.4}$$

where Q_1 and Q_1 are weighting functions.

A study that has assessed the LQG control law was performed by Pratt and Goodall [48]. Its aim was to compare traditional active secondary suspension between each bogie and the carbody with the alternative approach of active suspension between carbodies, so-called inter-vehicle suspension. The conclusion was drawn that active inter-vehicle suspension could achieve reduction of motions in either bounce or pitch direction, but not at the same time. Thus, it is a matter of trade-off and it depends on how the weighting of the cost function of the LQG theory is designed.

Another study by Pratt and Goodall [49] deals with the same subject of active intervehicle damping by means of LQG control law. The trade-off between ride quality and suspension deflection is dependent on the weighting of the cost function of the LQG controller. Simulations with an active three-car inter-vehicle model were performed and the results showed that ride comfort in the center carbody could be considerably improved compared to a corresponding passive inter-vehicle model. On the other hand, ride comfort in the two outer carbodies was deteriorated. Conclusions drawn from the simulations were that active inter-vehicle damping does not show significant improvement in ride comfort compared to passive inter-vehicle damping, but however, offers further development possibilities.

Tibaldi and Zattoni [50] have performed a study investigating LQ and LQG control law applied to active suspension design. A quarter-car vehicle model was used where a nonlinear hydraulic actuator was linearized in order to design the LQ and LQG controllers. Despite the fact that the LQG control law uses Kalman filtering to estimate immeasurable states it does not cause significant performance loss compared to the LQ controller.

2.4 Example of active secondary suspension

To conclude this chapter, some examples of active secondary suspension are presented: mainly this new technique is used for active lateral secondary suspension, while a real application of active yaw damper for secondary suspension is not used nowadays

The first full-scale demonstration of an active railway suspension was an active lateral secondary suspension using hydraulic actuators [51]. An actuator was fitted in parallel with the lateral secondary air suspension at each end of the vehicle, as can be seen in the left-hand side of Figure 2.16. The performance obtained from a comprehensive series of tests is shown on the right, from which it can be seen that a large improvement in ride quality was obtained: a 50% reduction compared to the passive suspension. The controller used a modal structure, shown in Figure 2.17, that provided independent control of the vehicle’s lateral and yaw suspension modes using the complementary filter technique.

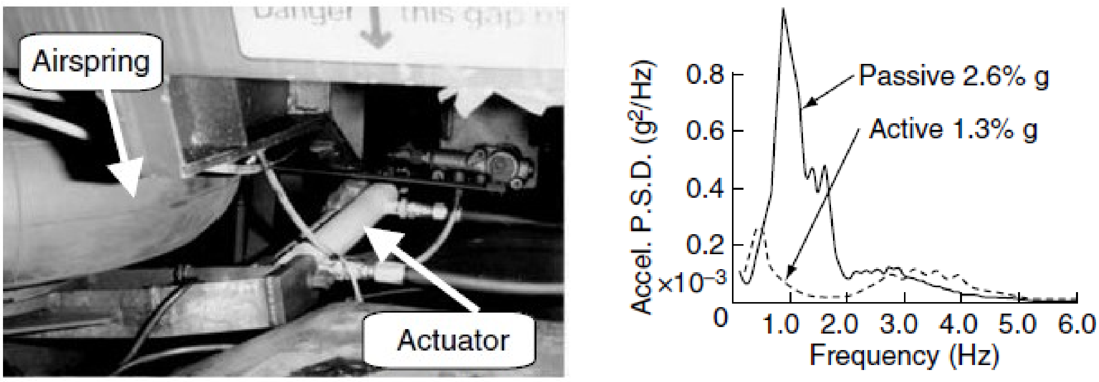

(a) (b)

Figure 2.16 Servo-hydraulic actuator (a) and experimental results for active lateral suspension (b) [16].

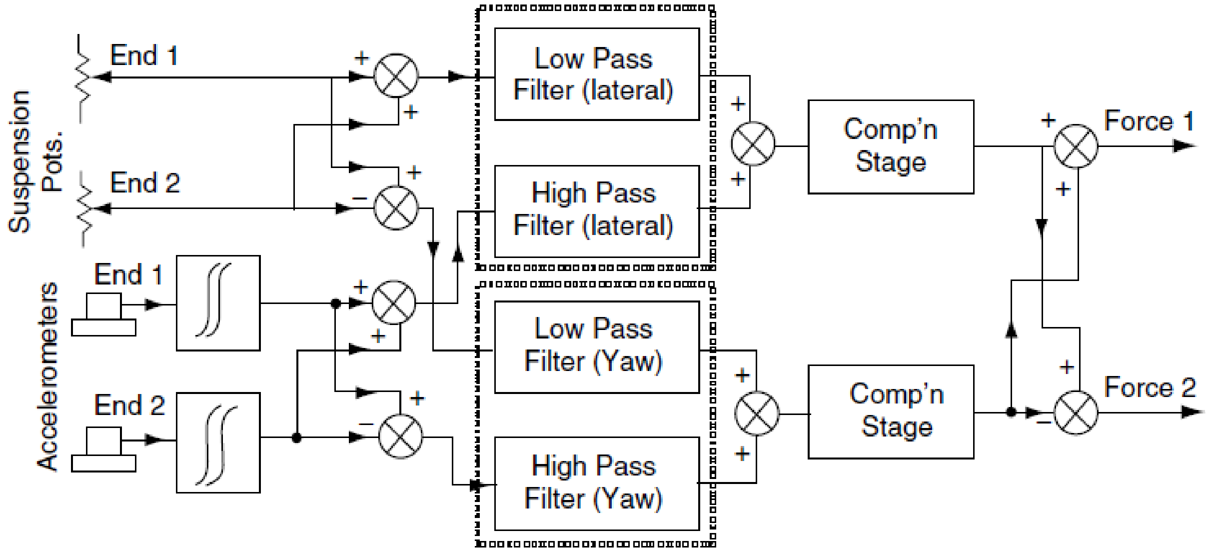

Figure 2.17 Controller for servo-hydraulic active lateral suspension [16].

The first commercial use of an active suspension was developed by Sumitomo for the East Japan Railway Company on their series E2-1000 and E3 Shinkansen vehicles, introduced in 2002 [52]. The main object of the control was the lateral vibration, *i.e.*, closely related with ride comfort, the aim being to reduce by more than half the lateral vibration in the frequency range from 1 to 3 Hz. A pneumatic actuator system was adopted which has the advantage of easy maintenance and low cost, and it is installed in parallel to a secondary suspension damper (Figure 2.18). The damper is electronically-switched from a soft setting when active control is enabled, to the normal harder setting for passive operation. An H_∞ controller was designed to provide robust vibration control using measurements from body-mounted accelerometers. It provides independent control of the yaw and lateral/roll modes, with the yaw controller driving the two actuators in opposition, and the lateral/roll controller driving them in the same direction. Figure 2.19 is a diagram of the overall control scheme.

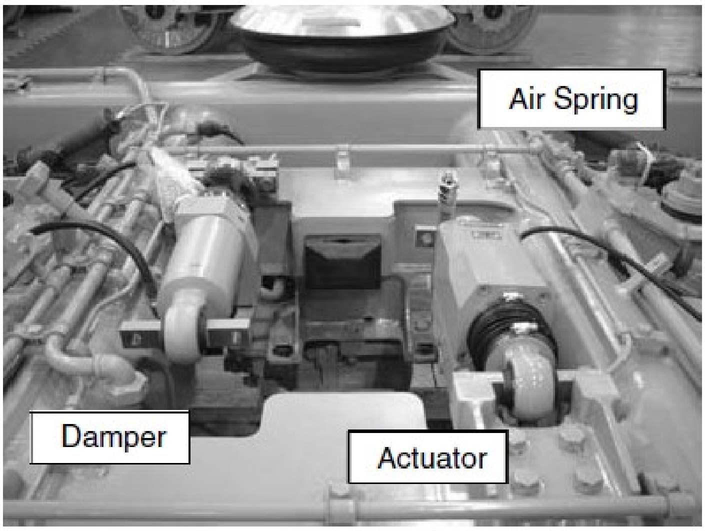

Figure 2.18 Actuator installation in bogie [16].

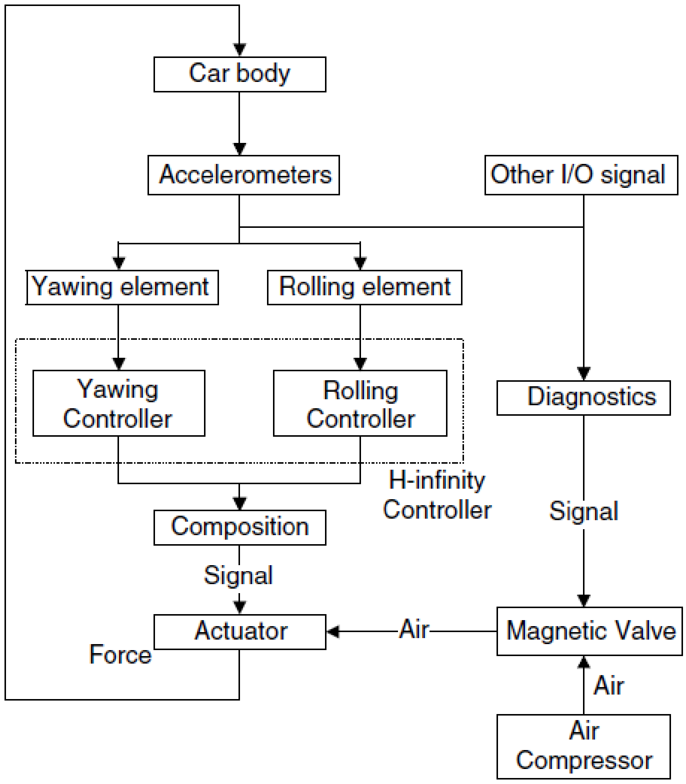

Figure 2.19 Overall scheme of control algorithm [16].

As mentioned above, there are no real application of active yaw damping in order to improve the dynamic behavior of high-speed railway vehicles. The concept of active secondary suspension is more related to the comfort of the passengers but usually is preferable semi-active secondary suspension than full-active. Probably there is only one example of active yaw damper actually applied and paradoxically it is not an example of high-speed train. There is a particular type hydraulic yaw actuator named ADD (German acronym of active yaw damper) from an Austrian company. It is basically a passive hydraulic yaw damper with a three-way valve with an internal displacement sensor. This actuator detects the internal displacement when the relative rotation between the bogie frame and the carbody is greater than a threshold value that establishes if the train is negotiating a sharp curve and combining this information with the running direction it is also possible to establish the direction of the curve. This information changes the position of the three-way valve and it is applied a force (with a fix value) that steering the bogie in the direction of the curve to help the negotiation of the curve itself. So, this is a passive component completed by an on/off active control. The main purpose of this application is not to increase the critical speed of the railway vehicle (it is sufficient the passive suspension) but is to improve the curve negotiation, especially in case of sharp curve that is an issue of low speed railway vehicle.

Finally, at the Mechanical Engineering Department of Politecnico di Milano the applicability and effectiveness of an active yaw damper has been investigated by means of in-line tests and numerical simulations. In this case, the proposed active device is based on an electro mechanical actuator and the results obtained show the possibility to significantly rise the critical speed of the vehicle as reported in [11].

Chapter 3 Semi-active and full-active hydraulic yaw dampers

This chapter provides an outline of the basic characteristics and the modelling of the actuating system that can be used for the yaw damper. The need to model actuating systems comes from the fact that this is an integral part of the system which, on account of its dynamics, modifies the response of the system itself. The actuating system achieves the necessary force (or torque) by means of a pressurized fluid.

Among the various type of actuators presented in Chapter 2, it has been chosen to use a hydraulic actuator for this particular application. Essentially, the reasons of this choice are due to the fact that the hydraulic solution allows to work in a frequency range suitable for the considered application and at the same time it allows a fail-safe design, so that also in case of failure it can guarantee a minimum operating condition in order to avoid safety problems. In fact, for example, the pneumatic actuator cannot work at the considered frequency range and on the contrary, the electromechanical one can work at the same range, but it can create very dangerous safety issues in case of failure.

The hydraulic actuators are fluid actuators in which the force (or torque) is obtained by using the pressure energy of an oil fluid which is converted into mechanical energy. A complete set of hydraulic actuator consists of five main components namely electro hydraulic powered spool valve, piston cylinder, hydraulic pump, reservoir and piping system as shown in Figure 3.1. Power supply is needed to drive the hydraulic pump through AC motor and to control the spool valve position. The spool valve position will control the fluid to come-in or come-out to the piston-cylinder which determines the amount of force produced by the hydraulic actuator [53].

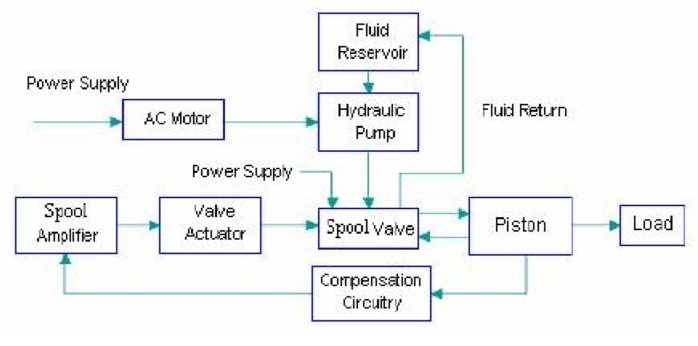

Figure 3.1 Diagram of a complete set of hydraulic actuators

The hydraulic cylinders essentially consist of a piston that is free to move within a closed guide (cylinder). Fluid under pressure, which uses a piston to exert the necessary force, is introduced into the cylinder. Depending on whether there are one or two chambers between the cylinder and the piston, this force can be exercised in either only one or both directions. In this work, it is assumed to have a double effect cylinder and its schematization is represented in Figure 3.2.

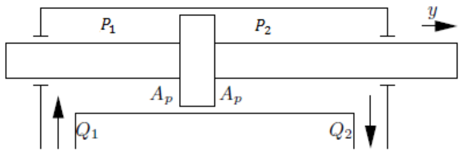

Figure 3.2 Double effect cylinder with through rod.

3.1 Concept of semi-active and full-active yaw damper

In order to size the hydraulic cylinder, it is important to know the force that the hydraulic cylinder has to produce, and the maximum pressure drop that can be achieved between the two chambers. Maximum pressure difference between the two chambers is assumed to be about 100 bar, while for the force that the hydraulic cylinder has to exert a value of 25 kN is estimated, that is the maximum value of the lateral forces obtained from preliminary multibody simulations of rail vehicle dynamics at high speed.

With these values of pressure and force, using the simple relation that defines the pressure, it is possible to find the effective area of the piston, that as shown in Figure 3.2 is represented by an annulus:

$$A_p = \frac{F}{P} \tag{3.1}$$

Finally, with these three values it is possible to choose from an actuator catalog appropriate dimensions of the piston rod like, for instance, diameter and area.

To obtain the value of the length of the chamber it is worth considering that despite this work considers a high-speed train, bogies have to be able to travel in a very sharp curve, like for example the curve to enter and exit deposit. By multiplying the value of the angle of rotation of the bogie (that depends on the semi-distance between the center of the two bogie of the same wagon) for the distance at which the yaw damper is applied with respect to the center of the bogie itself the value of the piston stroke that is directly connected with the value of the chamber's length is approximately obtained. Knowing the length of the chamber and the area, it is straightforward to calculate the volume of the actuator chamber. The main data of the hydraulic cylinder are shown in Table 3-1

Name	Value	Unit of measurement
Delta pressure	105	*bar*
Rating force	25	*kN*
Piston area	25.16	cm^2
Rod diameter	69.9	*mm*
Rod area	38.37	cm^2
Total area	63.53	cm^2
Cylinder diameter	89.94	*mm*
Chamber length	400	*mm*
Chamber volume	1	*l*

Table 3-1 Data of the hydraulic cylinder.

However, it is necessary to consider that the calculations done for the chamber length and the chamber volume have to be confirmed not only from a purely mechanical point of view but also from the point of view of the dynamics of the actuator by using the solution of the fluid motion field, that is shown in the following paragraphs.

It is worth to notice that despite the full-active and semi-active approaches have a significant difference, the main parameters of the hydraulic cylinder will be used both for the semi-active and full-active solution, and so the dimensioning of the hydraulic part is the same for the two models. The difference between the two different solutions are due to the fact that the full-active approach includes a fully-controllable force actuator that includes a power supply, whereas the semi-active concept utilizes a suspension component with a controllable characteristic. The energy flow of a semi-active suspension is controlled but not augmented, and furthermore the energy flow's direction is limited to one direction. More precisely, it is only possible to dissipate energy but not inject it (although with an accumulator it is possible to partly utilize the energy stored [54]), and this behavior results in a fundamentally nonlinear concept which offers less improvement compared with full-active. In principle any passive component whose characteristics can be changed electrically would comprise a semi-active device, but in practice a semi-active actuator is usually a conventional damper with the ability of variable damping by electro hydraulic or electro-rheological fluid devices. On the other side, full-active actuators mostly use electro-hydraulic, pneumatic or electro-mechanical technology [54].

In the following paragraphs semi-active and full-active models used in the study are presented and explained, underlining the different control strategies that will be used, in order to compare their relative performance using a consistent set of criteria.

3.2 Control strategies

The different control strategies both for the semi-active and the full-active device are now presented and explained. The control logics designed and implemented are non-model based controller. It does not require a complete model of the system since it is based on the direct measurement of the feedback variables. Another interesting feature of this kind of control logic is the low computational cost, that make it appealing for an industrial application.

3.2.1 Control strategies for semi-active

The first objective of the control logic is to decrease the lateral acceleration of the bogie and wheelset, measured according to European Standard EN 14363 [15]. Decreasing the lateral acceleration means not only improving the stability of the vehicle, but also increasing the critical speed of the vehicle, since it is strictly related with the lateral acceleration of the wheelset. The second purpose of the control logic is to limit the force exerted by the damper, to extend the life of the damping device and reduce transmission of vibrations to the carbody. Less stresses reduce the wear of the cylinder components, lowering also the maintenance costs. For the semi-active device, the following two different control strategies are implemented and used both in numerical simulation (Chapter 4) and in experimental tests (Chapter 5). It is important to consider that the two control strategies work in a quite different way. As a matter of fact, the MPPT control strategy is a relatively slow control logic since it changes the opening of the by-pass valve at discrete time intervals in the order of one second. On the contrary, the sky-hook control logic works with a continuous change of the opening valve using a very short time interval, shorter than the period of hunting oscillation, *i.e.* in the order of hundreds of milliseconds.

3.2.1.1 MPPT

As mentioned in Chapter 2, the Maximum Power Point Tracking (MPPT) control logic was developed in origin to adjust the controller variables with the aim of maximizing the power generated in a production plant. This control technique is here modified in order to reduce and control the hunting motion of a railway bogie.

The physical quantities that have to be decreased are included in the cost function J that is minimized by the algorithm. The expression of the cost function is:

$$J = k_{\ddot{x}}\left(\frac{RMS(\ddot{x}_{bogie})}{\ddot{x}_{lim}}\right)^2 + k_F\left(\frac{RMS(F)}{max(RMS(F))}\right)^2 \tag{3.2}$$

where $RMS(\ddot{x}_{bogie})$ is the root mean square of the lateral bogie acceleration computed following the normative EN14363 and $RMS(F)$ is the root mean square of the damper force. These two terms are weighted respectively by the lateral acceleration limit according to normative EN 14363 and by the maximum value of the root mean square of the damper force. The gain $k_{\ddot{x}}$ and k_F give different weights to the two terms of the cost function J.

The algorithm that compute the reference voltage minimizing the cost function is:

$$\begin{cases} V = V_{old} + sign(J, J_{old})k_J\left|\frac{J - J_{old}}{J_{max}}\right| \\ V = 0 \end{cases} \quad \text{if} \quad \begin{cases} J < J_{old} \\ J \geq J_{old} \end{cases} \tag{3.3}$$

in which k_J is the cost function gain, J_{max} is the maximum between J and J_{old} and the function $sign(J, J_{old})$ is computed in the following way:

$$\begin{cases} sign(J, J_{old}) = sign_{old}(J, J_{old}) \\ sign(J, J_{old}) = -sign_{old}(J, J_{old}) \end{cases} \quad \text{if} \quad \begin{cases} J < J_{old} \\ J \geq J_{old} \end{cases} \tag{3.4}$$

Moreover, an additional condition for the calculation of the input voltage is used and it is defined as:

$$V = V_{old} - \Delta V \qquad \text{if} \quad RMS(\ddot{x}_{bogie}) > \ddot{x}_{threshold} \tag{3.5}$$

in which ΔV is the maximum value of the voltage variation and $\ddot{x}_{threshold}$ is the threshold value for the lateral acceleration above which the system can be assumed unstable.

This control strategy works on considering records of the data acquired from the bogie frame and from the yaw damper and considers the value of the cost function J at a certain time instant and previous one and compares them each other. If the new value of the cost function J is lower than the old value, then the control continuous in the same direction as in the previous step. If otherwise the new value of the cost function is increased with respect to the previous one, then it changes the direction. Substantially, it is like empirically trying to find the way to minimize this function. It is worth to mention that this is in general a slowly behaving control strategy. No fast changes in the opening of the valve appears, the considered time steps are in the order of one second so every one second the new value for the opening of the valve is defined by the controller. In Figure 3.3 is shown the internal architecture of the MPPT control logic.

Moreover, it is possible consider two different types of control logic depending on the definition of the cost function J. The first way of defining the cost function J is just based on performances: the lateral acceleration of the bogie frame which is a measure of the degree of instability of the bogie itself is measured and the goal is to minimize the RMS of the filtered acceleration signal. In the second option the RMS of the force generated by the damper is also considered: in this case the aim of the control strategy is to minimize the hunting motion and at the same time reducing the force applied by the yaw damper.

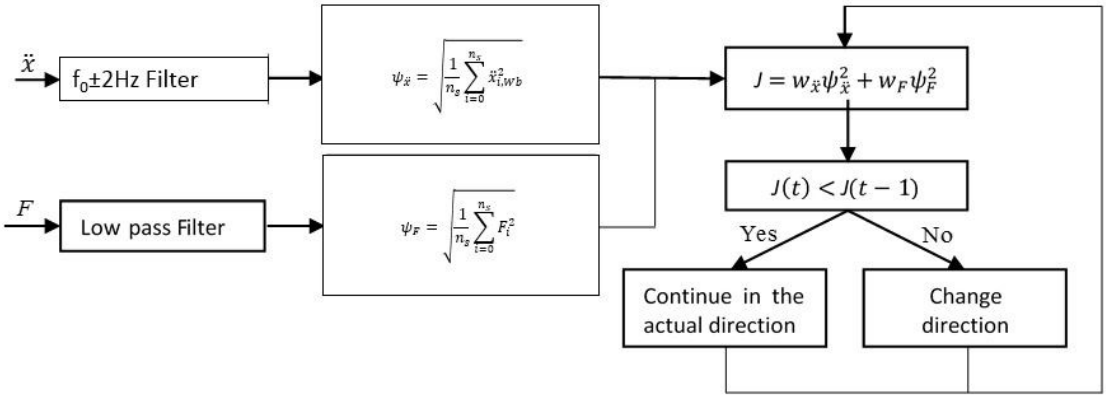

Figure 3.3 Internal architecture of the MPPT control logic.

3.2.1.2 Sky-hook

The other control strategy for the semi-active solution is sky-hook control, that is a widely used control strategy for controlling vibrations in mechanical systems. The idea is based on changing with time the damping coefficient for the semi-active yaw damper. This technique is used to emulate the presence of a viscous damper which instead of being attached to a moving body like the carbody, it is attached to a rigid frame (a sort of ground) that is following the motion of the bogie.

Semi-active dampers may be of the on-off type or of the continuously variable type. A damper of the first type is switched between "on" and "off" damping states in accordance with a suitable control algorithm. In its "on" state, the damping coefficient is relatively high, and in its "off" state, it is relatively low. Ideally the off-state damping should be zero, but in practical situations this is not possible. A continuously variable semi-active damper is also switched between "on" and "off" states. However, in its "on" state, the damping coefficient and corresponding damping force are varied. This concept is well illustrated in Figure 3.4, which shows the force-velocity characteristics for an on-off and a continuously variable damper. The shaded part of the graph on the right side represents the range of achievable damping coefficients for a continuously variable damper.

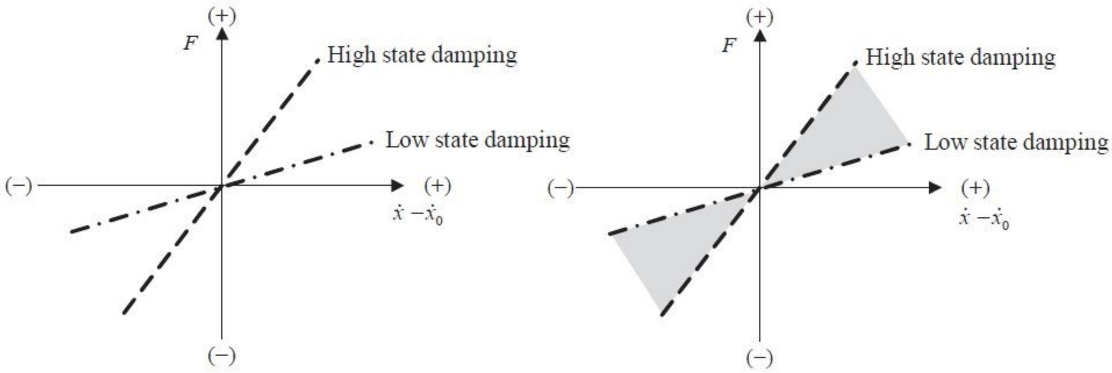

Figure 3.4 Semi-active damper concepts with on-off damper and continuously variable damper solutions.

In case of a system with a sky-hook damper, the damping force can be written as:

$$F_{sky} = c_{sky}\dot{x} \tag{3.6}$$

where F_{sky} is the sky-hook damping force, $\dot{x}$ is the velocity response of the bogie and c_{sky} is the damping coefficient of the sky-hook damper. The intention is to replicate such a sky-hook damping force with a semi-active yaw damper mounted conventionally between a "ground" and the bogie frame (Figure 3.5). However, since the passive damper can only absorb vibration energy, the product of the semi-active damping force F_{YD} and the relative velocity, $\dot{x}-\dot{x}_0$, across the damper must satisfy the inequality

$$F_{YD}(\dot{x}-\dot{x}_0) \geq 0 \tag{3.7}$$

The desired force is $c_{sky}\dot{x}$, but the semi-active yaw damper can only generate this force when $\dot{x}$ and $\dot{x}-\dot{x}_0$ have the same sign. When $\dot{x}$ and $\dot{x}-\dot{x}_0$ are opposite sign, the semi-active damper can only provide a force opposite to the desired force. In this situation, it is better to supply no force at all. The continuous semi-active sky-hook control algorithm is thus given by:

$$F_{YD} = \begin{cases} c_{sky}\dot{x}, & \dot{x}(\dot{x}-\dot{x}_0) \geq 0 \\ 0, & \dot{x}(\dot{x}-\dot{x}_0) < 0 \end{cases} \tag{3.8}$$

The switching of the device is controlled by the term $\dot{x}(\dot{x}-\dot{x}_0)$, which is called the condition function. When the damper is on, the damper force can be written as:

$$F_{YD} = c_{YD}(\dot{x}-\dot{x}_0) \tag{3.9}$$

where c_{YD} is the semi-active damping coefficient of the yaw damper. The value of c_{YD} must take to emulate a sky-hook damper may be found from equations (3.8) and (3.9):

$$c_{YD}=\begin{cases}\dfrac{c_{sky}\dot{x}}{(\dot{x}-\dot{x}_0)}, & \dot{x}(\dot{x}-\dot{x}_0)\geq 0\\ 0, & \dot{x}(\dot{x}-\dot{x}_0)<0\end{cases} \tag{3.10}$$

It is possible to see from (3.10) that when the relative velocity is very small, the required damping coefficient increases enormously and tends to infinity. However, in practice the semi-active yaw damper coefficient is limited by the physical parameters of the conventional damper, which means that there is both an upper bound, c_{max}, and a lower bound, c_{min}. The damping coefficient in equation (3.10) can thus be rewritten as

$$c_{YD}=\begin{cases}max\left[c_{min}, min\left[\dfrac{c_{sky}\dot{x}}{(\dot{x}-\dot{x}_0)}, c_{max}\right]\right], & \dot{x}(\dot{x}-\dot{x}_0)\geq 0\\ c_{min}, & \dot{x}(\dot{x}-\dot{x}_0)<0\end{cases} \tag{3.11}$$

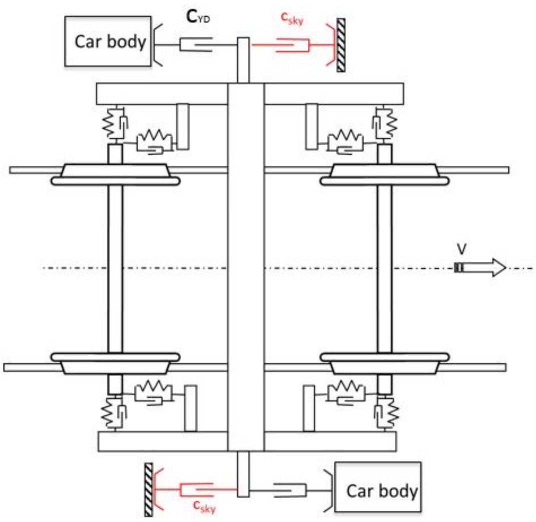

Figure 3.5 Sky-hook control strategy.

The control algorithm in equation (3.11) requires the damper coefficient to be continuously variable. To simplify the operation an on-off solution is proposed. The on-off yaw damper acts as a conventional passive yaw damper during the vibration attenuation portion of the vibration attenuation cycle, but a zero damping coefficient is assumed when the damping force generated by the semi-active yaw damper is in the opposite direction to the ideal sky-hook damping force. For on-off control, the damping force is governed by the control algorithm

$$F_{YD}=\begin{cases}c_{on}(\dot{x}-\dot{x}_0), & \dot{x}(\dot{x}-\dot{x}_0)\geq 0\\ 0, & \dot{x}(\dot{x}-\dot{x}_0)<0\end{cases} \tag{3.12}$$

where c_{on} is the on-state damping constant of the on-off damper. In practice, a zero damping coefficient is impossible when the damper is switched off. Therefore, the damping coefficient is switched between a high value and a low value, and the control algorithm in equation (3.12) can be rewritten as

$$c_{YD}=\begin{cases}c_{max}, & \dot{x}(\dot{x}-\dot{x}_0)\geq 0\\ c_{min}, & \dot{x}(\dot{x}-\dot{x}_0)<0\end{cases} \tag{3.13}$$

where c_{max} and c_{min} are the maximum and minimum coefficient of the on-off damper, respectively. The on-state damping c_{max} should be much greater than the off-state damping c_{min}, which should be as small as possible.

Both continuous sky-hook control and on-off sky-hook control algorithms attempt to produce the effect of sky-hook damping from a conventionally mounted damper.

As mentioned in paragraph 3.2.1, the sky-hook control strategy is a fast-acting control: the external valve is frequently closing and opening in a very short time interval.

3.2.2 Control strategy for full-active

The full-active control strategy aims at improving the performances of the railway vehicle at high speed. The following active control strategy is here implemented and used during the numerical multi-body simulation in the next chapter.

The maximum speed of the vehicle in tangent track is limited by the occurrence of hunting instability, which is a self-excited combined lateral and yaw oscillation of the bogie caused by the action of the wheel-rail contact forces typically occurring at high speeds. One possible way to suppress hunting instability is to use a damping force between the bogie and the carbody. In a passive vehicle this task is performed by oil dampers. However, in many cases, these devices prove to be rather inefficient, because of their internal flexibility [55], and therefore do not allow to raise sufficiently the vehicle's critical speed.

This simple control logic (Figure 3.6) is based on the definition of a reference force F_{ref} that is determined to achieve an ideal viscous damper and thus increasing the vehicle stability threshold. F_{ref} is proportional to the carbody-bogie relative speed as shown in (3.14):

$$F_{ref} = c_v v_{rel} \tag{3.14}$$

where c_v is the viscous damping gain [11].

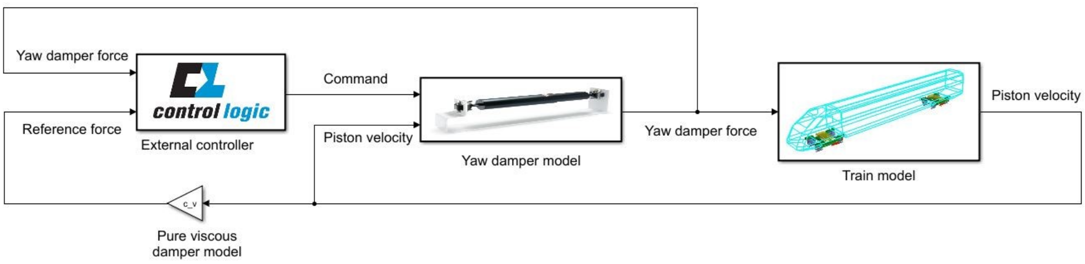

Figure 3.6 Ideal damper force (IDF) control scheme.

The external controller works as a simple proportional control between the yaw damper force and the ideal reference damper force. The input voltage command u used to regulate the characteristic of the yaw damper is given by:

$$u = k_p(F_{YD} - F_{ref}) \tag{3.15}$$

in which the proportional gain k_p is chosen by trial and error procedure in order to obtain that the yaw damper force follows in the best way the ideal reference damper force.

3.3 Model of the semi-active damper

In the following paragraph the Ferdek and Luczko model [56] is presented. First of all, the complete model is described and then the simplified reduced model is considered and analyzed, showing the main characteristics.

3.3.1 Full-order model

The damper that is taken into consideration for the semi-active model is a twin-tube damper and it is shown in Figure 3.7. The system consists of two cylinders: external one (compensatory chamber) (*1*) and the internal (working) one (*2*). Inside the working cylinder, a piston (*3*) is located attached to the rod (*4*). The piston rod is equipped with the rod guide (*6*) that limits its movement in relation to the cylinders, to the longitudinal direction only. In the lower part of the internal cylinder, a valve (*5*) is located. Four main chambers can be distinguished: chamber above the piston "External Chamber" (*A*), chamber below the piston "Compression Chamber" (*B*) and the compensatory tank "Reservoir Chamber", which consists of two parts: chamber (*C*) located above the oil level and chamber (*D*) located below it. Chamber (*D*) is filled with nitrogen under low pressure [56].

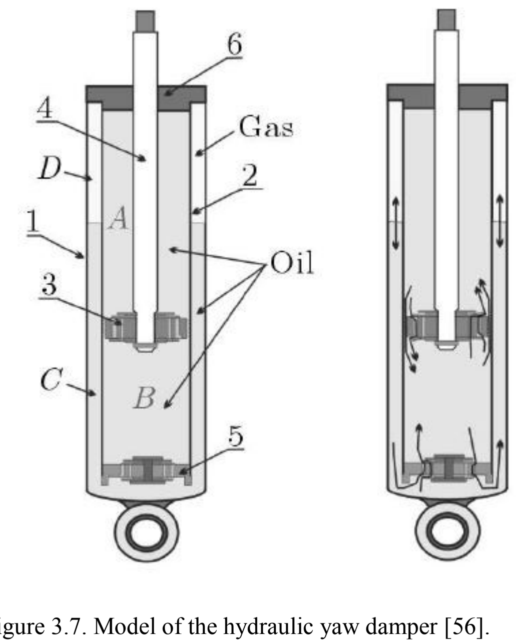

Figure 3.7. Model of the hydraulic yaw damper [56].

When the piston rod is pressed (and moves towards the bottom valve), the pressure in chamber B increases and the resistance force arises, which in turn causes the oil to flow through appropriate canals into the chamber A. The excess oil, passes through the bottom valve to the reservoir chamber, causing the pressure in chamber D to increase. In the rebound process, both piston and the rod move in the opposite direction, causing an increase of pressure in chamber A. The oil flows through the system of canals, back from the space above the piston, to the chamber below it. At the same time, oil from the compensatory tank flows through the bottom valve, in order to equalize the pressure in chamber B. The volume of the pumped fluid depends primarily on the piston displacement, while the flow rate depends on the piston velocity relative to the cylinder. The resistance force of the damper depends on the resultant force from pressure acting on the piston and from both dry and viscous friction. The force F_p exerted by the damper is given by:

$$F_p = (P_A - P_0)A_1 - (P_B - P_0)A_2 \tag{3.16}$$

in which P_A and P_B are the pressure in chamber A and chamber B, P_0 is the gas pressure in the auxiliary chamber, and A_1, A_2 are the area of the piston. The two area are different since a rod is attached on the top of the piston. With the purpose of computing the pressure in the three chambers the basic relation

$$\rho V = m \tag{3.17}$$

is taken into account and with the time differentiation and the inclusion of the equation

$$\frac{d\rho}{dP} = \frac{1}{K}\rho \tag{3.18}$$

the following relationship can be established for each i-th chamber:

$$\frac{1}{K_i}\dot{P}_i V_i + \dot{V}_i = \frac{\dot{m}_i}{\rho_i} \tag{3.19}$$

in which dots denote the time derivatives, V is the chamber volume, m is the mass of oil, ρ is the oil density and K is the oil compressibility modulus.

The changes in mass $\dot{m}_A$, $\dot{m}_B$ and $\dot{m}_C$ are described by using of the mass flow equations

$$\begin{aligned} \dot{m}_A &= \dot{m}_{BA} - \dot{m}_{AB} \\ \dot{m}_B &= \dot{m}_{AB} - \dot{m}_{BA} + \dot{m}_{CB} - \dot{m}_{BC} \\ \dot{m}_C &= \dot{m}_{BC} - \dot{m}_{CB} \end{aligned} \tag{3.20}$$

where the subscripts of the flow rates are associated with the chamber names between which the flow of oil occurs, proceeding from the chamber with the first subscript letter to the chamber with the last one.

By introducing the Heaviside's function, the previous flow rates can be substituted by the following equations:

$$\dot{m}_{AB} = \rho_A \beta A_{AB} H(P_A - P_B) \sqrt{\frac{2(P_A - P_B)}{\rho_A}}$$

$$\dot{m}_{BA} = \rho_B \beta A_{BA} H(P_B - P_A) \sqrt{\frac{2(P_B - P_A)}{\rho_B}}$$

$$\dot{m}_{BC} = \rho_B \beta A_{BC} H(P_B - P_C) \sqrt{\frac{2(P_B - P_C)}{\rho_A}} \qquad (3.21)$$

$$\dot{m}_{CB} = \rho_C \beta A_{CB} H(P_C - P_B) \sqrt{\frac{2(P_C - P_B)}{\rho_C}}$$

In order to obtain a very accurate model the fluid inside the piston cannot be considered uncompressible. Integrating the equation (3.18) an expression for variation of density according with the pressure can be computed for each chamber:

$$\rho_A = \rho_0 exp\left(\frac{P_A - P_{atm}}{K}\right)$$

$$\rho_B = \rho_0 exp\left(\frac{P_B - P_{atm}}{K}\right) \qquad (3.22)$$

$$\rho_C = \rho_0 exp\left(\frac{P_C - P_{atm}}{K}\right)$$

where ρ_0 is the density of oil under the influence of the atmospheric pressure P_{atm}.

In equations (3.20) the terms A_{ij} that represents the valve geometry, influence the mass flow rate. This term is function of the valve geometry and of the pressure difference across the valve:

$$A_{ij} = A_{ij}^{const} + A_{ij}^{var} \qquad (3.23)$$

where A_{ij}^{const} is the size of the cross-section area of the permanently open canals (including leakage) and A_{ij}^{var} is the area of the variable canals that is function of the difference on pressure across the valve

$$\Delta P = P_i - P_j \qquad (3.24)$$

and of a limit pressure P_k that is the pressure at which the valves begin to open:

$$A_{ij}^{var} = A_{ij}^{var}(P_i, P_j, P_k) \qquad (3.25)$$

In order to obtain the complete set of differential equations that describe the cylinder behavior the equation (3.3) needs to be replaced by:

$$V_A = A_1(l - x) \qquad (3.26)$$

$$V_B = A_2(l + x) \tag{3.27}$$

in which l is possible stroke.

An assumption is made here that complete length of the internal cylinder equals to

$$L = 2l + h \tag{3.28}$$

where h is the width of the piston valve, and that the displacement of the piston is given by the harmonic function

$$x = a \cdot sin(\omega t) \tag{3.29}$$

Knowing that the volume of the auxiliary chamber keeps constant, the relation

$$V_C + V_D = const \tag{3.30}$$

and its differentiation

$$\dot{V}_C = -\dot{V}_D \tag{3.31}$$

can be written.

Assuming that the gas volume V_D in the outer chamber satisfies the polytrophic equation, the following relation can be written:

$$P_D V_D^n = P_0 V_0^n = const \tag{3.32}$$

in which n is the polytrophic coefficient.

Assuming that pressure P_D is equal to pressure P_C, the rate of change in the volume V_D can be expressed as

$$\dot{V}_D = -\frac{\dot{P}_D V_D}{n P_D} \tag{3.33}$$

and introducing equation (3.32) and (3.33):

$$\dot{V}_C = -\frac{\dot{P}_D V_0 P_0^{\frac{1}{n}}}{n P_D^{1+\frac{1}{n}}} \tag{3.34}$$

Resuming, the equation that describes the change of oil pressure in chamber *A* and *B* are:

$$\dot{P}_A = \frac{K}{V_A}\left(\frac{\dot{m}_A}{\rho_A} + A_1 \dot{x}\right) \tag{3.35}$$

$$\dot{P}_B = \frac{K}{V_B}\left(\frac{\dot{m}_B}{\rho_B} - A_2 \dot{x}\right) \tag{3.36}$$

while introducing equation (3.33) into relation (3.19) it is possible to get:

$$\dot{P}_C = \frac{\dot{m}_C}{\rho_C} \frac{KnP_C^{1+\frac{1}{n}}}{V_C n P_C^{1+\frac{1}{n}} + KV_0 P_0^{\frac{1}{n}}} \tag{3.37}$$

This set of differential equation allows to compute the damping force of the hydraulic cylinder.

3.3.2 Simplified model

Although the complete model is very accurate in describing analytically the physical behavior of a twin tube hydraulic cylinder, it is difficult to be implemented on a numerical model since it presents high computational cost and some of its parameters are difficult to identify. Therefore, a simplification of the Fardek and Luczko model is now taken into consideration.

The force F_p exerted by the damper is written as:

$$F_p = A_{eff} \Delta P \tag{3.38}$$

where ΔP is the pressure difference between chamber A *a*nd chamber B and A_{eff} is an equivalent area that allows to obtain the same force value as in equation (3.16).

The oil density can be considered constant, as its variation with pressure can be neglected. This leads to a simplification of equation (3.35) and (3.36) that become respectively:

$$\dot{P}_A = \frac{K}{V_A}(Q_A + A_1 \dot{x}) \tag{3.39}$$

$$\dot{P}_B = \frac{K}{V_B}(Q_B - A_2 \dot{x}) \tag{3.40}$$

in which Q_A and Q_B are the volume flow rates relative to chambers *A* and *B*. In addition, the volumes V_A and V_B are considered constant because of the small stroke of the piston inside the inner cylinder:

$$V_A \cong V_B \cong V_0 \tag{3.41}$$

With this last assumption and by subtracting and then integrating equation (3.39) and (3.40), the damper force F_p can be expressed as a single state equation. It is worth to notice that the pressure P_C of the auxiliary chamber does not appear in the definition of the damper force since it can be considered a constant value.

The volume flow rate between chamber *A* and chamber *B* can be expressed by the Bernoulli equation:

$$Q = C_f \sqrt{\Delta P} sign(\Delta P) \tag{3.42}$$

The dependence of the damper force with the deflection velocity is modelled as a non-linear function of the piston velocity $\dot{x}_p$, leading to the final equation:

$$\Delta \dot{P} = \frac{K}{V_0}\left[-C_f \sqrt{\Delta P} sign(\Delta P) + f(\dot{x}_p)\right] \tag{3.43}$$

The term $f(\dot{x}_p)$ of equation (3.43) is designed as a cubic root function of the piston velocity $\dot{x}_p$ and it is plotted in Figure 3.8.

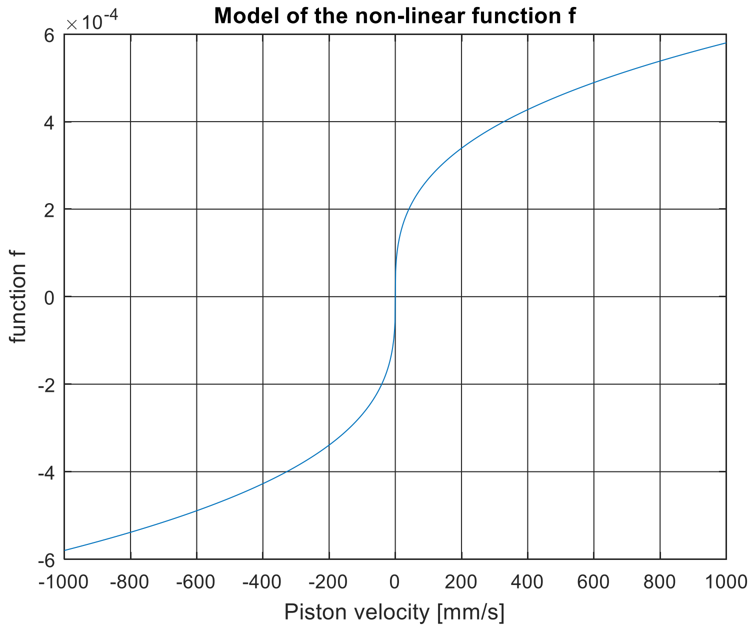

Figure 3.8 Model of the non-linear function of the piston velocity.

3.3.3 Proportional valve model

In order to define the model of the semi-active damper, the passive damper model presented in paragraph 3.3.2 must be extended introducing a model of the proportional valve. A connection pipe links the compression and the rebound chamber allowing the oil to flow in a by-pass channel. The controlled valve regulates the passage of oil in the by-pass channel, providing a tool to modify the damper characteristics. Figure 3.9 shows the scheme of the semi-active device obtained through the introduction of the by-pass channel.

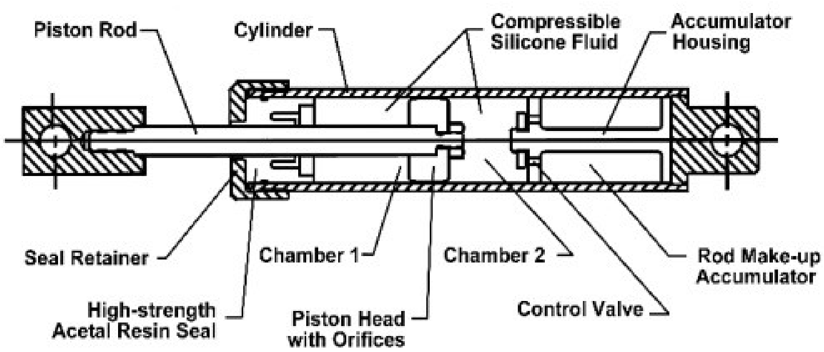

Figure 3.9 Semi-active hydraulic cylinder scheme [57].

From a modelling point of view the by-pass channel introduces an additional flow between rebound chamber A and compression chamber B. The Bernoulli equation is able to describe this flow Q_v across the valve as:

$$Q_v = c_d A_v x_v \sqrt{\frac{2\Delta P}{\rho}} sign(\Delta P) \tag{3.44}$$

where A_v is the area of oil passage through the valve when it is completely open, x_v is the valve spool position and c_d represents the contraction coefficient.

Matching together equation (3.43) and (3.44) it is possible to express the rate of change of delta pressure $\Delta\dot{P}$ between the two chambers as:

$$\Delta\dot{P} = \frac{K}{V_0}\left(-\left(C_f + c_d A_v x_v \sqrt{\frac{2\Delta P}{\rho}}\right)\sqrt{\Delta P} sign(\Delta P) + f(\dot{x}_p)\right) \tag{3.45}$$

With equation (3.45) the semi-active damper model is completely defined and it can be linked to the Simpack vehicle to perform the co-simulation (section 4.4).

3.3.4 Characterization of the semi-active damper model

In this paragraph a simple characterization of the yaw damper model introduced previously is made in order to understand its performances and to compare in a better way the results that will be obtained both during numerical simulations (Chapter 4) and HIL tests (Chapter 5).

In order to characterize the damper, a sinusoidal input for the displacement of the piston is given as input to the yaw damper model and the response of the damper in terms of force is analyzed for different frequencies of the input signal. This simple operation is repeated for different amplitude values of the displacement of the piston (1 mm and 3 mm) and for different values of the input voltage, that means for different opening values of the external servo-valve (0%, 20% 50% and 100%). As it is possible to notice from Figure 3.10 to Figure 3.13, the force exerted by the yaw damper is significantly influenced by the value of the opening valve since the maximum value can varies from 12-20 kN at 0% opening to 0.5-1 kN at 100% opening. The frequency of the sinusoidal input displacement of the piston considered in the following graphs is 4 Hz, that is more or less the frequency of the oscillation at which the limit cycle due to the hunting motion appears.

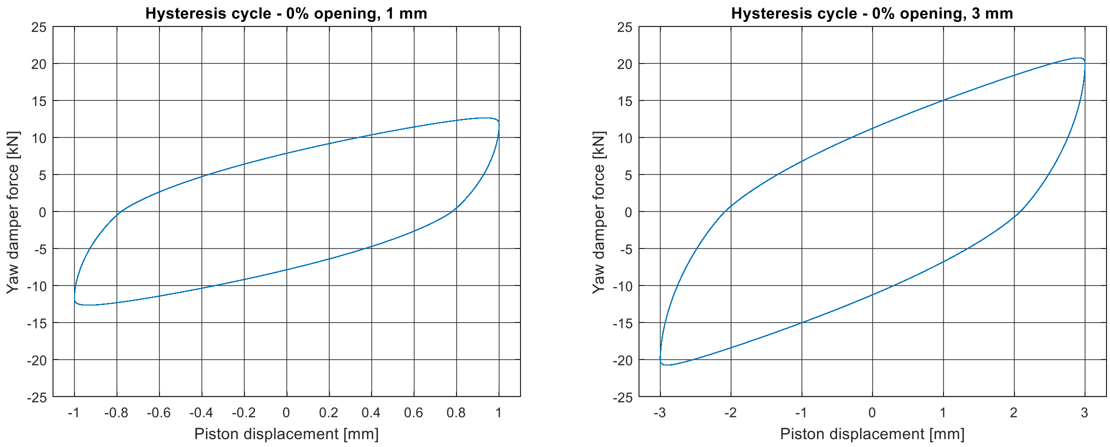

(a) (b)

Figure 3.10 Hysteresis cycle, 0% opening of the external valve, ± 1 mm amplitude of piston displacement (a), ± 3 mm amplitude of piston displacement (b).

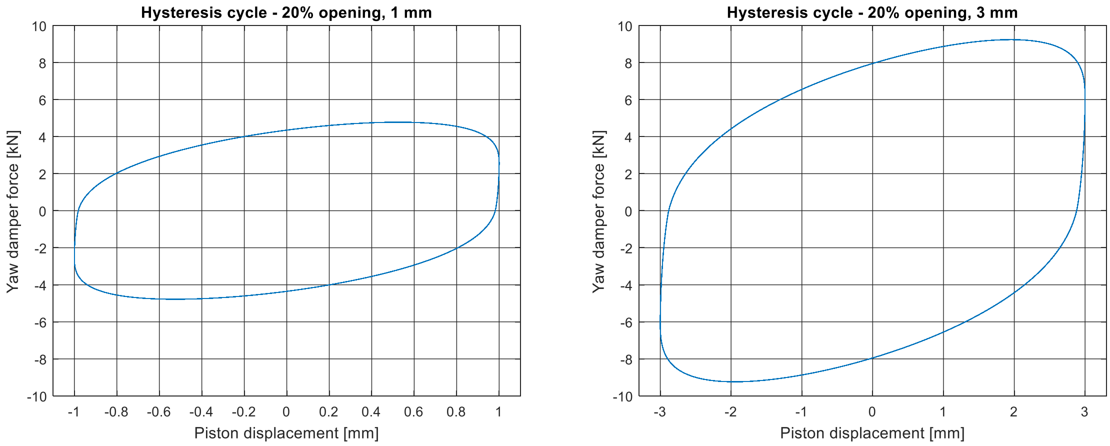

(a) (b)

Figure 3.11 Hysteresis cycle, 20% opening of the external valve, ± 1 mm amplitude of piston displacement (a), ± 3 mm amplitude of piston displacement (b).

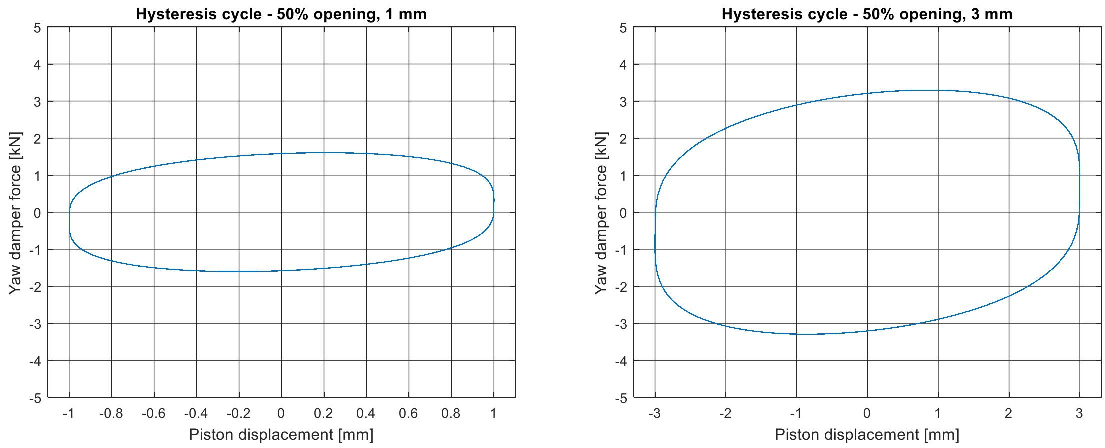

(a) (b)

Figure 3.12 Hysteresis cycle, 50% opening of the external valve, ± 1 mm amplitude of piston displacement (a), ± 3 mm amplitude of piston displacement (b).

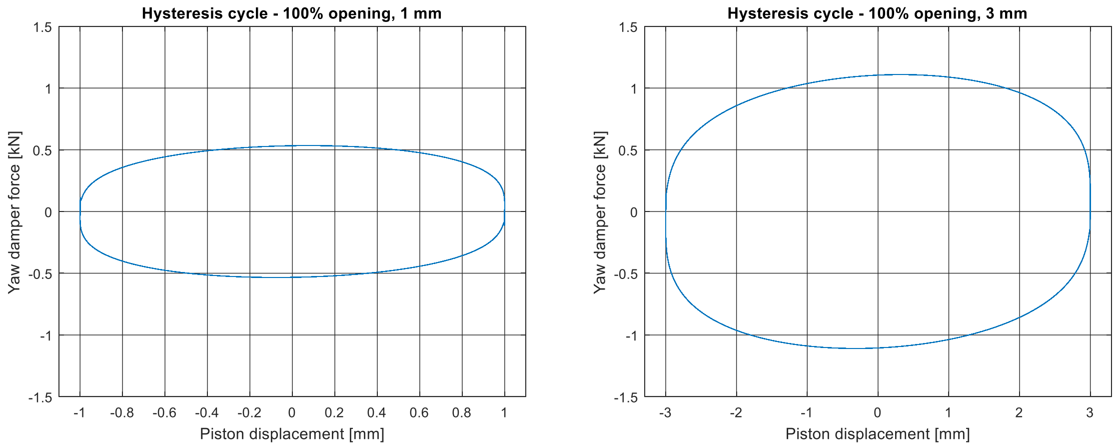

(a) (b)

Figure 3.13 Hysteresis cycle, 100% opening of the external valve, ± 1 mm amplitude of piston displacement (a), ± 3 mm amplitude of piston displacement (b).

Moreover, from the characterization tests it is possible to obtain the frequency response function between the piston displacement and the exerted force of the yaw damper evaluated for different values of opening valve as presented in Figure 3.14.

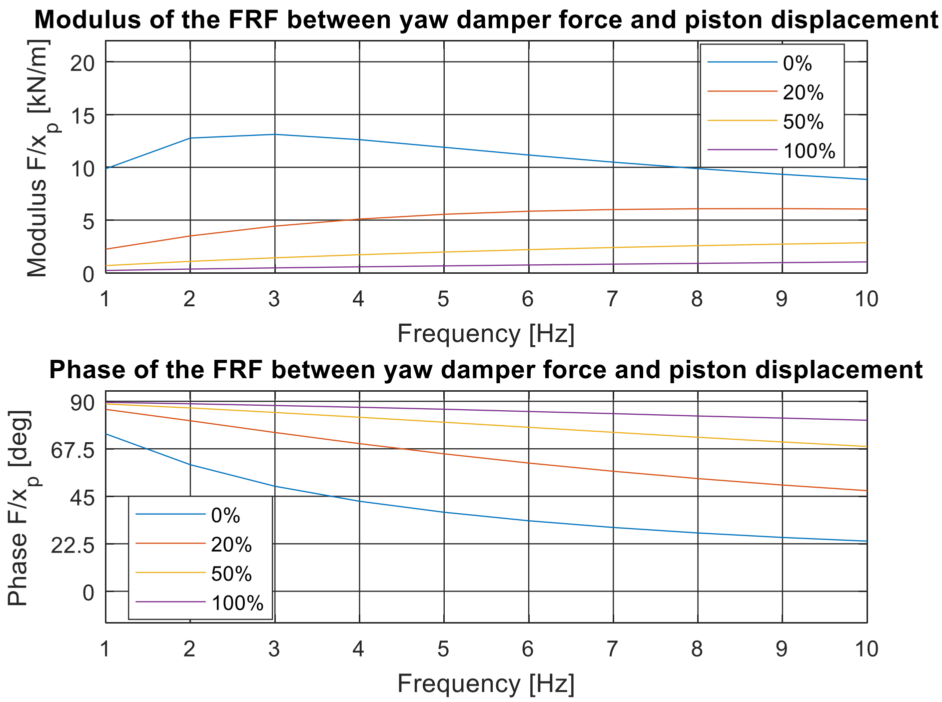

Figure 3.14 Frequency response function between yaw damper force and piston displacement (1 mm of amplitude).

The modulus diagram shows that with the openings of the valve the damper force decreases: when the valve is open the oil is no more forced to flow across the internal valve of the piston, but it can pass in the by-pass channel, where it finds less resistance. Another important feature of the semi-active damper model can be noticed from the phase diagram: opening the valve the phase rises up, approaching 90° when the valve is completely open. Opening the valve means increasing the ratio of the damping force to the elastic one. The rise up of the phase can be exploited by a control method that opens the valve in such a way to decrease the lateral acceleration of the bogies and wheelsets and increasing the critical velocity of the railway vehicle. However, it can be noticed that opening the valve the modulus of the force decreases, so a trade-off between increasing the damping coefficient and decreasing the total force has to be found by the controller.

Finally, again from the frequency response function, the equivalent stiffness and damping coefficient can be found. From Figure 3.15 it is possible to see how for the same value of the opening valve, increasing the frequency of motion means decreasing the damping coefficient and increasing the equivalent stiffness, so that at high frequency the hydraulic damper behaves more as a spring than as a damper.

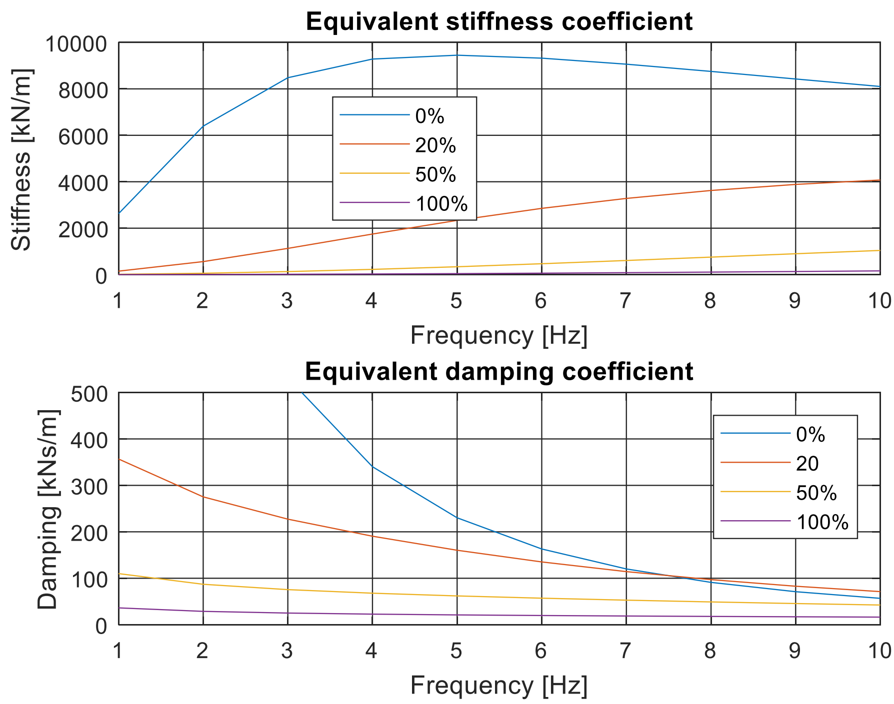

Figure 3.15 Equivalent stiffness and equivalent damping coefficients (1 mm of amplitude).

3.4 Model of the full-active damper

In this section the mathematical model of the full-active damper used in this thesis is presented. The model is based on the one developed by Ruderman [58].

3.4.1 Full-order model

First of all, the full-order model of hydraulic cylinder controlled by a directional control valve (based on [59]) is considered. The principal structure of hydraulic cylinder controlled by the directional control valve is represented in Figure 3.16. The pressure difference between the two chambers generates the hydraulic actuation force which moves the cylinder piston with a rod in direction of the pressure gradient. The external mechanical loads, inertial force, and cylinder friction counteract the induced pressure-gradient force, thus resulting in the motion dynamics of cylinder drive.

In standard conditions with constant supply pressure (due to a pump) the only control input available comes from the directional valve, u. In the simplest case, u is the coil voltage applied through an amplifier so as to energize the electro-magnetic circuits of the solenoid that compose the directional control valve. On the contrary, the more advanced and common case, which will be also considered from now on, is the case in which the control input u is directly proportional to the relative spool position. This means that the latter is low-level controlled by an embedded directional control valve electronics, which includes an internal coil current loop and external spool position loop. It is worth to notice that the spool relative displacement v, is provided by a single electro-magnetic solenoid that ensures a bidirectional spool actuation as shown in Figure 3.16.

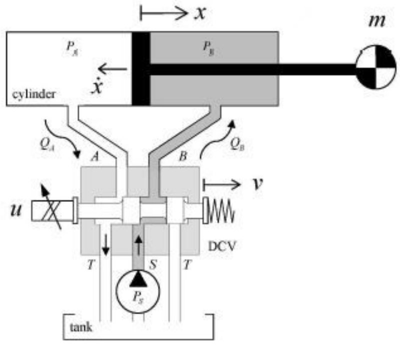

Figure 3.16 Structure of hydraulic cylinder controlled by directional control valve [58].

The low-level controlled directional control valve has the closed-loop transfer function characteristic of the second-order system described by

$$G(s) = \frac{v(s)}{u(s)} = \frac{\omega_0^2}{s^2 + 2\xi\omega_0 s + \omega_0^2} \tag{3.46}$$

The parameters of the directional control valve are the eigen-frequency ω_0, damping ratio ξ and, in the ideal case, unitary gain which ensures the steady state accuracy of the spool position control loop. The Bode diagram of the $G(s)$ transfer function is shown in Figure 3.17.

When the directional control valve assembly is equipped with a closed center spool, which is one of the most used configurations aimed to reduce the valve leakage and sensitivity to small input signals, the spool-controlled flow characteristics are inherently subject to a nonlinearity due to the presence of a dead-zone in the relationship between the flow rate through the valve and the position of the spool. It is a relative spool displacement below certain magnitude that does not lead to an orifice and therefore hydraulic flow. In addition, the orifice, which is governed by the spool displacement, is subject to saturations due to the maximally possible opening given by the inner structure of the valve body. Therefore, an internal flow-governing control variable z can be introduced as being related to the controlled spool position through two static nonlinearities, dead zone and saturation, connected in series [58].

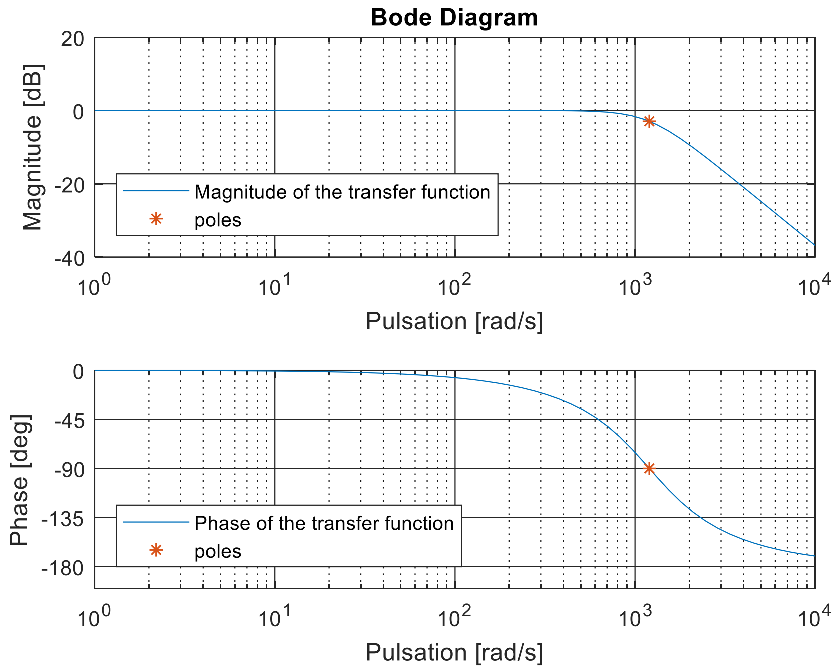

Figure 3.17 Bode diagram of the directional control valve closed loop transfer function.

The spool travel ν has been assumed as an available external input, therefore without considering its controlled behavior and associated internal dynamics.

Matching the directional control valve closed loop dynamics (3.46) with the total static nonlinearities described before:

$$h(\nu) = \begin{cases} \alpha \cdot sign(\nu), & if\ |\nu| \geq \alpha + \beta \\ 0, & if\ |\nu| \geq \beta \\ \nu - \beta \cdot sign(\nu), & otherwise \end{cases} \tag{3.47}$$

results in the mechanical sub-model of the directional control valve:

$$\ddot{\nu} + 2\xi\omega_0\dot{\nu} + \omega_0^2\nu = \omega_0^2 u \tag{3.48}$$

$$z = h(\nu) \tag{3.49}$$

where the output z is the orifice state which governs the valve flow. The parameters α and β denote the saturation level and the dead-zone size correspondingly.

The volumetric flow of hydraulic medium associated with both outer ports of the directional control valve, and thus with both chambers of the connected hydraulic cylinder, is governed by the corresponding pressure differences and given by the orifice equations:

$$Q_A(z) = \begin{cases} zK\sqrt{P_S - P_A}, & for\ z > 0 \\ zK\sqrt{P_A - P_T}, & for\ z < 0 \\ 0, & otherwise \end{cases} \tag{3.50}$$

$$Q_B(z) = \begin{cases} -zK\sqrt{P_B - P_T}, & for\ z > 0 \\ -zK\sqrt{P_S - P_B}, & for\ z < 0 \\ 0, & otherwise \end{cases} \tag{3.51}$$

In which P_S and P_T are the supply pressure and tank pressure respectively, while K is the valve flow coefficient

$$K = C_d w \sqrt{\frac{2}{\rho}} \tag{3.52}$$

denoted also as a valve gain, depends on the oil flow density ρ, discharge coefficient of the orifice C_d, and width of the rectangular orifice area w (area gradient).

Using the continuity equations, it is possible to obtain the gradient of pressure in both chambers:

$$\dot{P}_A = \frac{E}{V_A}\left(Q_A - A_A\dot{x} - C_L(P_A - P_B)\right) \tag{3.53}$$

$$\dot{P}_B = \frac{E}{V_B}\left(Q_B + A_B\dot{x} - C_L(P_B - P_A)\right) \tag{3.54}$$

where $A_{A/B}$ are the corresponding effective piston areas. Note that for this case (double-rod cylinder) the two areas are equal. The oil bulk modulus E, is defined as

$$E = -V\frac{dP}{dV} \tag{3.55}$$

and takes into account the compressibility of the hydraulic medium in cylinder. A further simplification assumption is made considering the bulk modulus as a constant parameter for the rated operation pressure of hydraulic system.

The total volume in hydraulic circuits

$$V_A = V_A^0 + A_A sat_h(x) \tag{3.56}$$

$$V_B = V_B^0 - A_B sat_h(x) \tag{3.57}$$

depends each on the rod drive position, while $V_{A/B}^0$ is the total chambers volume when the rod drive is in the initial zero position ($x = 0$). It is worth noticing that the drive displacement is subject to saturation, represented by sat_h operator in (3.56) and (3.57), while h is the half of the stroke of the hydraulic cylinder. C_L is an internal leakage of cylinder which characterizes an additional pressure drop due to penetration of the hydraulic medium between both chambers [58].

Using the Pascal's and the second Newton's law it is possible to formulate the equation for one translational degree-of-freedom of the mechanical sub-model of the cylinder:

$$m\ddot{x} = P_A A_A - P_B A_B - f(\dot{x}) - F_L \tag{3.58}$$

where m is the mass of the cylinder piston with the rod and F_L represents all the external counteracting forces (in case of stand-alone hydraulic cylinder can be assumed to be zero). The counteracting nonlinear friction f mainly depends on the relative velocity of the piston drive and acts as an inherent damping of the relative motion. This steady state friction force can be described by the Stribeck characteristic curve [60]:

$$f(\dot{x}) = sign(\dot{x})\left(F_c + (F_s - F_c)e^{-|\dot{x}|^{\delta}\chi^{-\delta}}\right) + c\dot{x} \tag{3.59}$$

which takes into account the constant Coulomb and linear viscous friction, plus the velocity-weakening effects in a low velocity range around zero. This model (3.58) is parameterized by the Coulomb friction coefficient F_c, Stribeck friction coefficient F_s, linear viscous friction coefficient c, and two Stribeck shape factors χ and δ.

Solving numerically the nonlinear equations, it is possible to obtain the frequency response function of the full-order model between the input command u and the output rod velocity $\dot{x}$. The frequency response functions have been obtained from the numerical simulation at different excitation amplitudes $|u| = \{\alpha, 0.3\alpha\}$, and in a range of frequency between 1 and 320 Hz. It is worth mentioning that the maximum frequency considering in this analysis is well beyond the frequency range in which the full-active yaw damper is supposed to work, but this value of the maximum frequency is chosen to analyze the effect of modelling the dynamics of the servo-valve. The Bode diagram of the full-order model is shown in Figure 3.18.

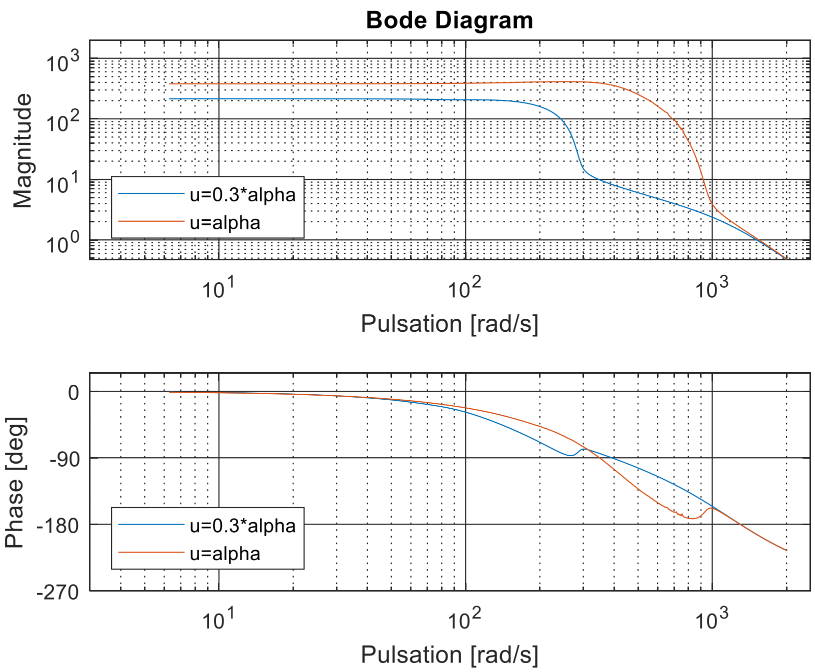

Figure 3.18 Frequency response function between the input command u and the output rod velocity $\dot{x}$ for the full-order model.

3.4.2 Reduced-order model

In this second case, it is assumed that the time-constants of hydraulic and mechanical sub-dynamics are significantly larger than that of the directional control valve by two to three orders of magnitude. Consequently, the input of the reduced model can be assumed as

$$u^* = v \tag{3.60}$$

which directly contains both nonlinearities expressed in (3.47).

It is possible to conclude that the reduced model contains only static nonlinearities in the input command, while thanks to the fast-directional control valve spool dynamics, the second order closed loop behavior of the directional control valve itself (3.46) can be neglected.

Introducing the load-relative pressure

$$P_L = P_A - P_B \tag{3.61}$$

and assuming a close hydraulic circuit, i.e.

$$|Q_A| = |Q_B| \tag{3.62}$$

the orifice equations (3.50), (3.51) presented in the full-order model can be grouped into one:

$$Q_L = zK\sqrt{\frac{1}{2}(P_S - sign(z)P_L)} \tag{3.63}$$

while it is valid:

$$P_A = \frac{P_S + P_L}{2}, \quad P_B = \frac{P_S - P_L}{2} \tag{3.64}$$

It is worth to notice that Q_L in (3.63) represents an average flow through the directional control valve and it imply further nonlinearities in the input command of the reduced model.

Using the same simplifying assumptions introduced in paragraph 3.3.2, the hydraulic continuity equations presented in (3.53), (3.54) can be transformed into one related to the load pressure gradient

$$\dot{P}_L = \frac{4E}{V_t}(Q_L - \bar{A}\dot{x} - C_L P_L) \tag{3.65}$$

in which $V_t = V_A^0 + V_B^0$ is the total hydraulic actuator volume and $\bar{A} = 0.5(A_A + A_B)$ is the average effective piston area.

Correspondingly, the dynamics of the mechanical part (3.58) in the reduced model becomes:

$$m\ddot{x} = P_L\bar{A} - f(\dot{x}) - F_L \tag{3.66}$$

with the cylinder drive velocity $\dot{x}$ as system output and the total friction force given always by (3.59).

Using the same consideration made for the full-order model, even in this case it is possible to obtain a numerical frequency response function between the input command u and the output rod velocity $\dot{x}$ (Figure 3.19). A comparison of the frequency response function of the full-order and reduced-order model is provided later in this chapter, but it can be anticipated that the two results are very close one to the other excepted at very high frequencies.

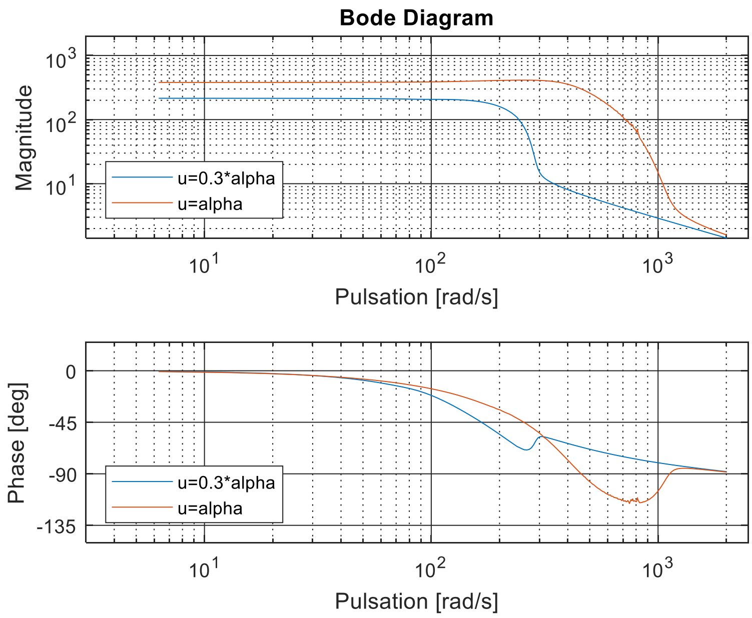

Figure 3.19 Frequency response function between the input command u and the output rod velocity $\dot{x}$ for the reduced model.

3.4.3 Linearized reduced-order model

Before comparing the full-order model and the reduced model, it could be interesting to provide a detailed analysis of the linearized reduced-order dynamics so as to discover the principal system behavior with impact of linearization.

Assuming for this time zero leakage coefficient and neglecting the nonlinear part of the system friction (this implies that the relative motion of the cylinder rod becomes solely damped by the viscous friction with a linear damping coefficient c) the reduced-order model can be directly linearized between the load flow and the rod velocity as:

$$G(s) = \frac{\dot{x}(s)}{Q_L(s)} = \frac{\bar{A}^{-1}}{\omega_c^{-2}s^2 + 2\xi\omega_c^{-1}s + 1} \tag{3.67}$$

with the cylinder eigenfrequency and the damping given by

$$\omega_c = 2\bar{A}\sqrt{\frac{E}{V_t m}} \tag{3.68}$$

$$\xi = \frac{\sigma}{4A}\sqrt{\frac{V_t}{Em}} \tag{3.69}$$

Despite the previous simplification, the linearized dynamics (3.67)-(3.69) offers a creditable estimation of the second order system behavior. It is evident that the gain between the flow and the cylinder velocity is inverse to the effective piston area, so that the cylinder with larger $\bar{A}$ can achieve higher velocities. Also, the eigenfrequency and therefore the achievable control bandwidth increases with $\bar{A}$, according to (3.68). At the same time, increasing $\bar{A}$ implies a reduction of the system damping (3.69) that involves additional issues of system stability. In addition, from (3.68) both the moving mass and the total hydraulic volume constitute the inertial terms which slow down the system eigenfrequency. The bulk modulus E appears as an equivalent stiffness of hydraulic medium so that larger E increases the system eigenfrequency, according to (3.68). It is possible to sum up that the parameters pair E/V_t, in addition to the effective piston area $\bar{A}$, is fundamental for the system eigenfrequency and damping, as related to the hydraulic circuits [58]. As mentioned before, for this reason it is important to verify the data obtained from the initial dimensioning of the hydraulic cylinder in order to guarantee the correct functionality of the hydraulic actuator.

Now, the impact of the load pressure feedback on the load flow according to (3.63) is considered. Keeping constant z value as a directional control valve operation point, the flow-pressure curve can be directly computed. For different value of z, starting from the neutral (closed) orifice state ($z = 0$) and going until its maximal value ($z = \alpha$), are represented in Figure 3.20.

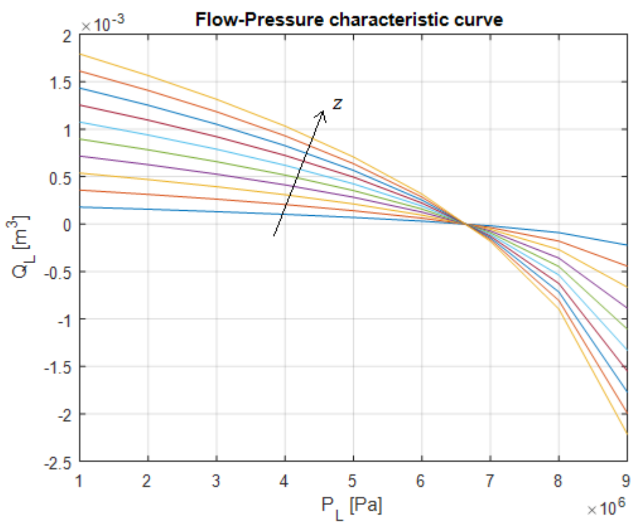

Figure 3.20 Static load flow-pressure characteristic curves.

Considering the working points $\hat{z}$ and $\hat{P}_L$ and positive directional control valve operation range it is possible to obtain:

$$\left.\frac{\partial Q_L}{\partial z}\right|_{\hat{P}_L} = K\sqrt{P_S - \hat{P}_L} =: C_q \tag{3.70}$$

$$\left.\frac{\partial Q_L}{\partial P_L}\right|_{\hat{z}} = -\frac{K\hat{z}}{2\sqrt{P_S - \hat{P}_L}} =: -C_{qp} \tag{3.71}$$

Both partial derivatives allow to introduce the so-called flow-gain coefficient C_q and the flow-pressure coefficient C_{qp}. Then, linearizing the orifice equation (3.63), it is possible to obtain:

$$\hat{Q}_L = C_q z - C_{qp} P_L \tag{3.72}$$

Analyzing equation (3.72) it is possible to notice how the pressure-dependent coefficient C_q amplifies the input orifice state z and, therefore introduces only an additional gain to the transfer function (3.67), while on the contrary, the pressure feedback coefficient C_{qp} reshapes the $G(s)$ dynamics so that the frequency response characteristic changes depending on the operation point [3].

Keeping in mind the previous considerations, it is possible to obtain the linearized transfer function between the orifice state z and the rod velocity $\dot{x}$, which can be obtained from (3.67)-(3.69) and (3.72) as:

$$\hat{G}(s) = \frac{\dot{x}(s)}{z(s)} = \frac{C_q G(s)}{1 + C_{qp}(ms + \sigma)\bar{A}^{-1}G(s)} \tag{3.73}$$

With the considerations used for the previous two model, in Figure 3.21 is shown the Bode diagram for the transfer function of the linearized model always between the input command u and the output rod velocity $\dot{x}$. It is important to notice that in this case it is necessary to linearize not only around the two input values of z (and so u) but also around a particular value of load pressure $\hat{P}_L = 0.75P_S$.

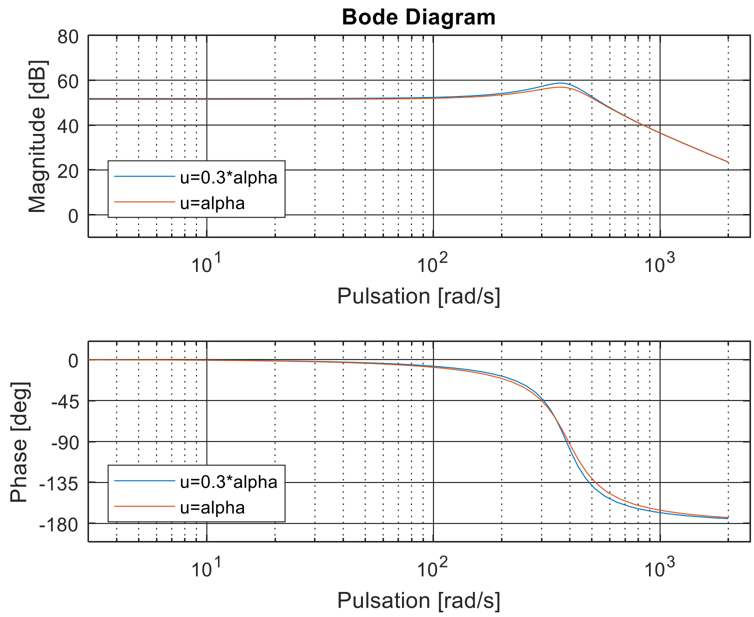

Figure 3.21 Frequency response function between the input command u and the output rod velocity $\dot{x}$ for the linearized reduced-order model.

3.4.4 Comparison among the three models

In this paragraph the dynamic properties of the three models will be discussed while making some qualitative comparison among them and demonstrating the differences in terms of measured frequency response functions. For the numerical simulations, the system parameters are listed in Table 3-1. It is worth to notice that the numerical values come from the previous hydraulic cylinder dimensioning and directional control valve data.

Param.	Value	Units	Param.	Value	Units
α	1e-3	*m*	A_A	25.16e-4	m^2
β	3e-4	*m*	A_B	25.16e-4	m^2
ω	1200	*rad/s*	V_A^0	1e-3	m^3
ξ	0.7	-	V_B^0	1e-3	m^3
C_d	0.65	-	m	12.39	*kg*
w	0.02	*m*	F_c	600	*N*
ρ	844.4	kg/m^3	F_s	900	*N*
E	1e8	*Pa*	c	2000	*kg/s*
P_S	1e7	*Pa*	χ	0.02	*m/s*
P_T	0	*Pa*	δ	0.8	-
C_L	7e-10	*1/s*	h	0.18	*m*

Table 3-2 System parameters of numerical simulation.

In Figure 3.22 is shown the comparison among the three different types of model, considering the input control command $|u| = \alpha$.

As already mentioned before in the previous three sub-paragraphs, the main differences among the three models are due to a different degree of complexity in the schematization. In fact, the full-order model schematizes the hydraulic actuator taking into account the most important nonlinearity components, in particular dead-zone nonlinearity and saturations of the spool displacement as well as the dynamics of the directional control valve. The reduced-order model is different from the full-order model mainly due to the fact that the dynamics of the spool is neglected. Finally, the linearized-reduced model linearizes the main quantities around an equilibrium position referred both to the load pressure P_L and the orifice state z (or control input command u). This model is very simplified with respect to the initial one, but it could be helpful for studying and implementing in a simple and effective way a particular control logic in order to transform the passive configuration of the hydraulic actuator in an active one.

From Figure 3.22 it is possible to notice how the dynamics of the directional control valve appears in the total system at very high frequency only (natural frequency of the directional control valve is $\omega_0 = 1200$ rad/s) and this is underlined by the fact that the full-order model (black line) and the reduced-order model (blue line) are very close until around 1000 rad/s, while for higher frequencies they become different due to the addition of two poles that come from the dynamics of the directional control valve. In fact, at high frequencies the modulus of the full-order model is influenced by the dynamics of the servo-valve and it decreases in a faster way with respect to the reduced-order model in which the dynamics of the directional control valve is neglected. Of course, this different behavior in the Bode diagram can be seen also in the phase graph: adding the pair of high-frequency poles the trend of the phase in the full-order model is lower than in the reduced-order model. It is possible to notice that there are differences also between the reduced-order model and the linearized reduced-order model but in this case too such changes can be observed only at high frequencies. Probably these differences in the Bode diagram are not due to the dynamics of the directional control valve as before because in both cases it is neglected, but they could be due to a linearization of some quantities in one model with respect to the other one.

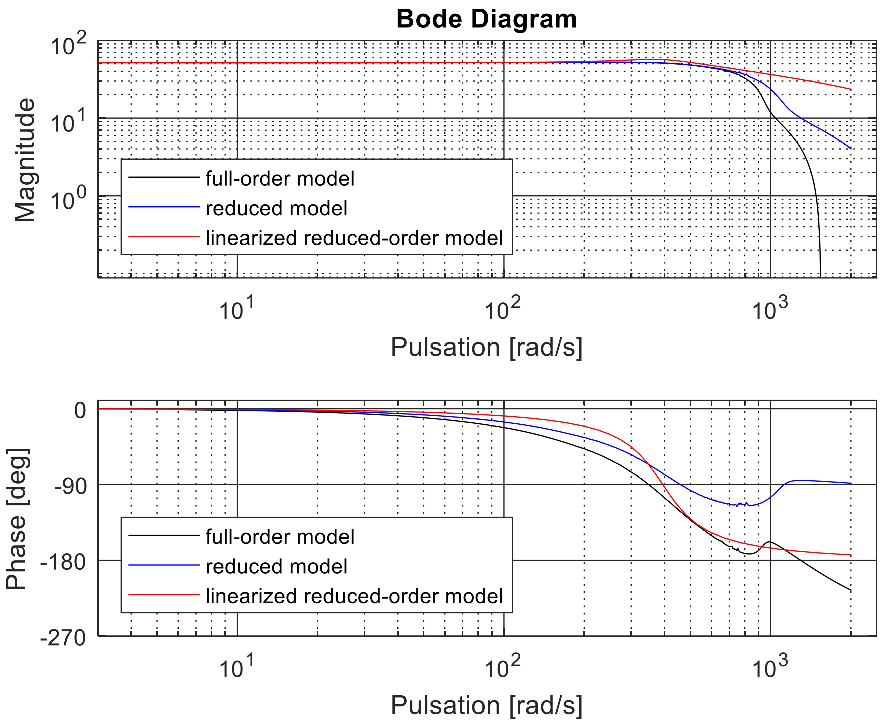

Figure 3.22 Comparison between the frequency response functions of the three different models.

In conclusion, for which concern the modulus of the transfer functions it is possible to consider the three cases very similar each other until $600\ rad/s$, while there are some remarkable differences in the phase diagram that cannot be neglected. Depending on the type of analysis it is possible to use one of the three models keeping in mind the above considerations.

Chapter 4 Vehicle dynamics model

The aim of this paragraph is to describe how the multibody model of the rail vehicle is used to investigate and assess the effect using a semi-active or full-active yaw damper, also compared with the case of the vehicle equipped with the standard passive damper. To study the problem and to perform the simulations, the model has to be robust and reliable. The complete railway vehicle is modelled through the multibody simulation software Simpack and the main features of this model are described in paragraph 4.1. In order to study the stability of the system a non-linear analysis will be done following the European Standard. Finally, the results of the passive, semi-active and full-active solutions will be compared and discuss in the last parts of the chapter.

4.1 Simpack multibody model

Modern trains are complex mechanical systems that can be better analyzed and designed using modern computational techniques. Developing detailed computer models of high-speed railway vehicles is necessary to study vehicle performance, to improve existing design, create new ones, and to develop safety guidelines for different operating and loading conditions. Computer dynamic simulations have in fact come to play a fundamental role in railway vehicle performance, in safety and accident evaluation, and in the design of new vehicles. The progresses in the fields of computational mechanics and numerical methods are directly applicable in the non-linear dynamics analysis of the railway vehicle systems.

Multibody system dynamics is a branch of the general field of computational mechanics that is concerned with developing and solving the linear and nonlinear equations that govern the motion of complex physical systems. The components of a multibody system can be subjected to large rotations and displacements. The motion of these components, however, is limited by kinematic constraints that are the result of mechanical joints and specified motion trajectories. Multibody system techniques are general and have been used in the analysis, design, and performance evaluation of numerous applications including vehicles, machines, space structures, biomechanical and biological systems, robotics and mechanisms, as well as many other applications. The equations of motion are developed in their most general form using the principle of mechanics. These equations are implemented on digital computers in order to develop programs that can automatically and systematically construct and numerically solve the equations of motion of a system that consists of an arbitrary number of bodies and joints [61].

There are several advantages for adopting multibody system methodologies in the computer analysis of railway vehicle systems. Among these advantages are their generality, their ability to systematically solve non-linear problems, and the direct implementation of special railway vehicle elements.

In this thesis, the railway vehicle model is defined using software Simpack and it is shown in Figure 4.1. It is a full vehicle model of the leading coach of a high-speed train set. The model has 72 degrees of freedom. The main rigid bodies are the car-body, two bogies and four wheelsets, two for each bogie.

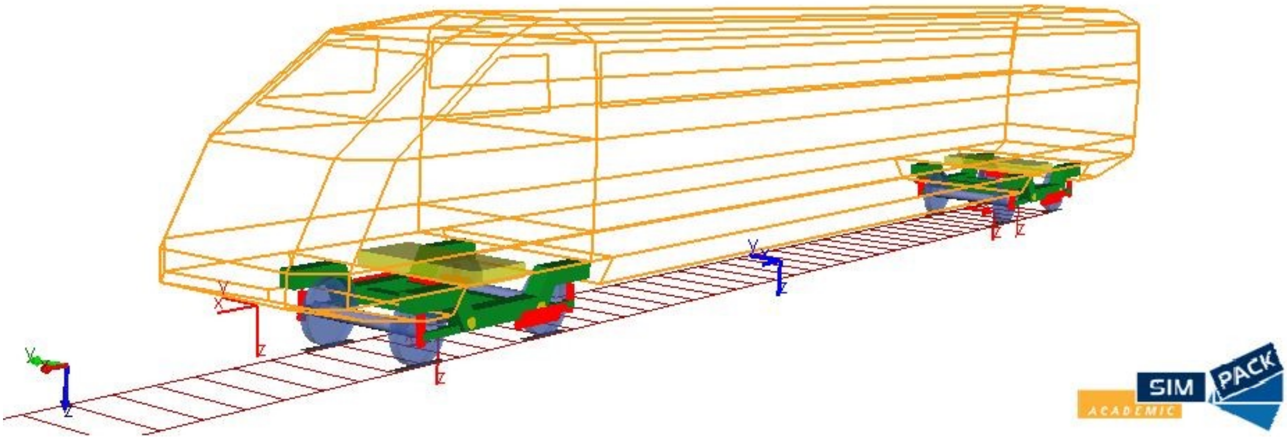

Figure 4.1 Multibody railway vehicle model in Simpack environment.

The main parameters of the model are shown in Table 4-1:

Name	Value	Unit of measurement
Load for each wheelset	27.52	*kN*
Wheelbase length	2.5	*m*
Distance between bogie frames	17.5	*m*

Table 4-1 Main parameters of the model.

The irregularity introduced in the multibody model is measured, while the wheel-rail contact is modelled through the Fastsim algorithm [16] derived from the Kalker linear theory [62].

Figure 4.2 shows the wheel-rail pairs, highlighting the contact points between the wheel and the rail. The wheel profile considered is the worn S1002, with a service life of 200000 km.

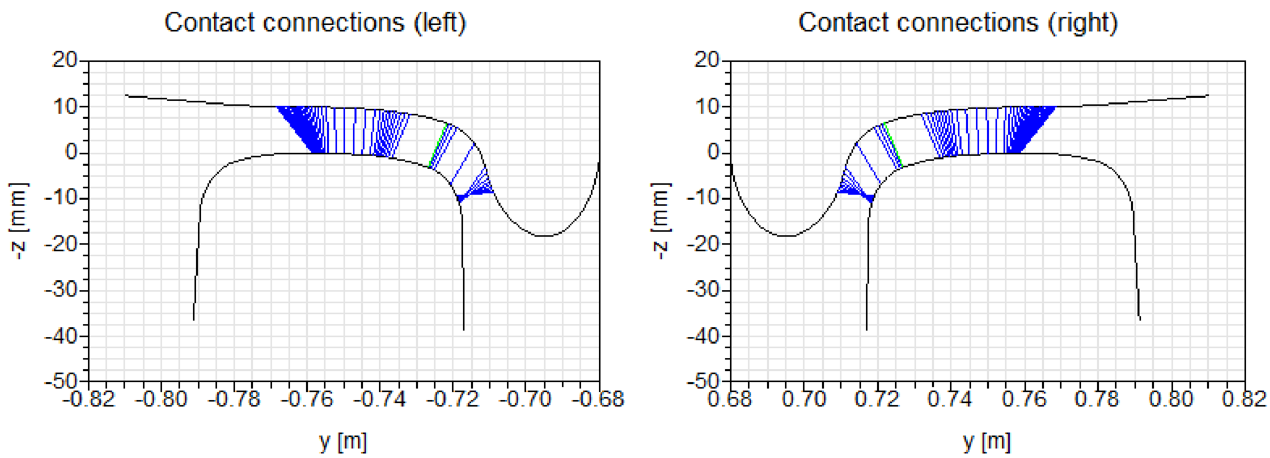

Figure 4.2 Wheel-rail pairs used in the Simpack multibody model.

4.2 Methods for stability assessment

In order to study the stability of the train vehicle both the linearized system and the non-linear one are considered. The main reasons for considering the linearized vehicle model are the utility of making a comparison with a two degrees of freedom model that will be introduced in the next chapter for the HIL tests and to see the importance of the non-linearities with respect to the linear model.

Regarding the stability of the system in terms of linear analysis, the eigenvalues/eigenvector method can be used. Considering a velocity versus damping plot, it is possible to identify the linear critical speed of the vehicle, that is the velocity for which the vehicle is assumed to become unstable and it is indicated by negative damping values.

More complex is the case of non-linear stability of the model. In fact, in this case it is not possible to perform an eigenvalues/eigenvectors analysis since the system is not linear anymore. For this case it is necessary to study the stability in time domain. It is possible to consider a time domain simulation starting from non-zero initial conditions and see how the motion of the vehicle (for example the bogie or wheelset lateral displacement) evolves with time. In particular, if the result is a convergent solution the system can be assumed as a stable system, while, if the solution is not convergent and a limit cycle appears the system can be assumed unstable at that considered velocity.

Moreover, in order to have a more accurate method for studying the stability of the system, the European Standard (EN 14363) can be used. The physical quantity to be considered according to the European standard is the lateral acceleration of the wheelset. In particular, the root mean square (*RMS*) of the lateral acceleration of each wheelset filtered with a band-pass filter that has a bandwidth of $\pm$ 2 Hz from the main peak of the lateral acceleration frequency response function has to be considered. The RMS is calculated over a spatial interval of 100 m, with a travelling window of 10 m. The RMS value is calculated for different running velocities in a track with random irregularities and it is compared with the acceleration threshold value (defined by the Standard) above which the hunting instability occurs. Using the EN 14363, the acceleration threshold value is defined as:

$$a_{lim} = \frac{12 - \frac{m_{bogie}}{5}}{2}$$

in which m_{bogie} is the mass of the bogie expressed in tons and a_{lim} for the considered railway vehicle is equal to 5.39 m/s^2.

4.3 Stability analysis for reference passive yaw damper

In this paragraph the stability analysis for reference vehicle with passive yaw damper will be discussed. In particular, both linear and non-linear analysis will be performed and compared each other.

Reference passive yaw damper means a damper with constant characteristic that cannot be controlled. The reference passive yaw damper is modelled based on the semi-active yaw damper model, considering a constant value for the opening valve that corresponds to an opening of 30%. In this way the reference passive yaw damper model is obtained and in the following two paragraphs will be compared with the semi-active and full-active solutions.

4.3.1 Linear analysis

A first effective analysis of the Simpack multibody model is done considering the linearized model. Linear model means that all the flexible elements (such as springs of suspensions and viscous damper elements) have a linear behavior and also the wheel-rail contact forces are calculated by the linear Kalker theory. In this way and with these assumptions the linear critical speed of the vehicle model can be calculated using an eigenvalues/eigenvectors analysis. The root locus plot for the Simpack model is shown in Figure 4.3.

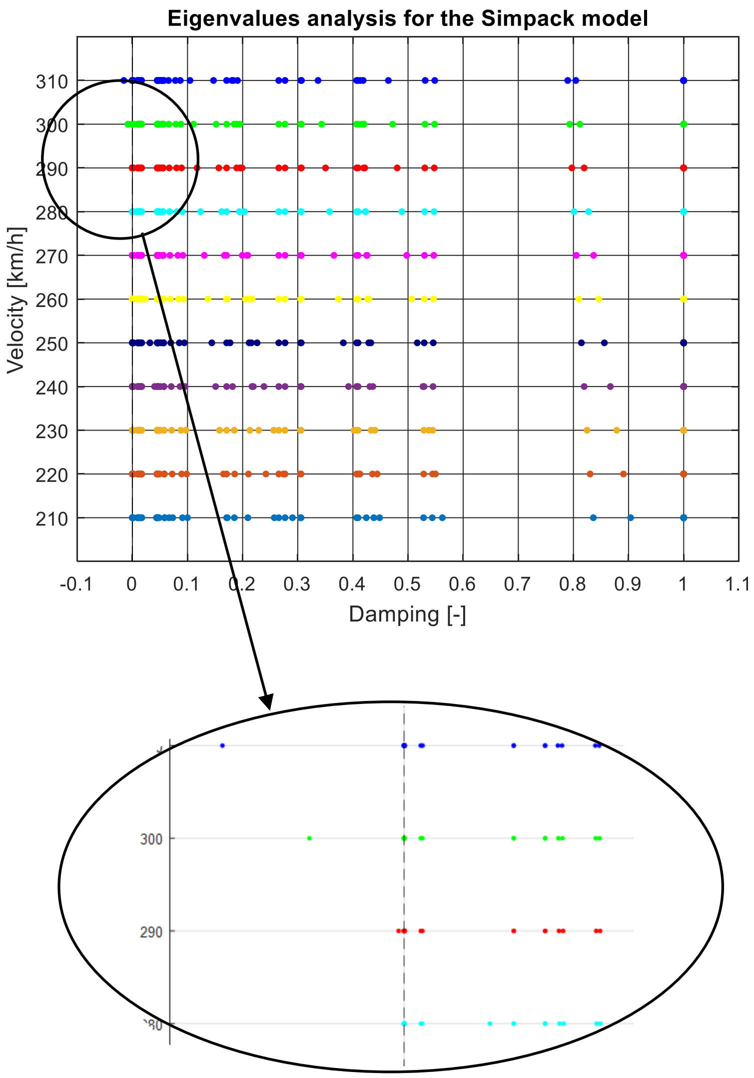

Figure 4.3 Eigenvalues analysis for the Simpack model.

The velocity versus damping plot allows to identify the linear critical speed of the vehicle, that is the velocity for which the vehicle is assumed to become unstable, and it is indicated by negative damping values. From the zoom of the eigenvalues analysis it is possible to notice that the negative damping values appears in correspondence of 280-290 km/h and so it is possible to conclude that the linear critical speed for the Simpack model with a reference passive yaw damper is in the range of 280-290 km/h.

4.3.2 Non-linear analysis

As mentioned in paragraph 4.2, for the non-linear stability analysis the eigenvalues/eigenvectors method is not suitable. For this reason, the stability analysis will be done referring to a time domain analysis.

First of all, after having imposed fixed initial conditions (lateral displacement of the bogie and yaw rotation of the bogie), the train is launched in a straight track section at constant speed. The results of the simulations in time domain considering the variation of the lateral displacement of the wheelset are presented in Figure 4.4, Figure 4.5 and Figure 4.6, that correspond to three different speeds. The first speed of the simulation is under the linear critical speed (240 km/h), the second one is close to the predicted linear critical speed (280 km/h) and finally, the third one is above the linear critical speed (300 km/h). From these three graphs it can be observed that in case of speed lower than the linear critical speed (240 km/h) the vehicle is in fully-stable condition, while in case of speed greater than the linear critical speed (300 km/h) the system is unstable as can be observed from the formation of a limit cycle of oscillation with amplitude of wheelset displacement of 6-7 mm corresponding to flange contact. In case of intermediate speed, a small limit cycle can be observed, but it does not lead to a continuous flange contact.

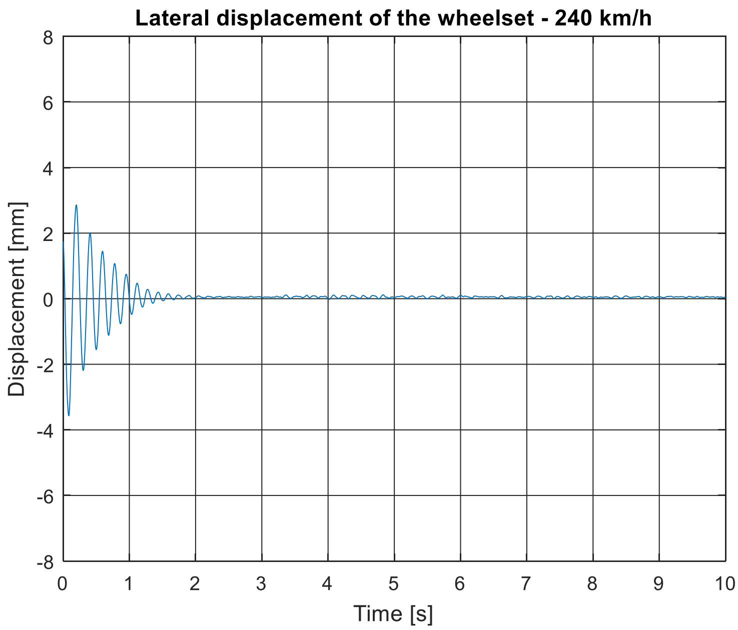

Figure 4.4 Time-history of the wheelset lateral displacement for non-zero initial condition, at 240 km/h (below the linear critical velocity).

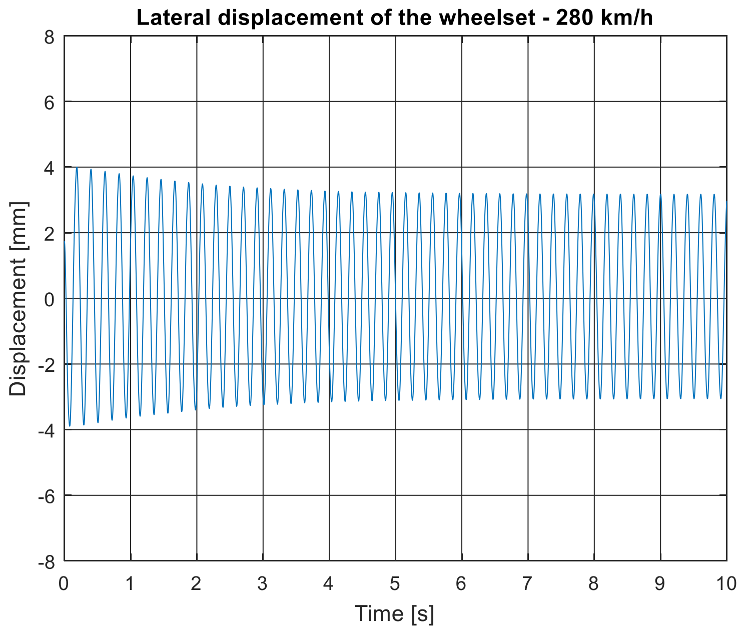

Figure 4.5 Time-history of the wheelset lateral displacement for non-zero initial condition, at 280 km/h (more or less the linear critical velocity).

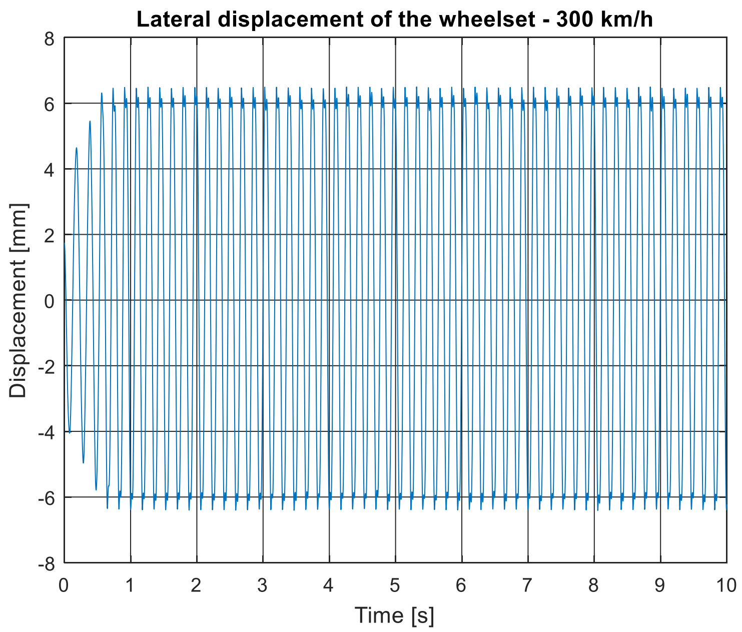

Figure 4.6 Time-history of the wheelset lateral displacement for non-zero initial condition, at 300 km/h (greater than the linear critical velocity).

The other method used for studying the stability of the system is based on the European Standard EN 14363. As mentioned in paragraph 4.2, the physical quantity to be considered according to the European Standard is the lateral acceleration of the bogie frame over one axle box. In Figure 4.7 the RMS values of the lateral acceleration of one wheelset calculated for different running velocities in a track with random irregularities are presented.

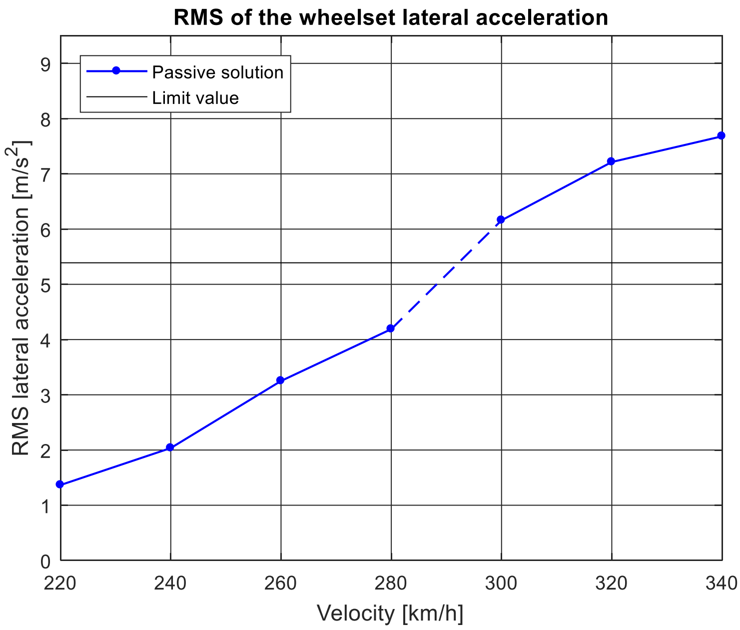

Figure 4.7 RMS of the wheelset lateral acceleration for different running velocities.

It is possible to notice that the RMS value of the lateral acceleration increases with increasing the speed until the acceleration threshold value set by the Standard is exceeded. This fact is highlighted in the graph in Figure 4.7 with a dashed line at the points where the instability conditions start to appear. Before the dashed line, visualizing the time history of one wheelset, no limit cycle can be notice (Figure 4.8). Vice versa, after the dashed lines, considering the time history of one wheelset, a limit cycle appears, and it is possible to see it despite the presence of the track irregularities as shown in Figure 4.9.

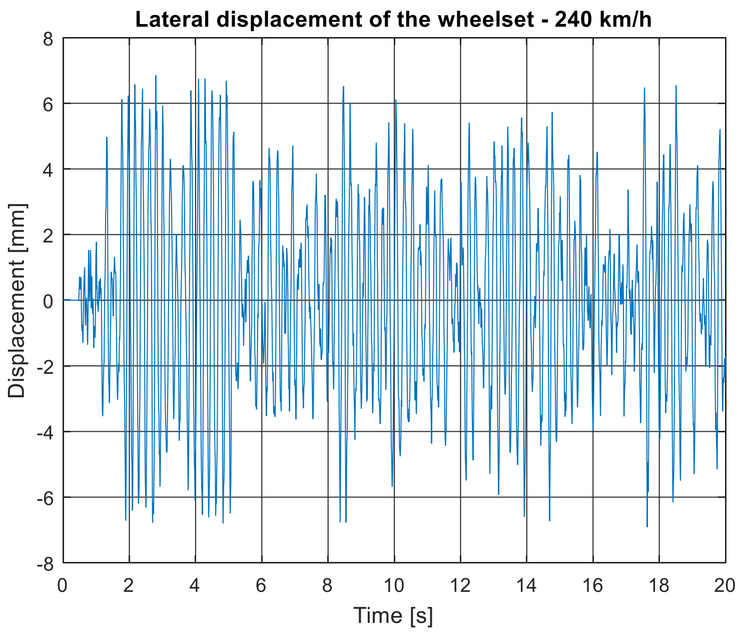

Figure 4.8 Time-history of the wheelset lateral displacement for a simulation with random track irregularity, at 240 km/h (lower than the linear critical velocity).

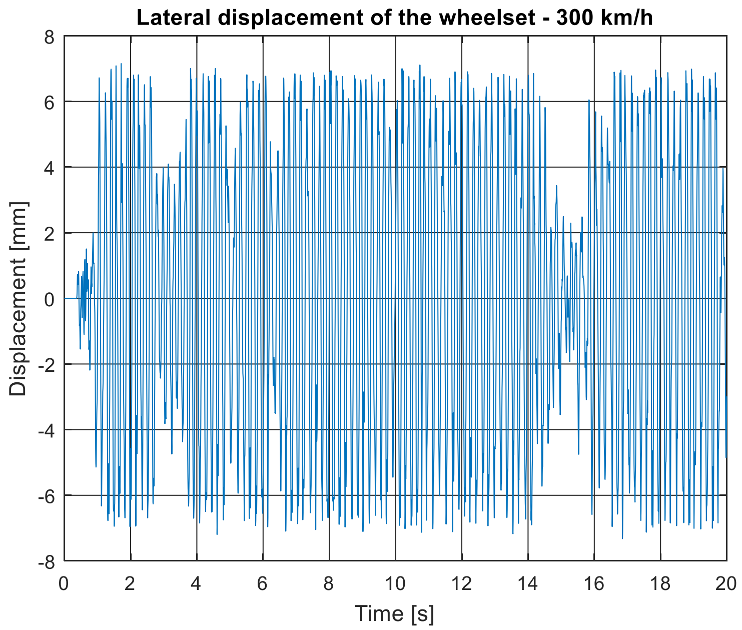

Figure 4.9 Time-history of the wheelset lateral displacement for a simulation with random track irregularity, at 300 km/h (greater than the linear critical velocity).

Moreover, in Figure 4.10 is reported the time-history of the lateral acceleration of one wheelset during the simulation in case of stable and unstable condition respectively. As it is possible to notice, the lateral acceleration in case of stable condition does not show particular variations and this is sign of stability of the vehicle.

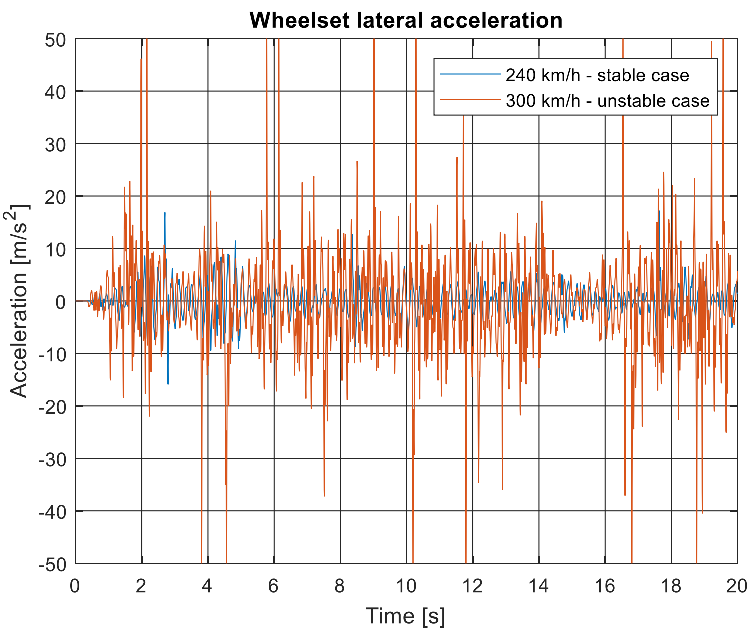

Figure 4.10 Time-history of the wheelset lateral acceleration in case of stable and unstable condition

Finally, it is also possible to notice how the non-linear critical velocity is not too much different from the linear one, in fact in both cases is around 280-300 km/h.

4.4 Stability analysis for vehicle with semi-active dampers

In order to model the vehicle with semi-active dampers the Simpack model of the passive vehicle described in section 4.1 is interfaced to the hydraulic model of the semi-active damper described in section 3.3. This latter part of the model is defined in Simulink. In order to connect the mechanical and hydraulic parts of the model, a co-simulation procedure between the Simpack model and the Simulink models is established. Thanks to this approach, the two models are able to exchange information online during the simulation (see scheme in Figure 4.11). The output of the Simpack model becomes the input for the Simulink block scheme and vice-versa. The Simpack outputs are the piston velocity of the yaw dampers and the lateral acceleration of the wheelsets. As input the multibody model receives the force exerted by the yaw dampers computed for each time step in the Simulink environment.

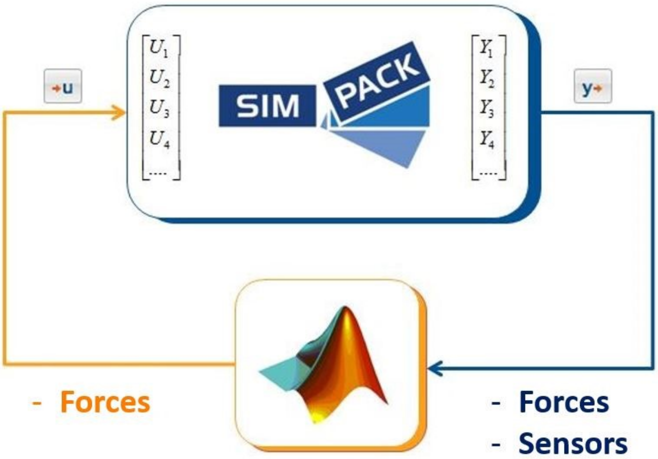

Figure 4.11 Simulink-Simpack co-simulation scheme.

The co-simulation results obtained with the semi-active yaw damper concepts are here presented. The control strategies introduced in paragraph 3.2.1 are applied to the semi-active devices and the results are compared with the case of reference passive yaw dampers in order to assess the effective benefits for the stability of the vehicle.

4.4.1 Stability analysis for the MPPT control stategy

The MPPT controller is implemented by a Simulink block and is linked to other parts of the system as represented in Figure 4.12.

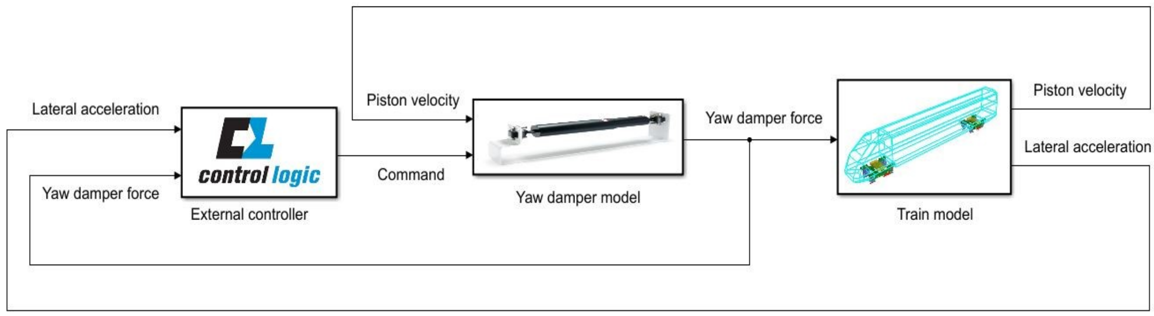

Figure 4.12 MPPT control scheme.

In the scheme above, the third block represents the mechanical model of the train vehicle that, through the co-simulation, communicates with the Simpack multi-body model. As shown in the scheme the inputs of this block are the forces exerted by the yaw dampers (one for each side of the bogie) and the outputs are the lateral accelerations of the bogies and the elongation velocity of the yaw dampers.

The second block contains the hydraulic cylinder model introduced in paragraph 3.3. The block inputs are the command for the proportional valve generated by the external controller, and the elongation velocity of the yaw damper, while the output is the force exerted by the hydraulic cylinder.

Finally, the first block represents the external controller that, according to the MPPT algorithm, takes as input the damper force and the lateral bogie acceleration and calculates as output the command that is fed to the control valve.

Figure 4.13 compares the results of the non-linear stability analysis for the vehicle with semi-active damper and MPPT control and the reference vehicle with passive damper. Both the MPPT control logics are considered. The one with the aim of minimizing only the lateral acceleration for the sake of simplicity is called $MPPT_1$, while the one with the aim of minimizing both lateral acceleration and yaw damper force is called $MPPT_2$. The weights for the two MPPT control strategies are shown in Table 4-2.

Control strategy	Weight of the aceleration	Weight of the force
$MPPT_1$	1	0
$MPPT_2$	1	4

Table 4-2 Weights of the MPPT control strategies.

As can be seen from the graph, the *RMS* values obtained for both MPPT solutions lead to the same results, especially at relatively high speed. As it is possible to notice, with the MPPT control logic, the stability threshold is exceeded at higher speed, with an increase of the critical speed of 70 km/h approximately. This means that with the semi-active solution the train vehicle can run at higher speed maintaining its stable behavior with respect to the passive solution.

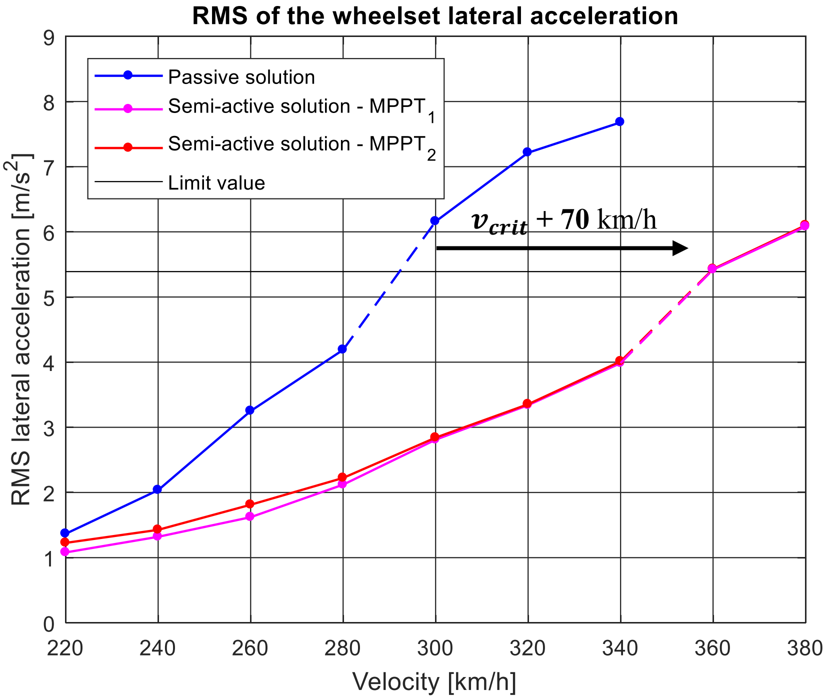

Figure 4.13 Comparison between the RMS of the wheelset lateral acceleration for the passive and MPPT semi-active solution ($k_{\ddot{x}} = 1, k_F = 4$) for different running velocities.

Another comparison between the passive and the semi-active case with the MPPT can be done comparing the time-history of the wheelset displacement. In Figure 4.14 and Figure 4.15 are shown the time-history for the case of velocity lower than the critical velocity and for velocity higher than the critical velocity obtained with the reference passive solution, respectively.

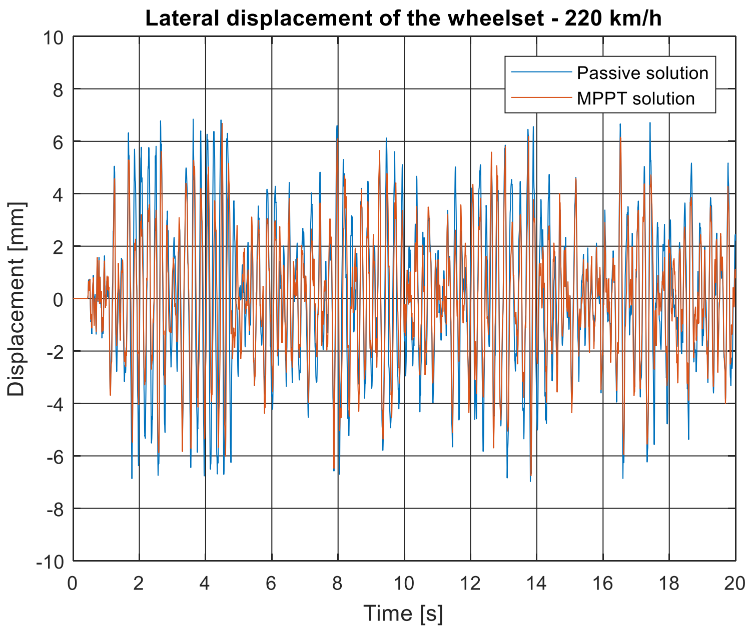

Figure 4.14 Comparison between the wheelset lateral displacement obtained with reference passive yaw damper and with MPPT control strategy at 220 km/h.

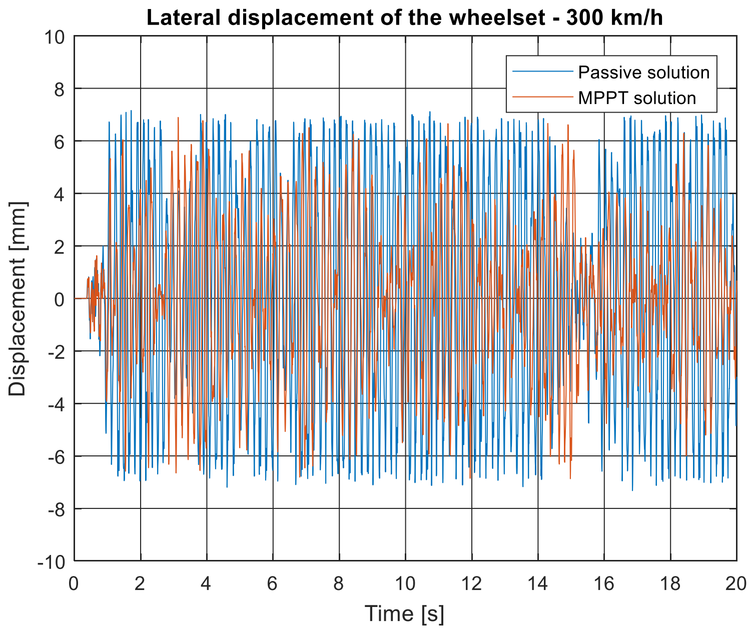

Figure 4.15 Comparison between the wheelset lateral displacement obtained with reference passive yaw damper and with MPPT control strategy at 300 km/h.

As it is possible to see, in the first case the lateral displacement of the wheelset for both solutions are quite similar since both models are in a stable condition. Vice versa, in the second case, it is possible to notice that the lateral displacement of the wheelset with the MPPT control logic is lower than the lateral displacement of the wheelset with the reference passive damper and this is sign of the stability of the vehicle for the velocity taken into account.

The MPPT algorithm computes the voltage command that control the opening of the external valve, optimizing the module and the phase of the damping force. The voltage command is in the range of 0-10 V, with 0 V that means valve completely closed and 10 V that corresponds to the valve completely open. This voltage command can be also expressed as a percentage of the opening external valve. In this case, 0% of opening command means 0 V applied to the opening valve and so the valve is fully closed; vice versa, 100% of opening command means 10 V applied to the opening valve and so the valve is fully open.

In Figure 4.16 is shown the time-history of the input voltage command considering the MPPT control strategy both in case of weight of the force gain equal to zero and in case of weight of the force gain equal to 4 and starting from the minim value of the command. For this simulation a low value of the velocity is considered so that the different effect of the two control logics can be appreciate in a better way. In particular, it is possible to notice that in case of zero weight of the force gain, since the aim of the controller is only to minimize the lateral acceleration of the bogie, the voltage command tends to remain to very low values (tending to zero). As a matter of fact, there is no reason for the voltage command to increase and consequently to decrease the yaw damper force, otherwise the lateral acceleration would increase, and this is in contrast with this specific target of the controller. Vice versa, considering the weight of the force gain equal to 4, it is possible to notice that the voltage command tends to increase somehow during the simulation. This behavior is due to the fact that the train is stable at this particular speed and since this control logic tries not only to minimize the lateral acceleration of the bogie but also to minimize the yaw damper force, it tries to open the valve considering a trade-off between minimizing the lateral acceleration of the bogie and minimizing the yaw damper force.

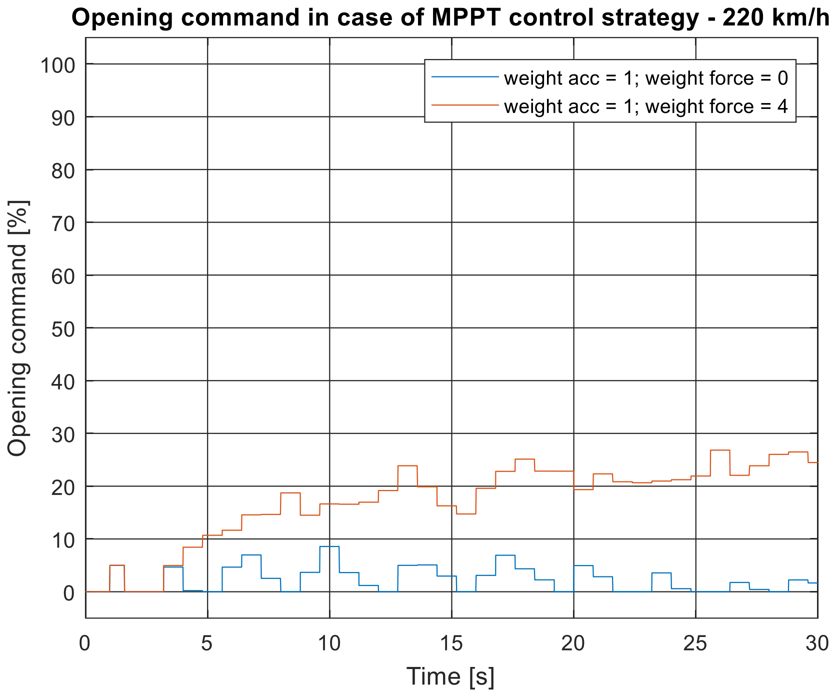

Figure 4.16 Command for MPPT control strategy starting from zero value of the opening valve.

Figure 4.17 shows the time-history of the opening command, starting from fully open valve and for the vehicle travelling at 300 km/h.

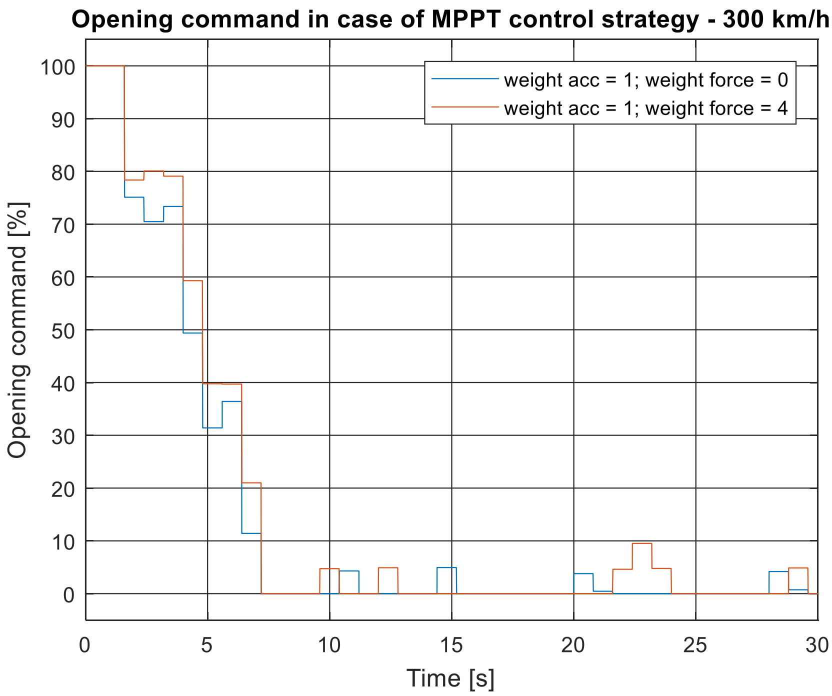

Figure 4.17 Command for MPPT control strategy starting from maximum value of the opening valve.

In this case, in the first part of the simulation the vehicle is unstable and for this reason the controller reduces the input voltage command in order to close the valve, increasing the yaw damper force and consequently reducing the lateral acceleration of the bogie and stabilize the vehicle. Once the vehicle is stable and the external valve is close, the voltage command remains more or less constant at zero value for both the MPPT control strategies. The different behavior with respect to the one shown in Figure 4.16 can be explained by the fact that in this case the velocity is higher and to reach the stability it is necessary to have a higher value of the damping force, that means very low input voltage command. However, even if the second part of the time-history is quite similar for the two different MPPT control logics, in the first part it is possible to notice that in case of zero value of the force gain the opening command decrease a bit more rapidly with respect to the case with a force gain equal to 4.

Finally, a complete time-history of the main quantities is shown in Figure 4.18. For the sake of brevity only the case with weights $k_{\ddot{x}} = 1, k_F = 4$ is reported. Lateral acceleration, wheelset displacement, yaw damper force and opening valve command are simultaneously reported.

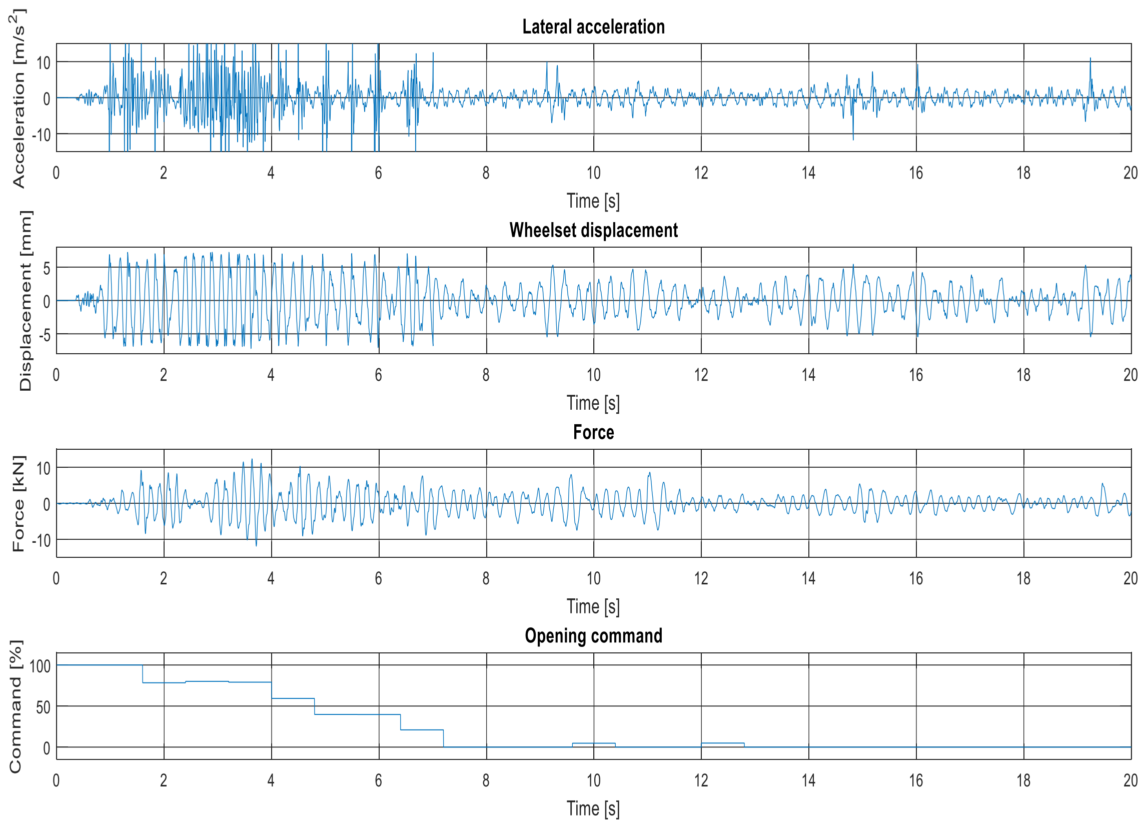

Figure 4.18 Time-history of a multibody simulation with MPPT control strategy at 300 km/h, with the aim of minimizing both the lateral acceleration and the yaw damper force, starting from the maximum value of the input voltage command.

Also in this case, an intermediate speed value is used in the simulation in order to better appreciate the effect of the MPPT control logic. As it is possible to notice, this figure summarizes all the comments made previously on the functioning of the MPPT control strategy. In the first part of the simulation, a large amplitude of the bogie hunting motion is observed in the two upper diagrams. This trigger the change of the opening command that happens approximately from 2 to 7 seconds.

Once the valve is sufficiently closed, the hunting motion is suppressed, the vehicle runs in a stable way and the opening command remains nearly constant.

4.4.2 Stability analysis for the sky-hook control strategy

The same analysis performed for the MPPT solution can be done also in case of sky-hook solution. In particular, considering the case of on/off sky-hook, the input voltage command can assume only two values that represent the fully open and fully closed configurations of the external opening valve and correspond to maximum and minimum value of the yaw damper force respectively. In this case, there is no big difference to start the simulation with the maximum or minimum value of the opening valve command, but it is still possible to appreciate the different behavior of the control logic considering two different velocities for the train vehicle.

In Figure 4.19 is shown a zoom of a time-history of the opening command taken from a numerical simulation made at 220 km/h. On the contrary, in Figure 4.20 the numerical simulation was performed at 300 km/h. As can be noticed, in case of relatively low speed of the vehicle the opening valve command is subjected to less variation between maximum and minimum value with respect to the case at relatively high speed.

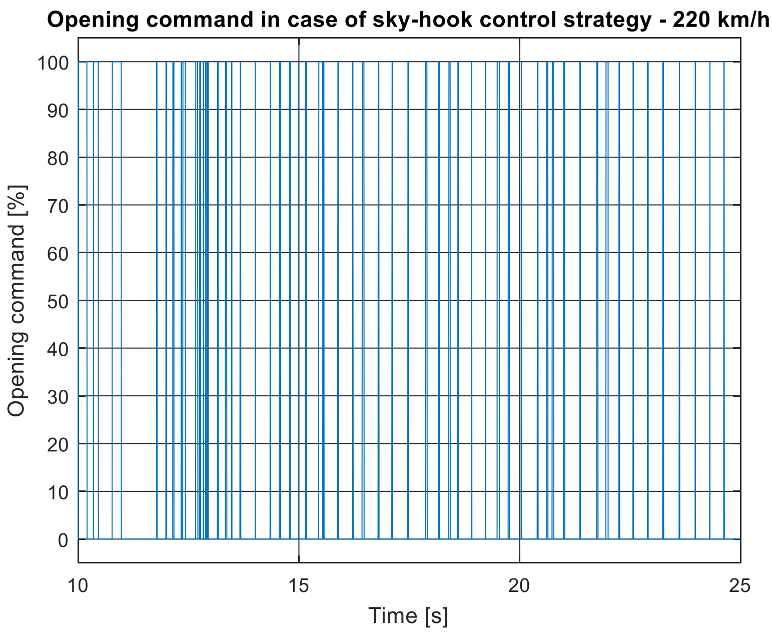

Figure 4.19 Command for sky-hook control strategy at 220 km/h.

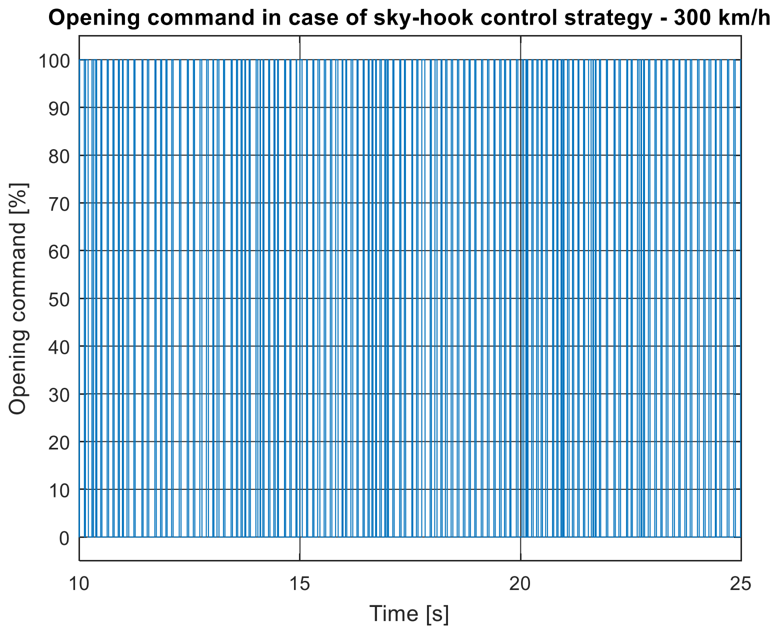

Figure 4.20 Command for sky-hook control strategy at 300 km/h.

As made for the MPPT control strategy, also in this case, a complete time-history of the main quantities that have to be considered during the simulation is shown in Figure 4.21.

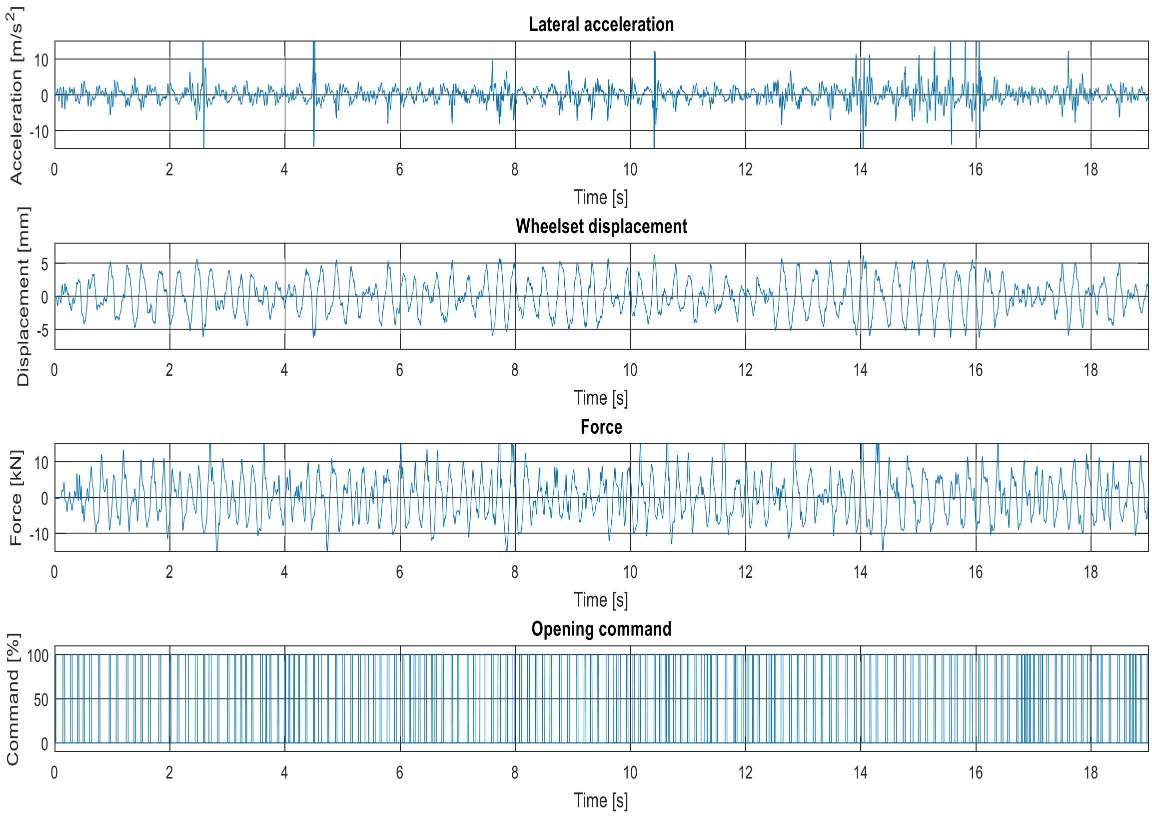

Figure 4.21 Time-history of a multibody simulation with sky-hook control strategy at 300 km/h.

During the entire simulation, the vehicle shows a stable behavior, with relatively low values of acceleration and wheelset displacement and with no sign of a limit cycle oscillation. The opening command is frequently switching between fully open and fully closed, as is inherent in the on/off sky-hook control strategy.

In Figure 4.22 is instead presented a zoom of the time-history of the opening command for the continuous sky-hook solution. As mentioned in paragraph 3.2.1.2 with the continuous solution the opening valve command can assume also intermediate values and not only the maximum and the minimum one. One of the remarkable advantages of this solution is that there are no step variations of the valve opening command (on/off sky-hook), which has instead a more smooth transition and this could be a key point especially when the real semi-active yaw damper will be considered. In fact, with the physical object, the dynamics of the opening and closing the valve might be non-negligible, depending on the hardware used.

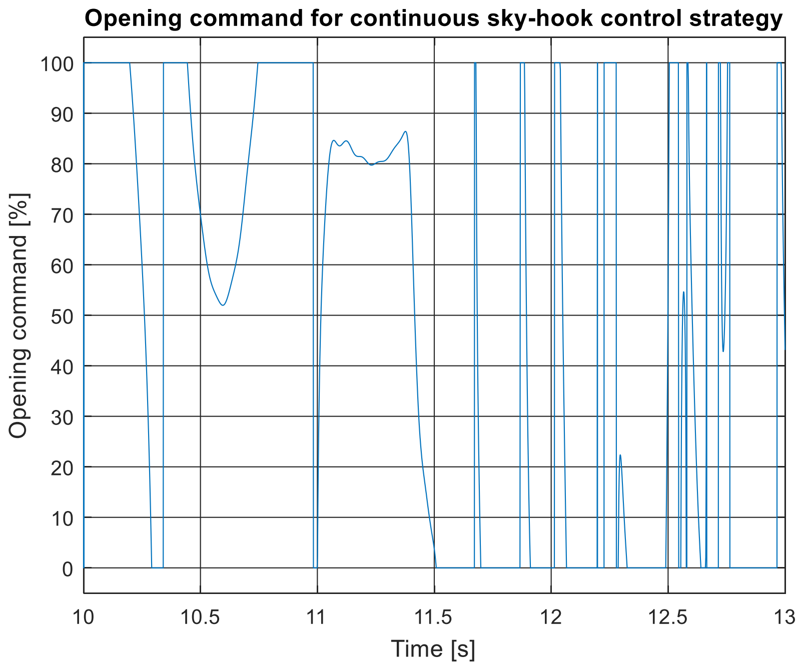

Figure 4.22 Opening valve command in case of continuous sky-hook control strategy.

Finally, in Figure 4.23 is presented the same graph shown in Figure 4.13 but with also the line that represents the sky-hook control strategy solution. To simplify the diagram, only one version of the MPPT controller ($k_{\ddot{x}} = 1, k_F = 4$) and one version of the sky-hook controller (on/off) are shown. As can be seen, there is no big difference between the two semi-active control strategies, at least regarding the RMS value of the lateral acceleration. So, it is possible to conclude that from the point of view of non-linear stability analysis, the two semi-active control strategies are quite similar to each other. The big difference between the two types of semi-active control strategies is the opening valve command. In case of MPPT solution, the opening valve values is calculated every second and it can only vary by a limited amount and not changing instantaneously from maximum to minimum value (or vice versa) as it happens in the sky-hook solution. This frequent opening and closing of the external valve have no consequences for the theoretical simulations. In fact, the yaw damper model assumes an ideal behavior for the proportional valve, so the opening and closing of the by-pass valve takes place instantaneously considering neither delay nor the dynamics of the valve itself.

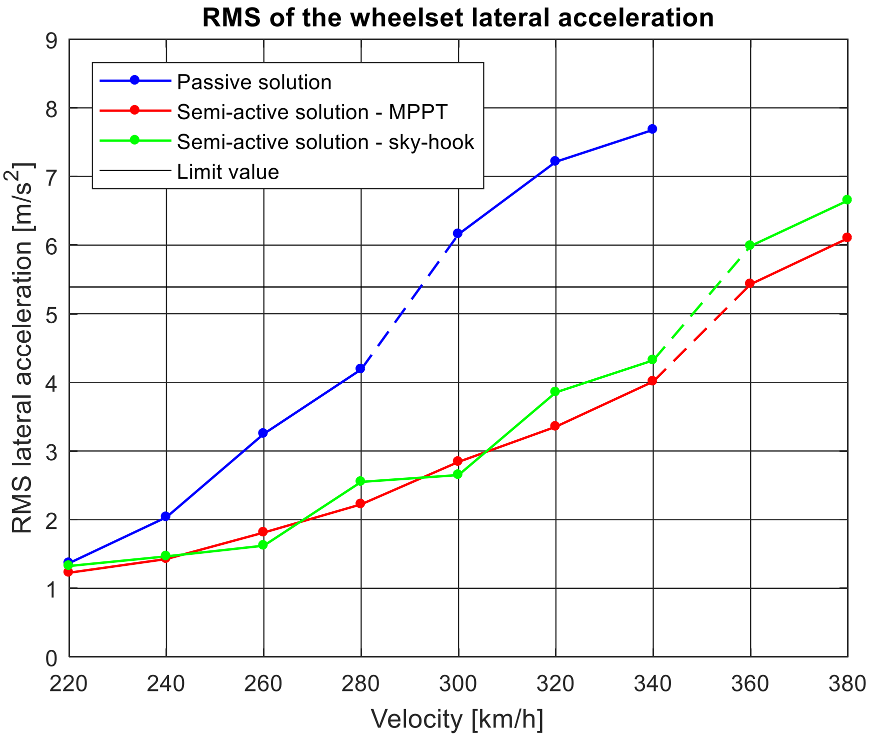

Figure 4.23 Comparison between the RMS of the wheelset lateral acceleration for the passive, MPPT and sky-hook semi-active solutions for different running velocities.

4.5 Stability analysis for the vehicle with full-active dampers

In this paragraph, the co-simulation results obtained with the full-active yaw damper concept are presented. The hydraulic actuator model introduced in paragraph 3.4 is connected to the mechanical multibody system of the rail vehicle presented in paragraph 4.1 through the co-simulation tool in the same way as previously described in this chapter. The gain c_v of the full-active control law (see section 3.2.2) was chosen by means of a sensitivity analysis. Of course, the performance of the full-active solution is strongly depending on this parameter. The simulation results are compared with the passive and semi-active solutions, with the aim of assessing the improvements in the vehicle stability performances.

First of all, the comparison in terms of RMS of wheelset lateral acceleration between the reference passive, semi-active and full-active solutions is presented in Figure 4.24. As it is possible to notice the limit value of the lateral acceleration is not exceeded in the entire range of speed considered for the vehicle equipped with full-active yaw damper. This means that the active concept has the best performances compared to the semi-active control logic, since there is no unstable condition at least up to 380 km/h.

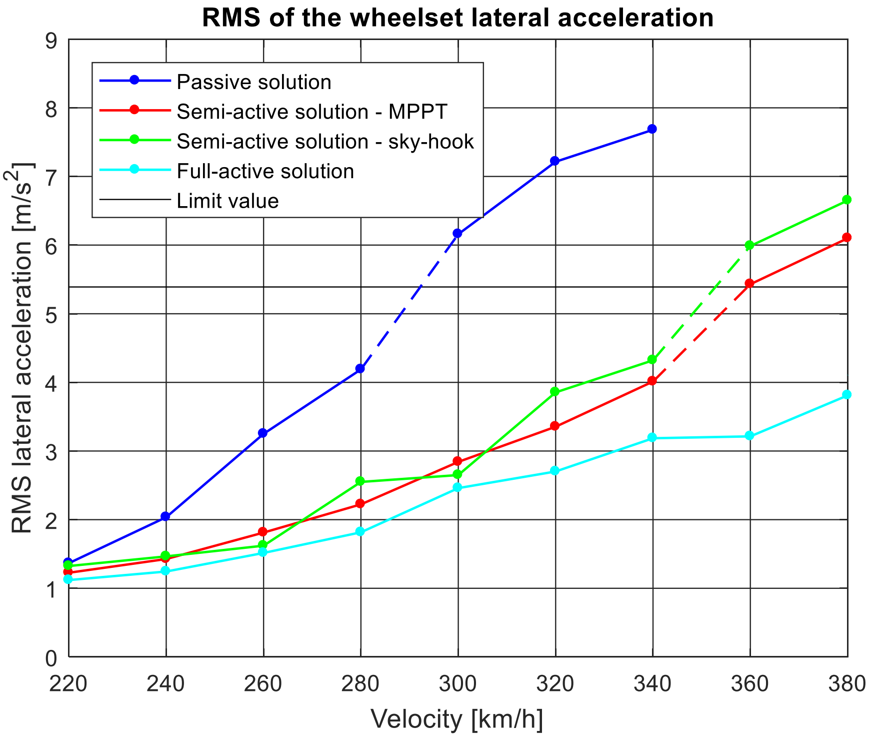

Figure 4.24 Comparison between the RMS of the wheelset lateral acceleration for the passive, semi-active (MPPT and sky-hook) and active solutions for different running velocities.

In Figure 4.25 the time-history of the lateral displacement of the wheelset is presented both for the passive and full-active solutions. As can be noticed, in the passive case a limit cycle appears while it is not evident for the case of full-active control strategy.

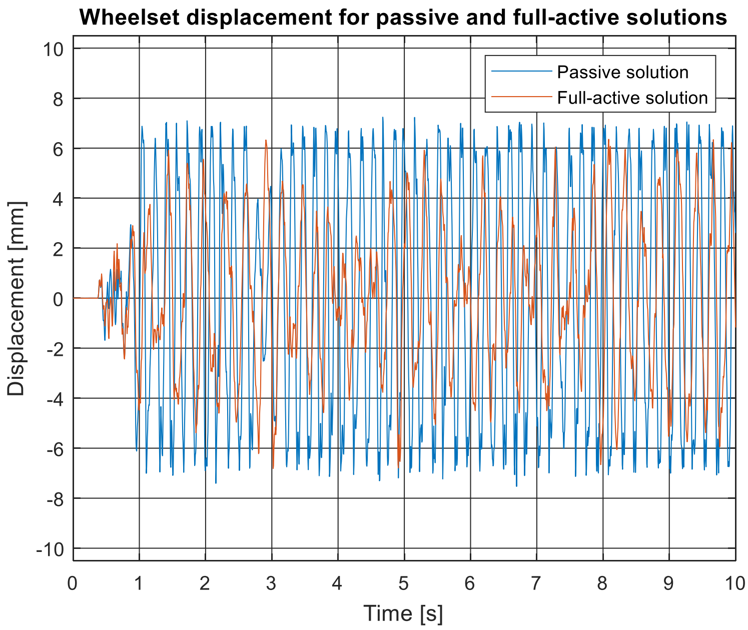

Figure 4.25 Comparison of wheelset lateral displacement between passive and full-active solution at 300 km/h (unstable condition in the passive case, stable condition in full-active case).

The stability improvement with the full-active solution can be also noted from the time-history of the wheelset lateral acceleration as presented in Figure 4.26. The magnitude of the wheelset lateral acceleration does not show particular variation during the entire time-history and this can be seen as another sign of the stability of the vehicle for the considered velocity.

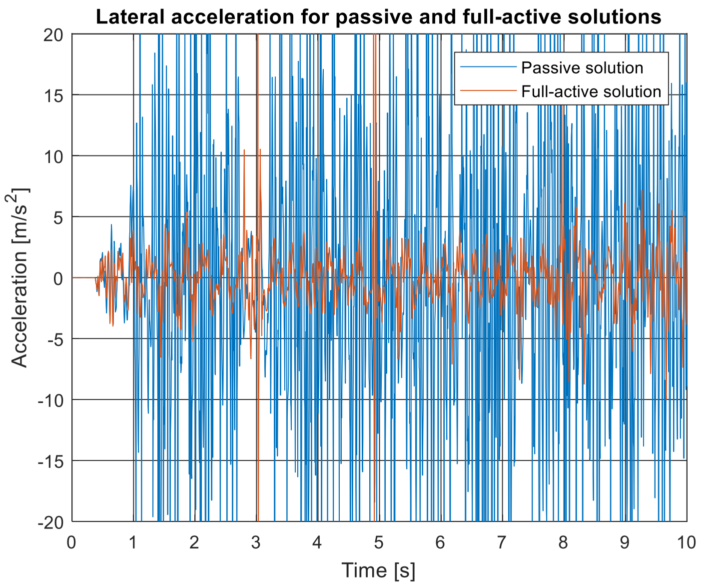

Figure 4.26 Comparison of lateral acceleration between passive and full-active solution at 300 km/h.

Finally, in Figure 4.27 is shown how the full-active control logic works. As mentioned in the description of the ideal damping force control logic in paragraph 3.2.2 the aim is to replicate the effect of an ideal viscous damper through a proportional control based on the difference between the ideal reference damping force and the effective force produced by the full-active damper model. It is observed that the actual force generated by the full-active damper follows closely the reference force which is the force that would be generated by a linear viscous damper with damping coefficient c_v equal to 330 kNs/m.

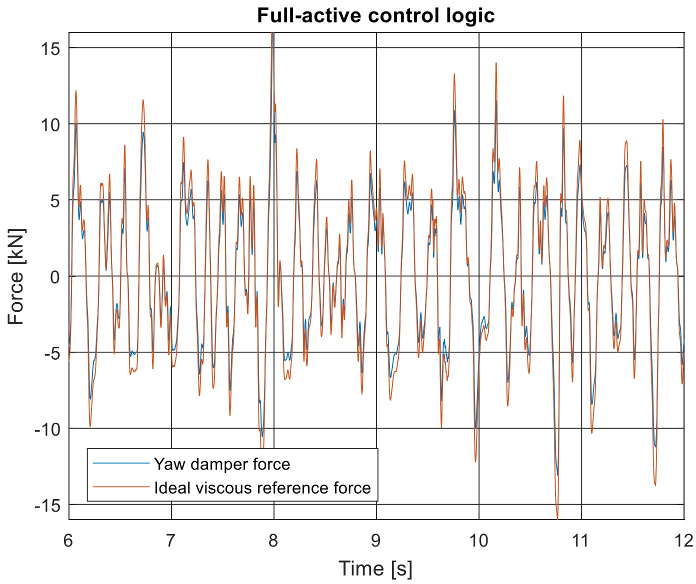

Figure 4.27 Example of how the full-active control logic works compared with ideal viscous reference force.

As mentioned in the first part of this section, the gain c_v of the full-active control law was chosen by means of a sensitivity analysis. The choice represents a good trade-off between performances in terms of lateral acceleration and limited maximum force. For sake of brevity, in Table 4-3 are reported the main parameters that have to be considered for the choice of the gain c_v.

$c_v\ [kNs/m]$	$RMS_{acc}\ [m/s^2]$	$F_{max}\ [kN]$	$RMS_P\ [kW]$
210	7.08	20.369	0.357
270	5.98	23.491	0.280
330	3.91	23.100	0.242
390	2.63	24.570	0.194

Table 4-3 Sensitivity analysis for gain c_v.

As predicted, the stability of the bogie improves with increasing values of the c_v coefficient, and also force increases but the root mean square of the dissipated power does not. Therefore, a value of c_v coefficient equal to 330 kNm/s is a suitable compromise between an oversizing of the actuator and its good performances, even better than the semi-active solution.

Chapter 5 HIL testing

In this chapter, the concept of hardware in the loop (HIL) and the experimental tests results there will be presented and discussed. It is important to underline how the HIL tests allow to pass from purely numerical simulations to the real experimental tests, in which the simplified model of the yaw damper is no longer considered, and it is replaced by the real physical object with all its complexities and functionalities. Therefore, results obtained from the HIL tests are a good indicator for the correct functioning of the physical yaw damper. Since the Simpack multibody model of the railway vehicle is too complex for running in real-time, the introduction of a simplified model of the bogie is necessary. In this way, with a simpler model, the simulations can run in real-time and the HIL concept can be used.

It is worth to notice that the yaw damper used for the HIL tests is not exactly the one modelled in Chapter 3. Moreover, the HIL tests are limited to the semi-active yaw damper solution, since the prototype of the full-active one was not available.

5.1 HIL testing concept

Hardware-in-the-Loop simulation, is a technique that is used in the development and test of complex real time embedded systems. HIL simulations provides an effective platform by adding the complexity of the plant under control to the test platform. The complexity of the plant under control is included in test and development by adding a mathematical representation of all related dynamics systems. These mathematical representations are referred to as the “plant simulation”. The embedded system to be tested interacts with this plant simulation.

A HIL simulation must include electrical emulation sensors and actuators. These electrical emulations act as the interface between the plant simulation and the embedded system under test. The value of each electrically emulated sensor is controlled by the plant simulation and is read by the embedded system under test (feedback loop). Likewise, the embedded system under test implements its control algorithms by outputting actuator control signals. Changes in the control signals result in changes to variable values in the plant simulation.

The HIL bench is constituted by:

- sensors: input devices;
- actuators: used to perform an action following the control unit input;
- electrical and electronic wiring and relative connections: the electrical system and the network that interconnects the control units with the relative terminators *i.e.* sensors and actuators;
- models: the computer programs that emulates everything that is non-physically presented in the bench and send the signals to the connected devices.

The final purpose of the HIL tests is to simulate the real behavior of the physical yaw damper without considering the effective presence of the other components of the train and represent the step just before the on-line tests.

5.2 Description of test rig

Figure 5.1 shows the test rig setup used during the experimental phase. The main components that can be seen are the hydraulic actuator which is used to test and move the damper, a load cell in between the actuator and the effective semi-active yaw damper itself with another load cell.

Figure 5.1 HIL experimental setup.

Instead, in Figure 5.2 is presented a schematization of the test rig in order to understand how the hydraulic actuator and the semi-active yaw damper are connected to the other units.

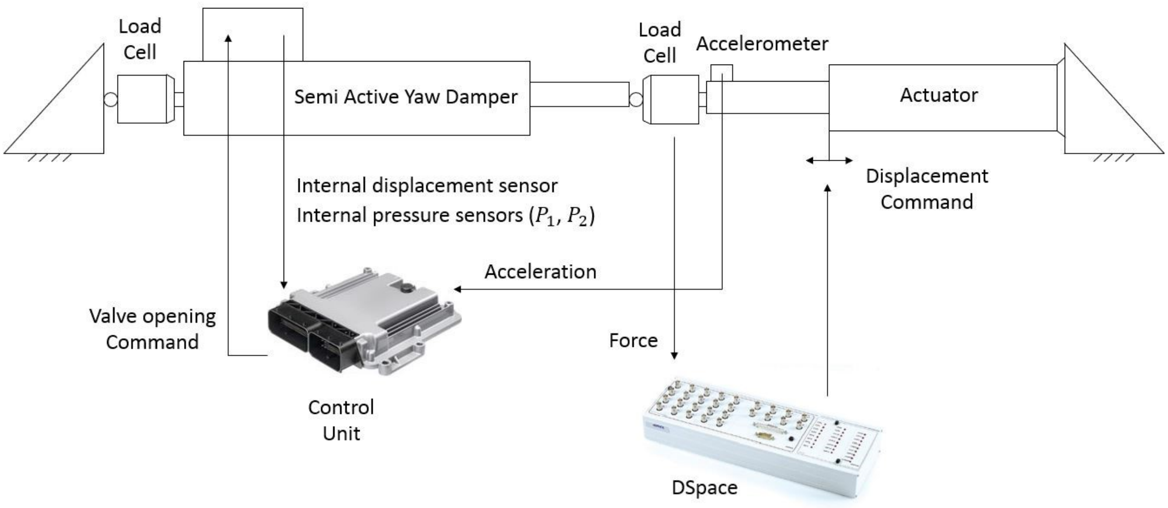

Figure 5.2 Scheme of the HIL setup and connection with the other units.

The inputs of the control unit driving the semi-active yaw damper are the acceleration signal that comes from the accelerometer mounted on the moving end of the hydraulic actuator (interface between the hydraulic actuator and the semi-active yaw damper) and the force signal that comes from the two internal pressure sensors mounted inside the semi-active yaw damper. The output of the control board is the valve opening command which defines the opening of the variable restriction valve of the semi-active yaw damper. The other unit used for the HIL tests is a real-time board by DSpace and it is used to drive the hydraulic actuator, realizing the HIL feedback loop. The input of the DSpace is the force measured from the load cell and its output is the displacement realized by the hydraulic actuator. It provides the reference for the actuator displacement based on the output of the simplified train vehicle model integrated on it.

Finally, in Figure 5.3 it is possible to see in more detail the two control boards as described previously and other laboratory tools principally used for converting and acquiring signals.

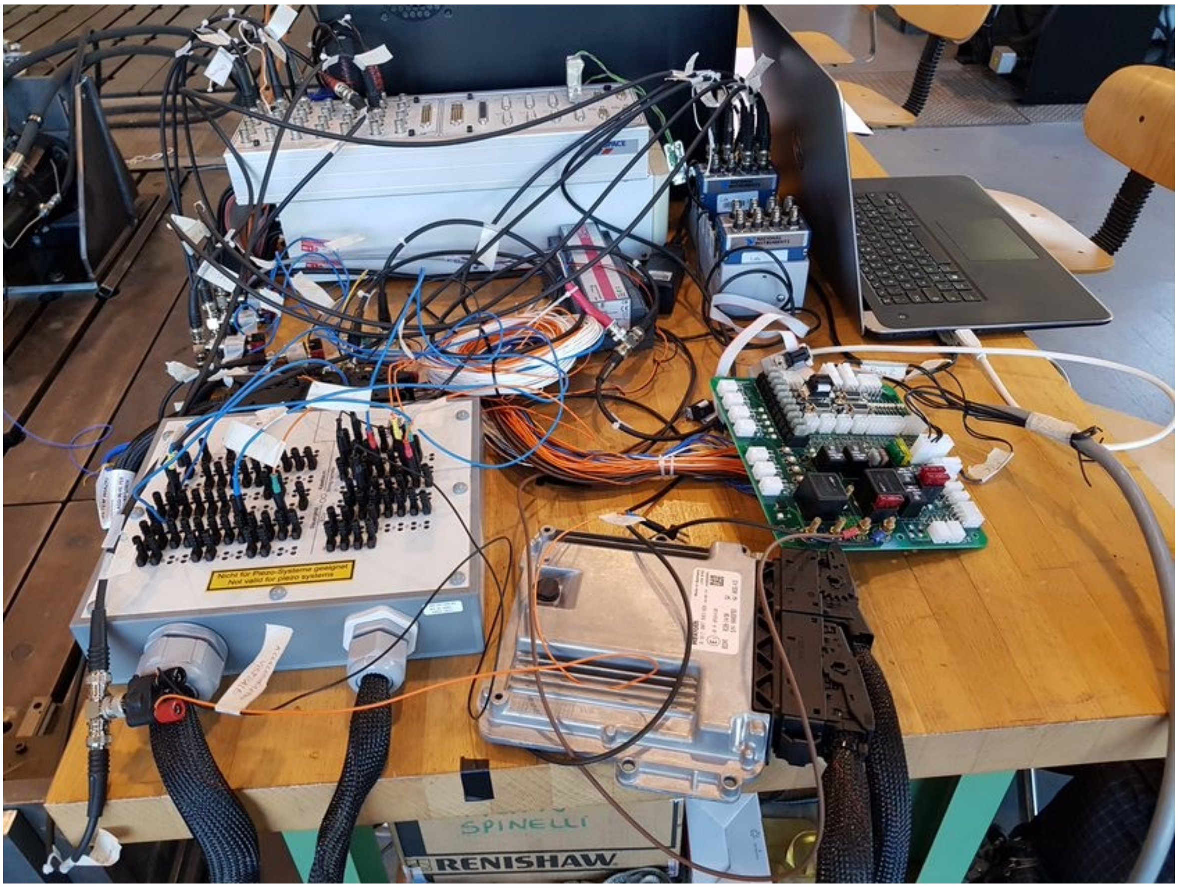

Figure 5.3 Control unit used to drive the semi-active yaw damper, DSpace real-time board and other laboratory tools.

5.3 2-dof model of the vehicle

As mentioned in the introduction of this chapter, the multibody model in Simpack is useless for writing the equation of motion of the system and for the HIL test bench since it is too complex, having 72 degrees of freedom. These are the reasons why a two degrees of freedom simplified mechanical model of the system is introduced as shown in Figure 5.4.

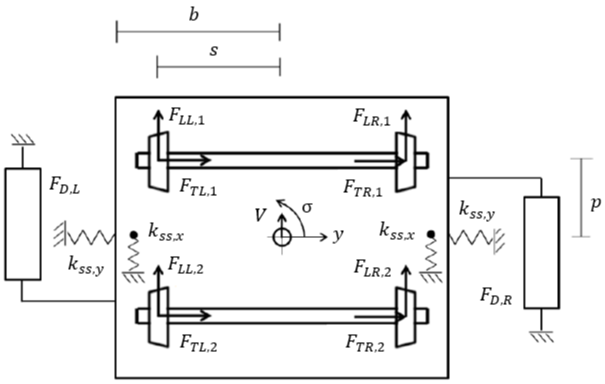

Figure 5.4 2-dof schematization of the train vehicle.

The assumptions that are used in this simplified model are the following:

1. the system is formed by three rigid bodies: two wheelsets and the bogie frame (Figure 5.5). Frequencies involved with hunting instability motions are always below 10 Hz (in particular between 3-6 Hz) whereas flexibility effects in wheelsets and bogie frame are to be found in a high frequency range, at least 60 Hz or more. All bodies are moving in longitudinal direction with speed V.
2. The carbody is assumed to move longitudinally with speed V and with no lateral/yaw oscillations due to the low coupling provided by the secondary suspensions.
3. Completely rigid primary suspensions, since the longitudinal and transversal stiffness values of the multibody model are very large.

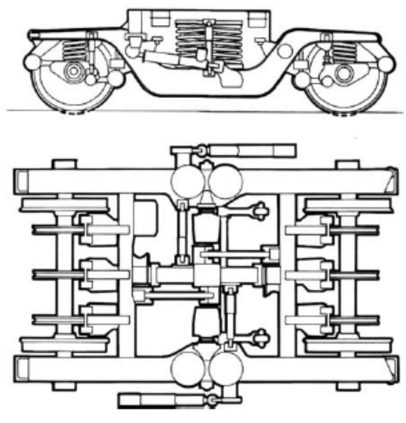

Figure 5.5 Model of the system: two wheelsets and one bogie frame.

With the third assumption (completely rigid primary suspensions) the two wheelsets are moving rigidly together with the bogie frame except for one additional degree of freedom which is the rotation of the body around its axis of revolution. The only flexibility that is possible to consider is the one for the secondary suspension: a longitudinal and a transversal stiffness k_{ssx}, k_{ssy}. With this assumption, the only degrees of freedom are a lateral displacement evaluated at the center of the bogie frame y and a yaw ration for the bogie σ. The lateral displacements at the front and rear wheelsets y_F, y_R and as well as the yaw rotation for the two wheelsets σ_F, σ_R become kinematic variables that are depending on y and σ. The wheel-rail contact forces are decoupled in two directions, longitudinal and transversal and they are present in each wheel. Finally, F_{DL}, F_{DR} are the forces exerted by the yaw dampers.

With these general considerations on the simplified mathematical model, in the following two paragraphs will be presented both the linearization of the two degrees of freedom model and the "complete" schematization of the model itself, in which the main effects due to non-linearities will be also included.

5.3.1 Linear model

Considering the linearized simplified two degrees of freedom model, with respect to Figure 5.4 the equations that describe the dynamics of the system can be written as:

$$\begin{cases} m\ddot{y} + 2k_{ssy}y = F_{TR1} + F_{TL1} + F_{TR2} + F_{TL2} \\ J\ddot{\sigma} + 2k_{ssx}b^2\sigma = s[(F_{LR1} + F_{LR2}) - (F_{LL1} + F_{LL2})] + p[(F_{TL2} + F_{TR2}) - (F_{TL1} + F_{TR1})] - b(F_{DL} + F_{DR}) \end{cases} \quad (5.1)$$

in which m represents the mass of the bogie plus the masses of the two wheelsets and J is the moment of inertia of the bogie and the two wheelsets rigidly connected. In equation (5.1), s represents the semi-gauge, p is the semi-wheelbase length and b is the distance between the point of application of the force of the yaw dampers and the center of the track.

Using the linearized model, it is necessary to consider some additional assumptions in addition to the previous three in order to schematize in a correct way the dynamics of the train model. For this reason, small displacements, conical wheel profiles, linear relationship between creepages and creep force, negligible effect of spin and spin moment are assumed. According to this fourth hypothesis of the model, the wheel-rail contact forces in transversal and longitudinal direction can be expressed according to Kalker's linear theory in the following way [62]:

$$\begin{cases} F_{TR1} = -f_{22}\varepsilon_{TR1} \\ F_{TL1} = -f_{22}\varepsilon_{TL1} \\ F_{TR2} = -f_{22}\varepsilon_{TR2} \\ F_{TL2} = -f_{22}\varepsilon_{TL2} \end{cases} \quad (5.2)$$

$$\begin{cases} F_{LR1} = -f_{11}\varepsilon_{LR1} \\ F_{LL1} = -f_{11}\varepsilon_{LL1} \\ F_{LR2} = -f_{11}\varepsilon_{LR2} \\ F_{LL2} = -f_{11}\varepsilon_{LL2} \end{cases} \quad (5.3)$$

in which the two linear coefficients f_{22} and f_{11} are respectively:

$$f_{22} = GabC_{22} \quad (5.4)$$

$$f_{11} = GabC_{11} \quad (5.5)$$

where G is the shear modulus of the material, a and b are the semi-axis of the wheel-rail contact ellipse (obtained by the Simpack model of the train), C_{11} and C_{22} are the Kalker's coefficients that depend on the ratio b/a in the following way [16]:

$$C_{22} = 3.2893 + \frac{0.975}{b/a} - \frac{0.012}{(b/a)^2} \tag{5.6}$$

$$C_{11} = 2.4014 + \frac{1.3179}{b/a} - \frac{0.02}{(b/a)^2} \tag{5.7}$$

The creepages in transversal and longitudinal direction can be expressed as functions of the state variables:

$$\varepsilon_{TR1} = \varepsilon_{TL1} = \frac{\dot{y} + V\sigma - p\dot{\sigma}}{V} \tag{5.8}$$

$$\varepsilon_{TR2} = \varepsilon_{TL2} = \frac{\dot{y} + V\sigma + p\dot{\sigma}}{V} \tag{5.9}$$

$$\varepsilon_{LR1} = \varepsilon_{LR2} = \frac{V - \dot{y}\sigma + s\dot{\sigma} - \Omega R_R}{V} \tag{5.10}$$

$$\varepsilon_{LL1} = \varepsilon_{LL2} = \frac{V - \dot{y}\sigma - s\dot{\sigma} - \Omega R_L}{V} \tag{5.11}$$

Moreover, assuming the wheels shape to be conical (Figure 5.6), the rolling radius on the right and left wheel is defined as:

$$R_R = R_0 + \gamma y \tag{5.12}$$

$$R_L = R_0 - \gamma y \tag{5.13}$$

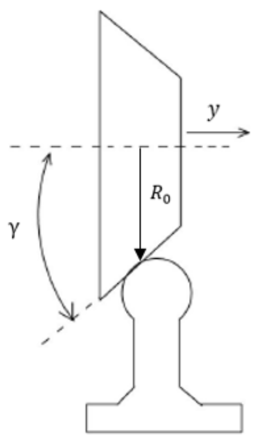

Figure 5.6 Schematization of the linear conical profile of the wheel.

In this way, using the previous linear relationships between the rolling radius and the lateral displacement it is possible to obtain the following expression for the longitudinal creepages:

$$\varepsilon_{LR1} = \varepsilon_{LR2} = \frac{s\dot{\sigma}}{V} - \frac{\gamma y}{R_0} \tag{5.14}$$

$$\varepsilon_{LL1} = \varepsilon_{LL2} = -\frac{s\dot{\sigma}}{V} + \frac{\gamma y}{R_0} \tag{5.15}$$

Defining $\bar{x} = \begin{Bmatrix} y \\ \sigma \end{Bmatrix}$ and introducing all the relations from (5.2) to (5.15) into equation (5.1), it is possible to obtain the following matrix expression:

$$\begin{bmatrix} m & 0 \\ 0 & J \end{bmatrix} \ddot{\bar{x}} + \begin{bmatrix} \frac{4f_{22}}{V} & 0 \\ 0 & \frac{4f_{11}s^2}{V} + \frac{4f_{22}p^2}{V} \end{bmatrix} \dot{\bar{x}} + \begin{bmatrix} 2k_{ssy} & 4f_{22} \\ -\frac{4f_{11}s\gamma}{R_0} & 2k_{ssx}b^2 \end{bmatrix} \bar{x} = \\ = \begin{bmatrix} 0 & 0 \\ -b & -b \end{bmatrix} \begin{bmatrix} F_{DR} \\ F_{DL} \end{bmatrix} \tag{5.16}$$

The force F_{DR} and F_{DL} are functions of the damping and stiffness coefficient of the two elements that compose the yaw dampers themselves. In particular, since these two elements are in series configuration and this would involve the addition of further degrees of freedom to describe the entire model, as a first approximation it is possible to consider the stiffness of the yaw damper as infinitely rigid. In this way, the presence of the ideal spring can be neglected, and the yaw damper can be schematized only with an ideal damper. With this simplification it is possible to write the two forces in the following way:

$$F_{DR} = F_{DL} = c_0 b\dot{\sigma} \tag{5.17}$$

where c_0 is the damping coefficient taken from the passive reference damper model.

Introducing (5.17) into equation (5.16) it results:

$$\begin{bmatrix} m & 0 \\ 0 & J \end{bmatrix} \ddot{\bar{x}} + \begin{bmatrix} \frac{4f_{22}}{V} & 0 \\ 0 & \frac{4f_{11}s^2}{V} + \frac{4f_{22}p^2}{V} + 2c_0b^2 \end{bmatrix} \dot{\bar{x}} \\ + \begin{bmatrix} 2k_{ss,y} & 4f_{22} \\ -\frac{4f_{11}s\gamma}{R_0} & 2k_{ss,x}b^2 \end{bmatrix} \bar{x} = \begin{bmatrix} 0 \\ 0 \end{bmatrix} \tag{5.18}$$

Equation (5.18) represent the complete equations of motion of the linearized simplified two degrees of freedom model of the train.

5.3.2 Non-linear model

First of all, for the non-linear model it is necessary to remove the hypothesis of constant equivalent conicity of the wheels. In this case, relations (5.12) and (5.13) are not valid anymore and the wheel's radius increases as a function of the wheelset displacement in the following way:

$$R_{L,R} = R_0 + \Delta R_{L,R}(y_{wheelset}) \tag{5.19}$$

in which $R_{L,R}$ is the effective contact radius of the left/right wheel, R_0 is the nominal rolling radius and $\Delta R_{L,R}$ is the variation of the rolling radius with the lateral displacement of the wheelset for the left/right wheel. The rolling radius variation functions are taken directly from software Simpack considering the train wheels profile and they are represented for the right and left wheel in Figure 5.7.

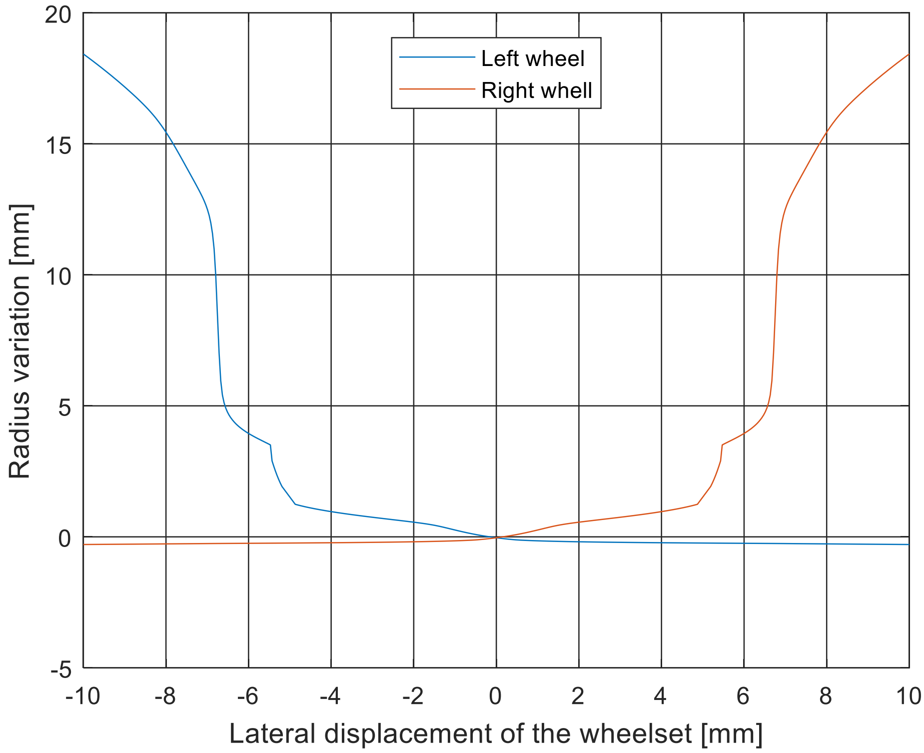

Figure 5.7 Functions for the radius variations of the left and right wheel.

Another non-linear component that is present in the wheel-rail contact schematization is a lateral force that affects each wheel. This force is proportional to the tangent of the contact angle ($\tan\gamma$) in the following way:

$$F_{B\ L,R} = P \cdot \tan\gamma_{L,R} = P \cdot \tan\left(\gamma_{L,R}(y_{wheelset})\right) \tag{5.20}$$

in which P is the vertical load for each wheel, while $\tan\gamma$ is a function of the lateral displacement of the wheelset. As done for the radius variations, also in this case the contact gradient on rail for the two wheels are taken directly from the Simpack model in order to have a better comparison between the two models, and it is represented in Figure 5.8.

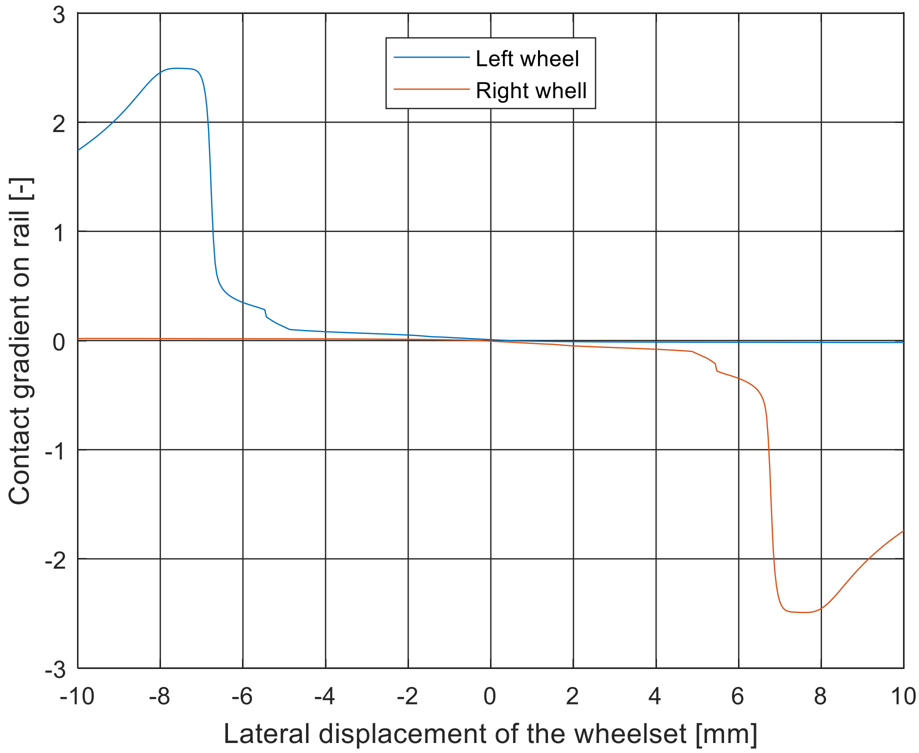

Figure 5.8 Contact gradient on rail, plot of $\tan\gamma$ as a function of the wheelset lateral displacement.

A very practical way for improving the Kalker contact linear theory is to use what is known as Heuristic laws (Figure 5.9): the starting point is always the linear theory by Kalker, and therefore linear forces and parameter τ are defined. Finally, a saturation law that is basically a third order polynomial which provides a kind of smooth transition from the linear region of the diagram (which is predicted by the linear theory of Kalker) to the saturation limit ($\tau > 1$) is applied. In this way, the redistribution of the longitudinal and transversal creep forces considering the cubic saturation law is obtained:

$$\begin{cases} F_{TR1}^{sat} = \dfrac{F'_{R1}}{F_{R1}^{res}} F_{TR1} \\ F_{TL1}^{sat} = \dfrac{F'_{L1}}{F_{L1}^{res}} F_{TL1} \\ F_{TR2}^{sat} = \dfrac{F'_{R2}}{F_{R2}^{res}} F_{TR2} \\ F_{TL2}^{sat} = \dfrac{F'_{L2}}{F_{L2}^{res}} F_{TL2} \end{cases} \tag{5.21}$$

$$\begin{cases} F_{LR1}^{sat} = \dfrac{F'_{R1}}{F_{R1}^{res}} F_{LR1} \\ F_{LL1}^{sat} = \dfrac{F'_{L1}}{F_{L1}^{res}} F_{LL1} \\ F_{LR2}^{sat} = \dfrac{F'_{R2}}{F_{R2}^{res}} F_{LR2} \\ F_{LL2}^{sat} = \dfrac{F'_{L2}}{F_{L2}^{res}} F_{LL2} \end{cases} \tag{5.22}$$

in which, the linear creep forces, $F_{L\,L,R\,1,2}$ and $F_{T\,L,R\,1,2}$, are taken from the Kalker's linear theory ((5.2), (5.3)), the resultant linear force for each wheel, $F_{R,L\,1,2}^{res}$, is defined as the sum in quadrature of the longitudinal and transversal linear creep forces:

$$F_{L,R\,1,2}^{res} = \sqrt{\left(F_{T\,L,R\,1,2}\right)^2 + \left(F_{L\,L,R\,1,2}\right)^2} \tag{5.23}$$

the cubic saturation curve has the following equation:

$$F'_{L,R\,1,2} = \mu P\left(1 - \left(1 - \tau_{L,R\,1,2}\right)^3\right) \tag{5.24}$$

and the parameter $\tau_{L,R\,1,2}$ is defined for each wheel as:

$$\tau_{L,R\,1,2} = \frac{F_{L,R\,1,2}^{res}}{3\mu P} \tag{5.25}$$

where μ is the friction coefficient existing between the wheel and the rail.

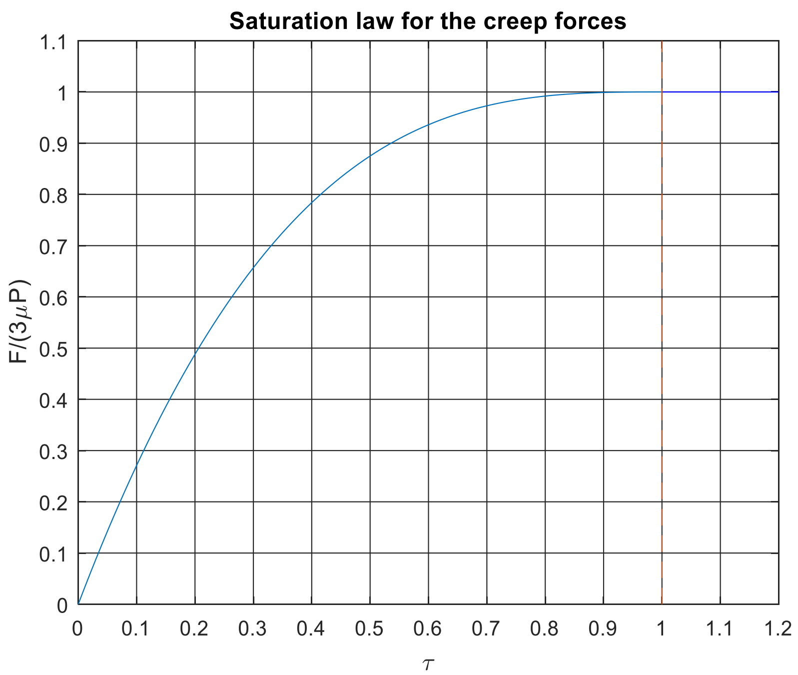

Figure 5.9 Heuristic law for the saturation creep forces: Vermeulen-Johnson law.

Finally, in order to obtain a more complete model, other two degrees of freedom are introduced, that are the additional independent rotations of each wheelset β_1 and β_2, relative to the un-perturbed rolling motion of the wheelset. In this way, the angular speed of each wheelset can be written as:

$$\omega = \Omega + \dot{\beta} \tag{5.26}$$

The introduction of these additional independent coordinates is useful to deal with the large variation of longitudinal creepages occurring when flange contact occurs considering the non-linear rolling radius variation shown in Figure 5.7.

It is worth to notice that for the sake of simplicity, even though the non-linear model is now a four degrees of freedom one, it will in any case be referred to as a non-linear model with two degrees of freedom, simply referring to the yaw rotation of the bogie and to the lateral displacement of the bogie itself. The two additional degrees of freedom are used only in the equations of motion in order to have a more realistic comparison between the two models.

With these additional assumptions it is possible to obtain the equations of motion of the non-linear model writing the equilibrium equations for the lateral displacement, yaw rotation, torques around the front and rear wheelsets.

$$\begin{cases} m\ddot{y} + 2k_{ssy}y = F_{TR1}^{sat} + F_{TL1}^{sat} + F_{TR2}^{sat} + F_{TL2}^{sat} + F_{BR1} + F_{BL1} + F_{BR2} + F_{BL2} \\ J\ddot{\sigma} + 2k_{ssx}b^2\sigma = s[(F_{LR1}^{sat} + F_{LR2}^{sat}) - (F_{LL1}^{sat} + F_{LL2}^{sat})] + p[(F_{TL2}^{sat} + F_{TR2}^{sat}) - (F_{TL1}^{sat} + F_{TR1}^{sat})] + \\ +p[(F_{BR2} + F_{BL2}) - (F_{BR1} + F_{BL1})] - b(F_{DL} + F_{DR}) \\ J_{w1}\ddot{\beta}_1 + F_{LL1}^{sat}R_{L1} + F_{LR1}^{sat}R_{R1} = 0 \\ J_{w2}\ddot{\beta}_2 + F_{LL2}^{sat}R_{L2} + F_{LR2}^{sat}R_{R2} = 0 \end{cases} \tag{5.27}$$

As it can be noticed from (5.27), the main differences with respect to the liner case are the non-linear saturated creep forces, the contact forces in lateral direction due to the contact gradient on rail and the two additional equilibrium equations due to the independent rotations of each wheelset.

5.3.3 Comparison between the Simpack multibody model and the reduced 2-dof model

In this section the results of the comparison between the Simpack model and the reduced two degrees of freedom model both in linear and in non-linear form are presented. In addition, it will be briefly discuss also the difference between the linear and non-linear model of the two degrees of freedom schematization of the train vehicle. The simulations are done with an ideal pure viscous yaw damper in which the equivalent damping coefficient is taken directly from the characterization of the semi-active yaw damper presented in section 3.3.4 at 4 Hz and with a constant opening of the valve equal to 30%.

5.3.3.1 Linear Simpack model vs linear simplified 2-dof model

For what concerns the linear critical velocity of the two degrees of freedom simplified model it will be used an eigenvalues/eigenvectors analysis as it was done for the linear Simpack model (paragraph 4.3.1). The equations of motion in (5.18) can be generalized in a matrix form as:

$$[M]\ddot{\bar{x}} + [C]\dot{\bar{x}} + [K]\bar{x} = [0] \tag{5.28}$$

Introducing the state variable $\bar{z} = \begin{Bmatrix} \dot{\bar{x}} \\ \bar{x} \end{Bmatrix}$ and his derivative $\dot{\bar{z}} = \begin{Bmatrix} \ddot{\bar{x}} \\ \dot{\bar{x}} \end{Bmatrix}$ it is possible to obtain the state space representation:

$$\begin{bmatrix} [M] & [0] \\ [0] & [M] \end{bmatrix} \begin{Bmatrix} \ddot{\bar{x}} \\ \dot{\bar{x}} \end{Bmatrix} + \begin{bmatrix} [C] & [K] \\ -[M] & [0] \end{bmatrix} \begin{Bmatrix} \dot{\bar{x}} \\ \bar{x} \end{Bmatrix} = \begin{Bmatrix} 0 \\ 0 \end{Bmatrix} \tag{5.29}$$

$$[A_1]\dot{\bar{z}} + [B_1]\bar{z} = 0 \quad \rightarrow \quad \dot{\bar{z}} = -[A_1]^{-1}[B_1]\bar{z} \quad \rightarrow \quad \dot{\bar{z}} = [A]\bar{z} \tag{5.30}$$

where the state matrix is a function of the vehicle velocity, $[A] = [A(V)]$.

Imposing the steady state solution:

$$\underline{z} = \underline{Z}e^{\lambda t} \tag{5.31}$$

it is possible to obtain:

$$\begin{gathered} \lambda\underline{Z}e^{\lambda t} = [A(V)]\underline{Z}e^{\lambda t} \quad \rightarrow \quad (-\lambda[I] + [A(V)])\underline{Z} = \underline{0} \quad \rightarrow \\ \rightarrow \quad det(-\lambda[I] + [A(V)]) = 0 \end{gathered} \tag{5.32}$$

that represents an eigenvalues problem of the state matrix $[A(V)]$.

Generally, the λ values are pairs of complex and conjugate numbers:

$$\lambda(V) = -\alpha(V) \pm i\omega(V) \tag{5.33}$$

By analyzing the real part of the eigenvalues, it is possible to study the stability of the system: if all the real parts are negative the system is stable, otherwise, if at least one of the real parts is positive the system is unstable. The imaginary part of the eigenvalues provides information on the frequency of the oscillation.

One of the most used way of showing the results for this analysis is the well-known root locus visualization (Figure 5.10): it is based on repeating an eigenvalue/eigenvector analysis for the state matrix of the system for different longitudinal speed of the vehicle which is increased in discrete steps (5 km/h). The results are represented in a complex plane where the horizontal axis is the axis of the real part of the solutions, and the vertical axis is the axis of the imaginary part of the solutions. Each complex and conjugate pair is represented by two points which are placed symmetrically with respect to the horizontal axis. If the speed can change in discrete steps, then the couples of points are moving in the complex plane and the root locus is obtained. It is possible to notice that if the speed of the vehicle is increasing then the system will go into an unstable condition. Moreover, it is worth to notice that this type of analysis gives also some information on the frequency of the motion on the vertical axis. The imaginary part of the first eigenvalues with positive real part is more or less 21 (the imaginary part corresponds to the pulsation frequency ω expressed in rad/s) and so it is possible to conclude that the frequency of the hunting motion is slightly higher than 3 Hz.

As mentioned before, the instability is reached when the real part of the maximum eigenvalue crosses the zero, becoming positive. So, from this sensibility analysis it is possible to conclude that the reduced model has a linear critical velocity of 270 km/h, while the linear critical speed of the Simpack train model is around 280-290 km/h (paragraph 4.3.1). The proximity of the two critical velocities confirms the reliability of the simplified model and although the linear model introduced is a very simplified one, with two degrees of freedom only, it can reproduce in an accurate way the lateral dynamics of the railway vehicle, as testified by its linear critical velocity that is very close to the linear critical velocity of the Simpack linearized model.

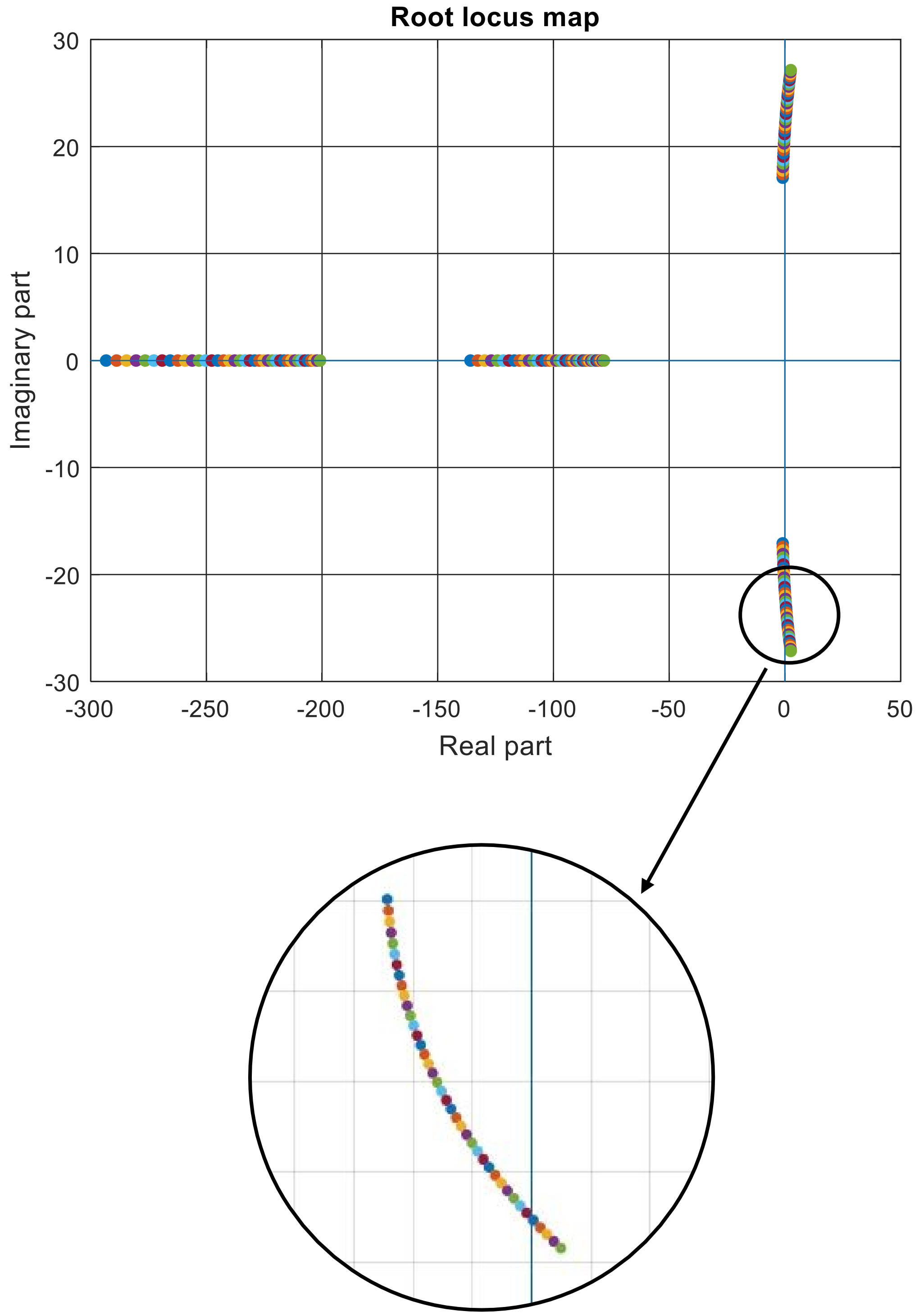

Figure 5.10 Root locus map: dependence on the running velocity.

5.3.3.2 Linear simplified 2-dof model vs non-linear 2-dof model

In this section the difference between the linear two degrees of freedom simplified model and the non-linear two degrees of freedom model will be briefly discussed. As mentioned in paragraph 5.3.2, the main difference between these two mathematical models of the train vehicle is the way on how the wheel-rail contact forces are calculated. In particular, in the linearized model an equivalent constant wheel conicity was used in order to calculate the rolling radius variation, while with the non-linear model it was used the real wheel profile. Of course, since the comparison is between a linear and a non-linear model, it makes no sense to use the eigenvalues/eigenvectors analysis and calculate the linear critical speed. For this reason, the comparison between these two models will be done only referring to a simplified time domain analysis, in which, after having imposed fixed initial conditions (lateral displacement of the bogie and yaw rotation of the bogie itself), the train is launched in a straight track section at constant speed. The results of the two models are then compared in time domain considering the variation of the lateral displacement for both models. The results are presented in Figure 5.11, Figure 5.12 and Figure 5.13 that correspond to three different velocities: the first velocity of the simulation is under the linear critical velocity (220 km/h), the second one is close to the predicted linear critical velocity (285 km/h) and finally, the third one is above the linear critical velocity (320 km/h).

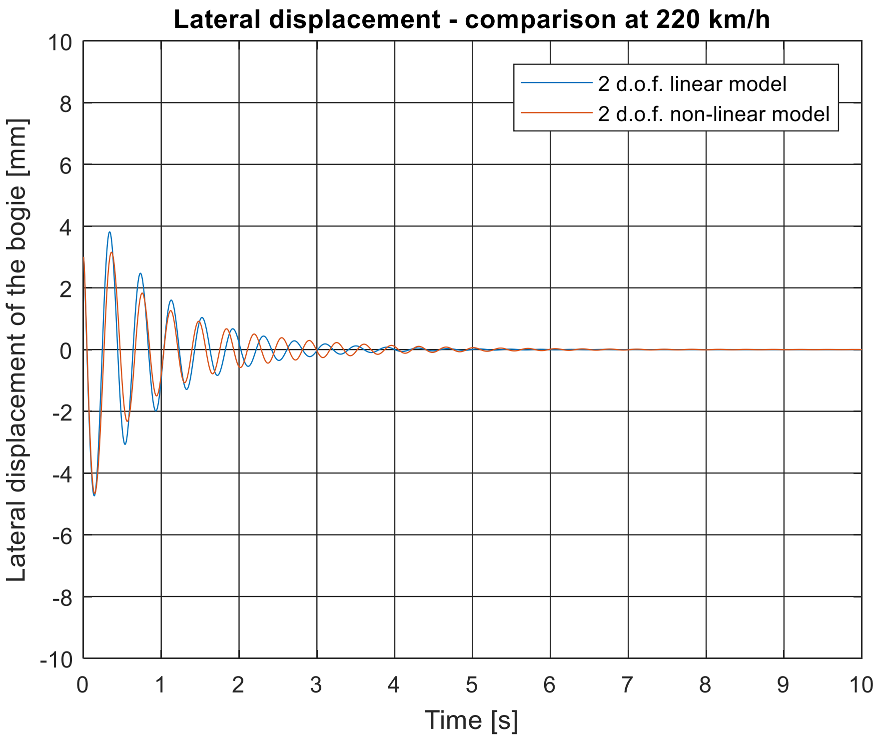

Figure 5.11 Comparison between linear and non-linear simplified two degrees of freedom model at 220 km/h (lower than the linear critical velocity).

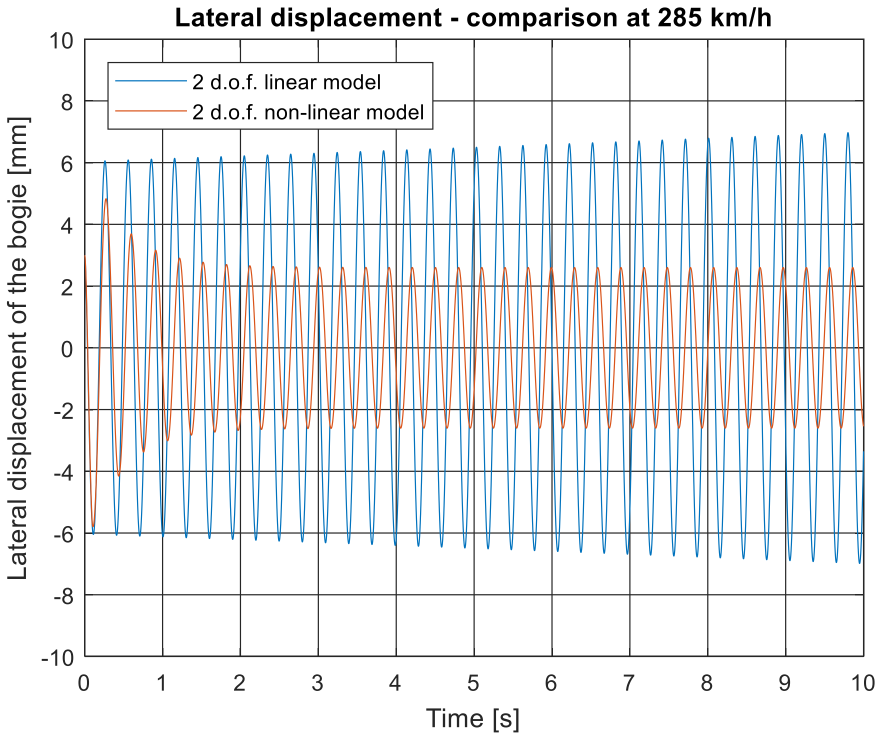

Figure 5.12 Comparison between linear and non-linear simplified two degrees of freedom model at 285 km/h (approximately the linear critical velocity).

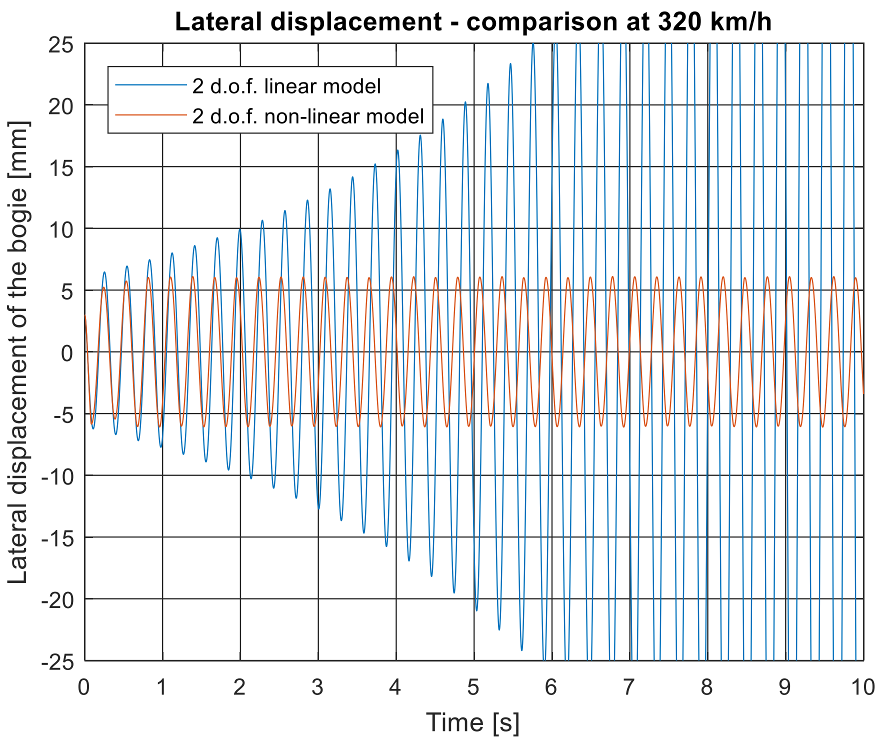

Figure 5.13 Comparison between linear and non-linear simplified two degrees of freedom model at 320 km/h (higher then linear critical velocity).

As it can be noticed, the non-linear model has an important difference with respect to the linear one: in fact, for the velocities near or greater than the linear critical velocity a limit cycle appears. This limit cycle is due to the non-linear effects of the wheel-rail contact that is the main difference between the two models. However, it is possible to notice how in case of velocity lower than the linear critical velocity (Figure 5.11) the two responses are almost the same. This fact can be justified considering that in case of low wheelset displacement the non-linear effects due to the radius variation and the contact gradient on rail are negligible with respect to the linear. In the other cases, with greater velocities a limit cycle appears in the non-linear model and for this reason it is not as trivial as in the linear case to find the critical velocity of the non-linear two degrees of freedom model, since there is no pure expansive solution. The other difference that can be noticed is that the frequencies of the hunting motion in the two cases are not exactly the same, but this can be justified by the fact that in the non-linear model there are two additional degrees of freedom (additional rotation of each wheelset) with respect to the linear model and also the non-linearities are considered. However, even if the two frequencies are not exactly equal, both are of the order of 3-4 Hz which correspond to the oscillation frequency due to the hunting motion of the rail vehicle. Finally, it can be confirmed the linear critical speed of the two degrees of freedom model also in time domain: for speed equal to 285 km/h and 320 km/h the solutions are expanded with time (Figure 5.12 and Figure 5.13), while for velocity equal to 220 km/h the solution is convergent (Figure 5.11) that means that the velocity is under the linear critical velocity of the vehicle.

5.3.3.3 Simpack multibody model vs non-linear 2-dof model

After having compared the linear Simpack model with the simplified two degrees of freedom linear model and the simplified two degrees of freedom linear model with the non-linear one, the non-linear Simpack model is compared with the non-linear two degrees of freedom model. As mentioned in the introduction of this chapter, the validation of the two degrees of freedom model with respect to the Simpack multibody model is very important since it allows to use a yet accurate for the *HIL* tests. In fact, the Simpack model is a very complicated model and it cannot run in real-time applications.

Figure 5.14 and Figure 5.15 show the comparison of the two models considering the vehicle running on an irregular track at speed 240 and 300 km/h respectively. Although the two degrees of freedom model is a very simple model, the agreement with the Simpack multibody model can be considered quite good. In particular there is a good matching of the two models in terms of predicting a stable running of the vehicle at 240 km/h (wheelset displacement only occasionally exceed 6 mm, no limit cycle visible) to unstable running at 300 km/h as can be observed from the formation of a limit cycle of oscillation with amplitude of wheelset displacement of 6-7 mm corresponding to flange contact.

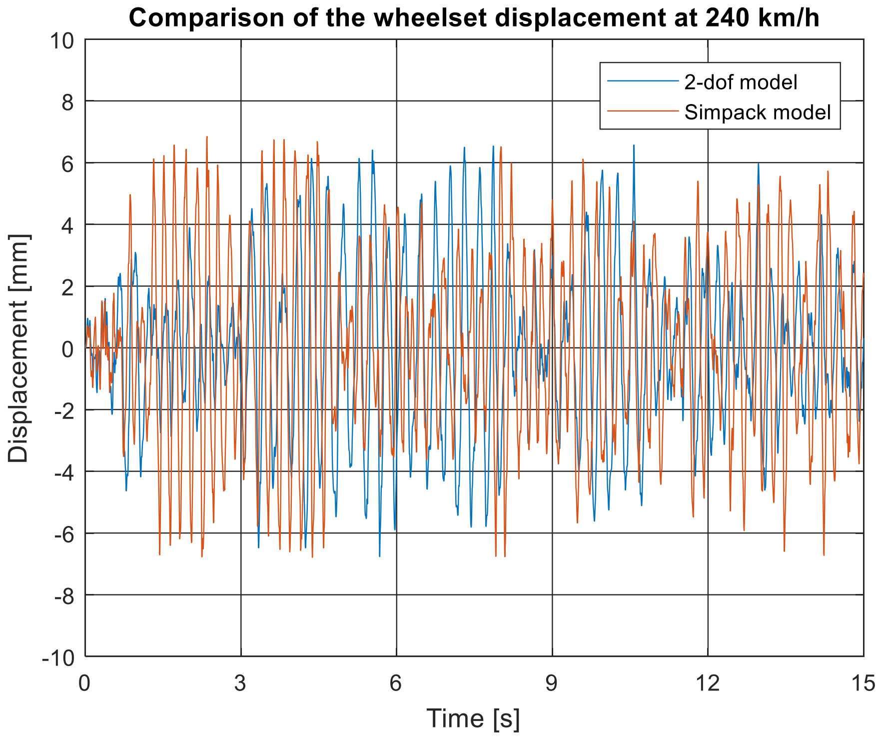

Figure 5.14 Comparison between two degrees of freedom model and Simpack multibody model, lateral wheelset displacement at 240 km/h (stable condition).

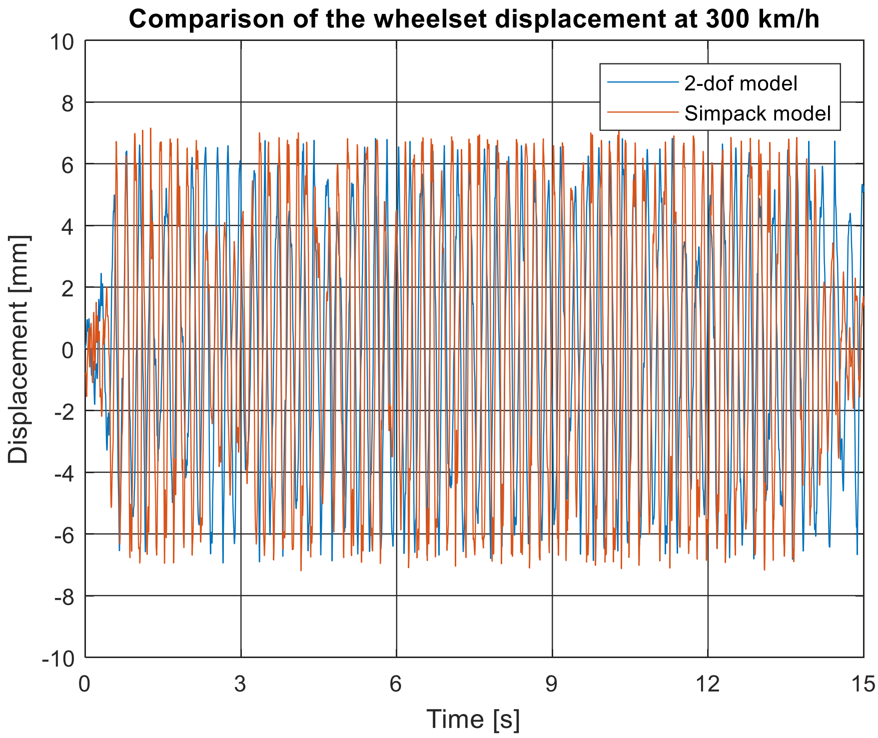

Figure 5.15 Comparison between two degrees of freedom model and Simpack multibody model, lateral wheelset displacement at 300 km/h (unstable condition).

Finally, in order to have further confirmation of the good quality of the two results, a time domain analysis starting from an initial condition of lateral displacement and yaw rotation of the bogie at different velocities has been performed. Figure 5.16, Figure 5.17 and Figure 5.18 show the comparison of the time response of the two different model respectively at 220 km/h, 285 km/h and 320 km/h. As it is possible to notice, at very relatively speed both of the time responses show a decaying oscillation (Figure 5.16) even if the Simpack one is more damped than the other, but as mentioned before, this different behavior can be justified by the different number of degrees of freedom of the two models and the simplifications used for the two degrees of freedom one. At 285 km/h (Figure 5.17) in both models a with small amplitude appears for both models. The amplitude of the limit cycle being similar in the two cases and not large enough to produce flange contact. At 320 km/h (Figure 5.18) for both model it is possible to see a fully developed limit cycle with an amplitude of ± 6 mm, that means that flange contact occurs at each oscillation. Based on these considerations, it can be concluded that also this analysis confirms the goodness of the simplifications made and the similarity between the multibody Simpack model and the non-linear two degrees of freedom model.

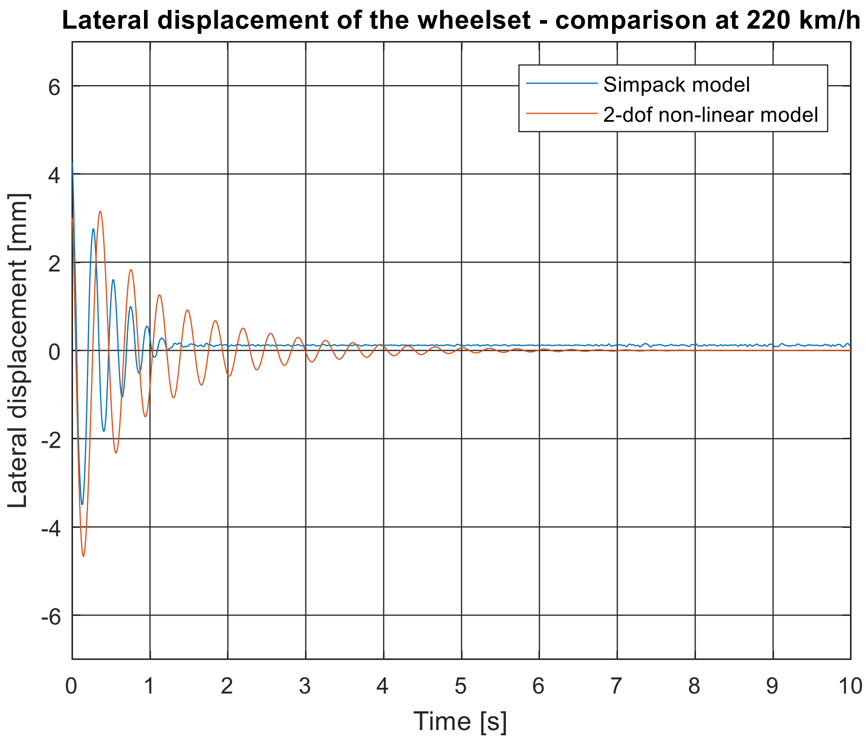

Figure 5.16 Comparison between the two models for lateral displacement of the wheelset at 220 km/h (lower than the critical velocity).

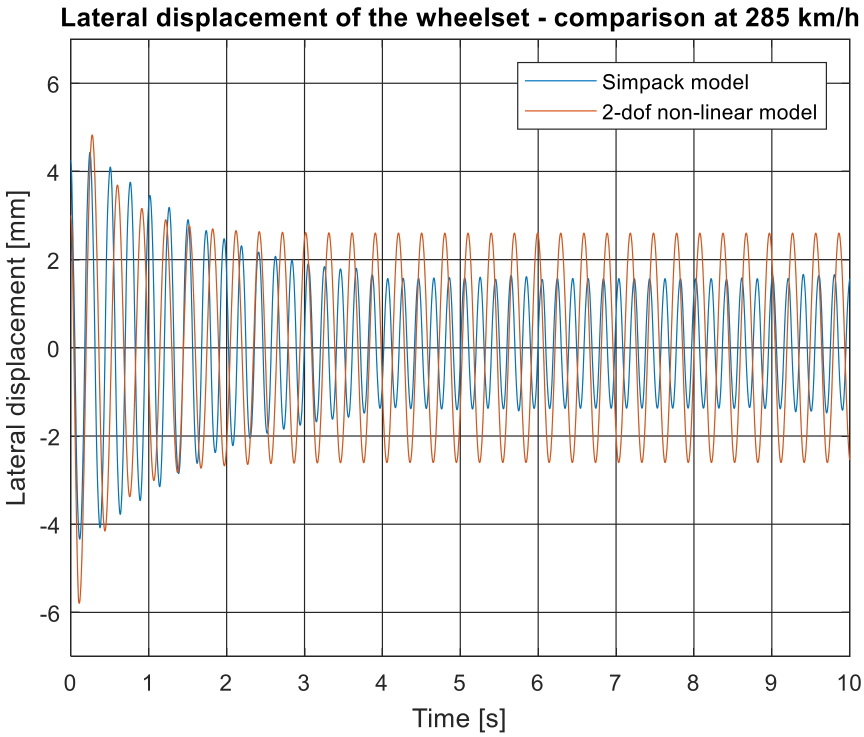

Figure 5.17 Comparison between the two models for lateral displacement of the wheelset at 285 km/h (approximately the linear critical velocity).

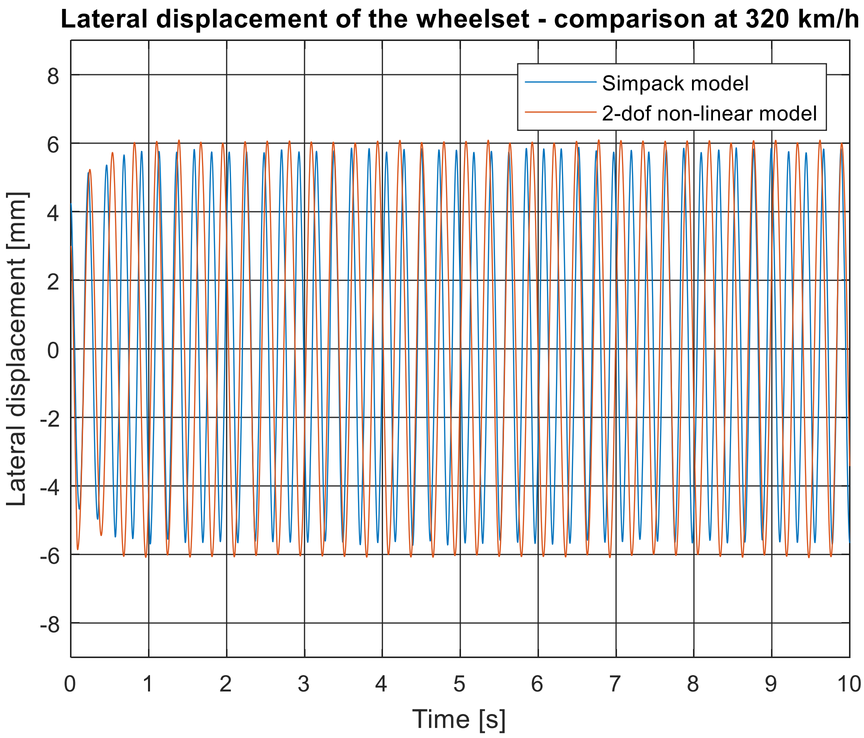

Figure 5.18 Comparison between the two models for lateral displacement of the wheelset at 320 km/h (higher than the critical velocity).

5.4 HIL experimental tests

In this section the HIL experimental tests will be presented and discussed. The focus will be on the results obtained with the two different control logics presented in paragraph 3.2.1, analysing the advantages and disadvantages for each one of the two. It is worth to notice that the semi-active yaw damper used in the HIL tests is not exactly the same as the one introduced in the paragraph 3.3 and for this reason it is not possible to have an exact quantitative comparison between the two results. However, it still can be interesting and useful to have a qualitative comparison between the ideal mathematical model and the real physical model in order to understand which are the practical aspects that appear in the real case and that are neglected and not taken into account during the numerical simulations.

5.4.1 Results of HIL tests with MPPT control strategy

In order to see the benefits of the MPPT control logic on the stability and dynamics performance of the railway vehicle, the experimental HIL tests are performed in the following way. First of all, a fixed value of speed of the vehicle is imposed. This value has to be sufficiently large to be sure that the vehicle becomes unstable after a perturbation is applied. In the first part of the tests, before switching on the track-irregularity since the bogie is not subjected to any perturbation, it just going straight without increasing neither the lateral acceleration nor the lateral wheelset displacement. Then, the track-irregularities are switched on and their effect is introduced in the real time model which is run on the DSpace board. In this phase, it is decided to deliberately start with the valve fully open, so the amount of damping is limited and the bogie has a low critical speed. After track irregularity is switched on, the behavior of the system is observed in terms of the oscillation of the bogie and reaction of the control board. It is expected that the control strategy succeeds with bringing back the bogie to a stable running behavior.

In the figures that will be used to present the results of the tests the time-history of four main quantities are shown. In particular will be considered the lateral acceleration of the bogie taken from the accelerometer signal placed on the tip of the hydraulic actuator, the wheelset displacement that is obtained by a virtual sensor generated from the DSpace board, the force of the semi-active yaw damper taken from the internal pressure sensors of the damper itself, and the valve opening command in the range of 0-100%.

In Figure 5.19 is presented the results of the test in which the weight of the force contribution of the cost function J is set to zero. After the onset of instability, the control board implementing the *MPPT* algorithm reacts to the unstable behavior of the bogie and sends a command to progressively close the proportional valve. Since this control strategy is not trying to minimize the force but just the lateral vibration, then, once the valve is sufficiently close, there is no reason for the controller to reopen it. So, it remains more or less at the same opening condition of the remaining part of the test. In fact, the controller is simple trying to minimize the lateral acceleration of the bogie and the best way is to stay at this opening valve condition, with a low vale of the valve opening command.

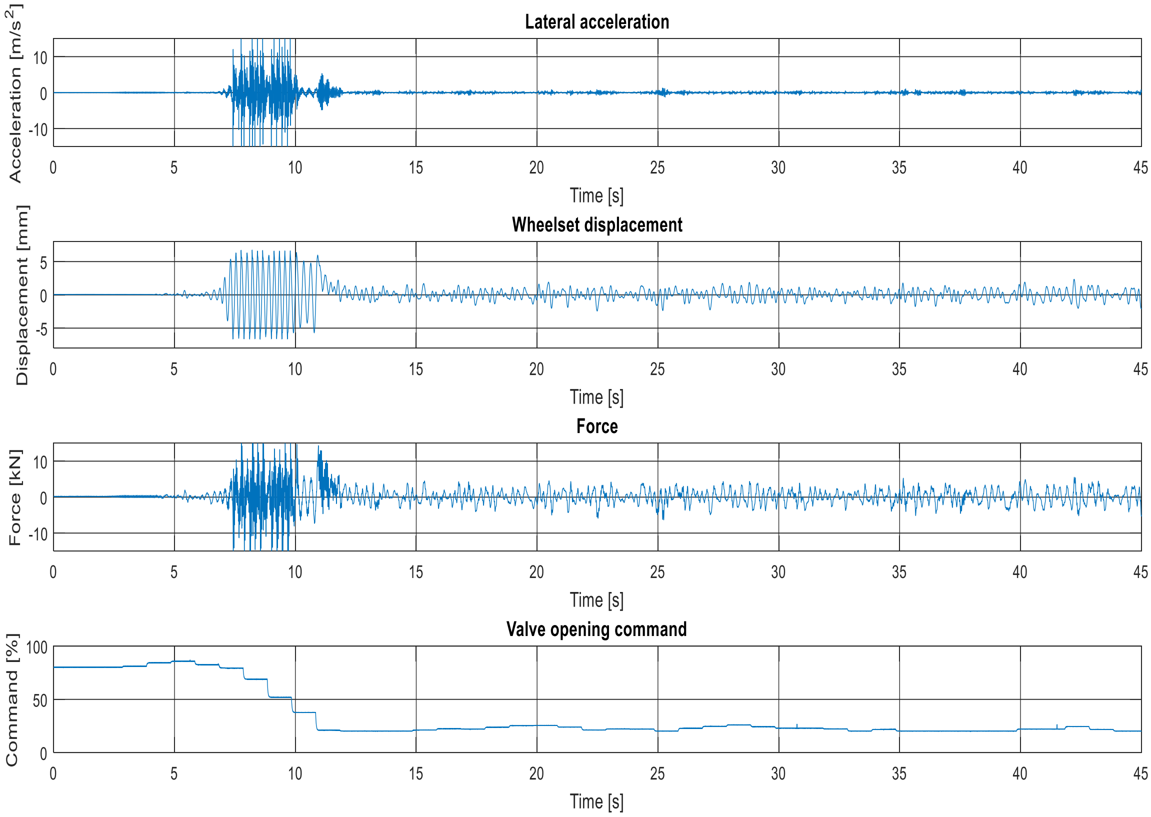

Figure 5.19 Result of HIL test with MPPT control strategy at 260 km/h, with zero value of the weight of the force in the definition of the cost function J and starting from fully open valve (80%).

In order to confirm the analysis done so far, it is possible to repeat the same test as before but starting from lower value of the valve opening command, that means valve almost fully closed. In this case the vehicle model is stable and the lateral acceleration value for the bogie is low as can be seen from Figure 5.21. According to this control logic, there is no need to re-open the valve since this should only lead to an increase of the lateral acceleration which is exactly what the control logic is trying to avoid.

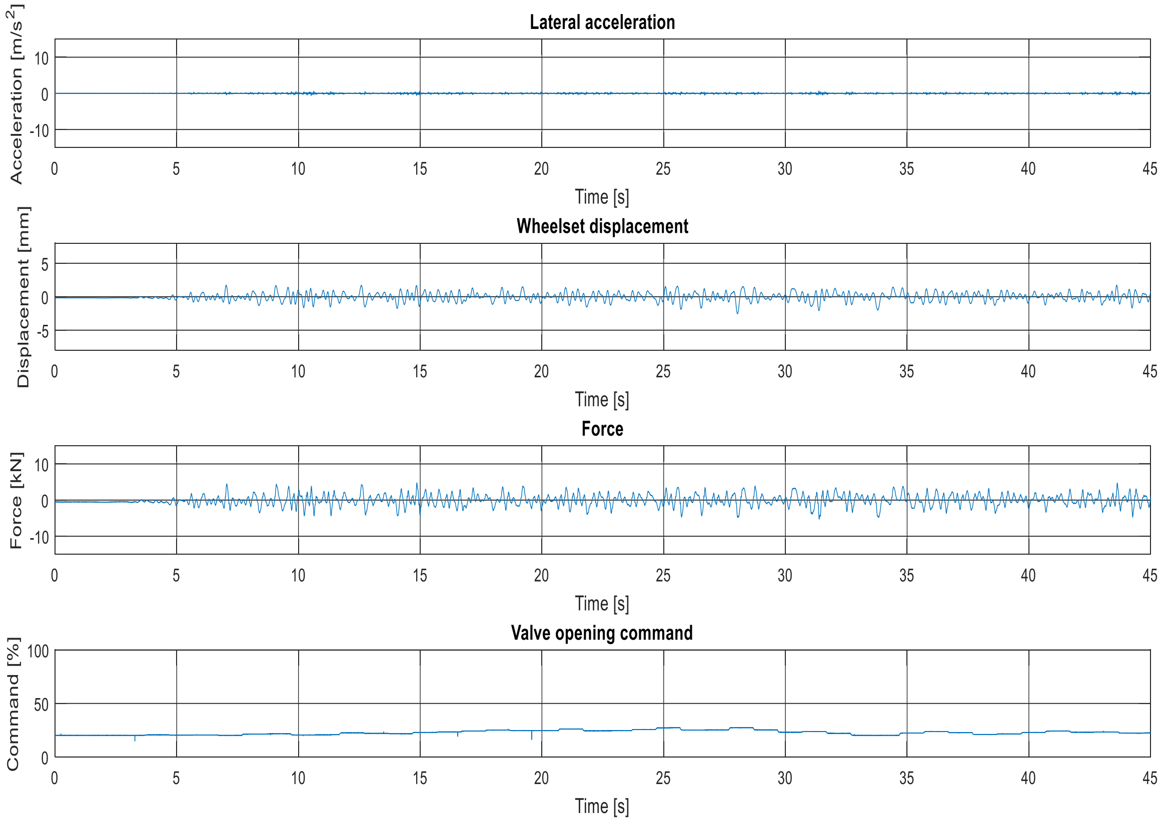

Figure 5.20 Result of HIL test with MPPT control strategy at 260 km/h, with zero value of the weight of the force in the definition of the cost function J and starting from closed valve (20%).

Figure 5.21 shows the results of a test performed at the same speed, considering a non-zero weight for the RMS of the force. In this case, after the instability is suppressed and the RMS of the bogie acceleration is reduced, the controller attempts to reduce the force generated by the damper, partially re-opening the valve. In the final part of the test, a constant intermediate opening value is reached which is still capable of ensuring the stable running of the bogie.

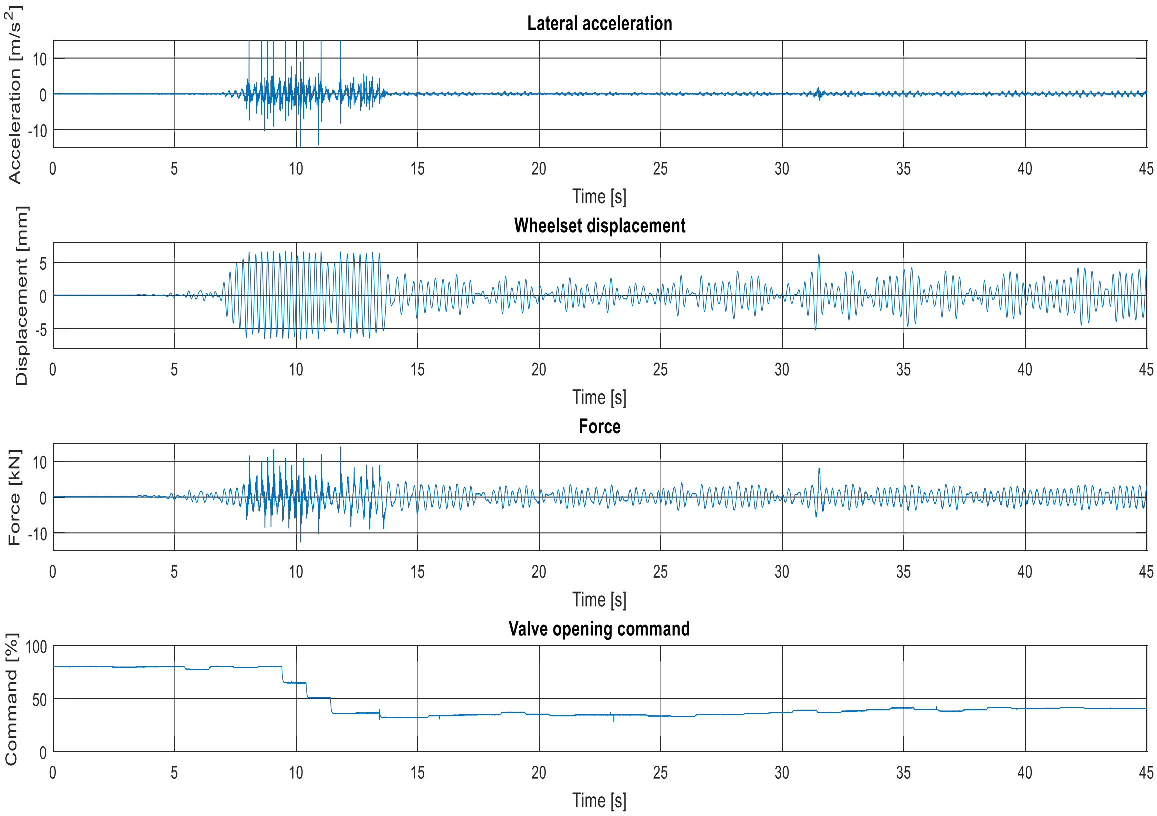

Figure 5.21 Result of HIL test with MPPT control strategy at 260 km/h, with the aim of minimizing both the lateral acceleration and the yaw damper force, starting from fully open valve (80%).

Figure 5.22 compares the time-history of the valve opening for the two tests performed with different weights of functional J. It is observed that in the initial phase of the test the controller reacts to the onset of instability in the same way for the two cases, but in the final part of the test the behavior is different and only if the RMS of the force is considered in the functional J the controller attempts to re-open the valve.

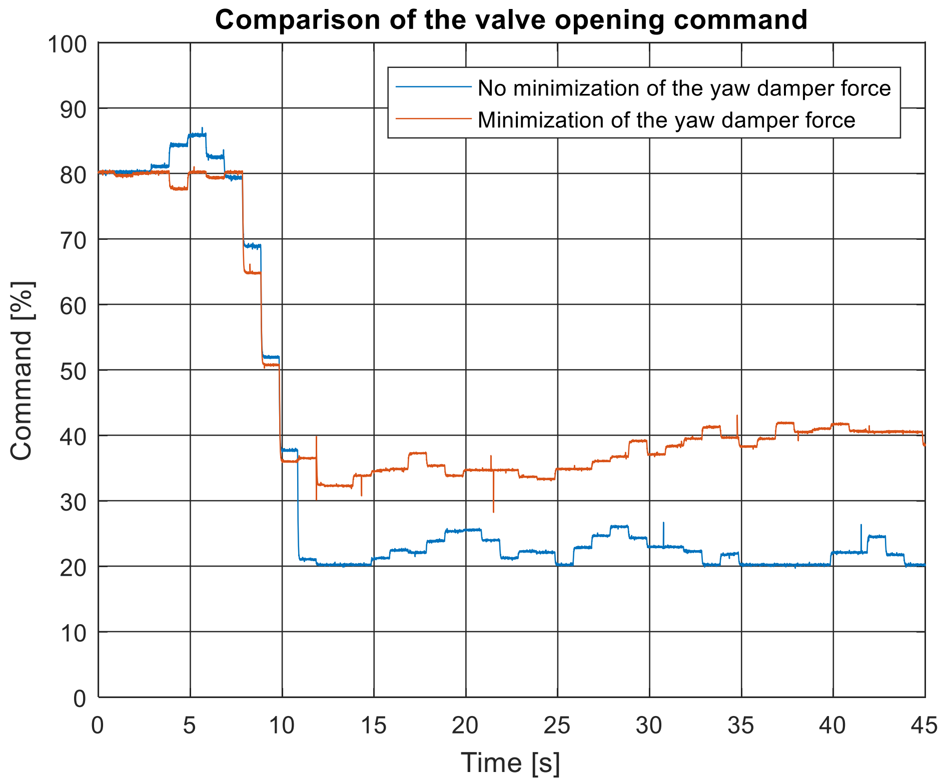

Figure 5.22 Comparison between the valve opening command obtained from the two different MPPT control strategies.

This type of control strategy was subsequently tested for different values of initial speed of the vehicle up to 380 km/h and it is working at all used speeds. It is possible to conclude that with this configuration of the semi-active yaw damper there is virtually no speed at which the vehicle may become unstable. This is due to the fact that if the valve is fully closed (valve opening command is around 20%) the damper becomes very stiff and there is no chance for instability to take place. The negative aspect of this situation is that if the damper becomes very stiff, a lot of transmission of vibrations from the bogie to the carbody can be expected.

5.4.2 Results of HIL tests with sky-hook control strategy

In order to evaluate the performances of the sky-hook control, HIL tests are performed in the same way as done for the MPPT control strategy. Tests are performed considering a constant value of vehicle speed. This value has to be sufficiently large to be sure that the vehicle becomes unstable after a perturbation is applied. In the first part of the tests, before switching on the track-irregularity since the bogie is not subjected to any perturbation, no appreciable lateral movement takes place, as visible in the time histories of the lateral acceleration and lateral wheelset displacement. Then, the track-irregularities are switched on and their effect is introduced in the real time model. After track irregularity is switched on, the behavior of the system is observed in terms of the oscillation of the bogie and reaction of the controller.

The results of the tests considering the two different types of sky-hook control logic, on/off sky-hook and continuous sky-hook, are presented in Figure 5.23 and Figure 5.24, respectively. Contrary to the results obtained with the MPPT control logic, in this case the sky-hook control strategy does not lead to any appreciable improvements regarding the stability of the bogie. As a matter of fact, the lateral displacement of the wheelset undergoes an oscillation with amplitude in the range of 6 mm and also the lateral acceleration does not show any significant reduction for the remaining part of the test.

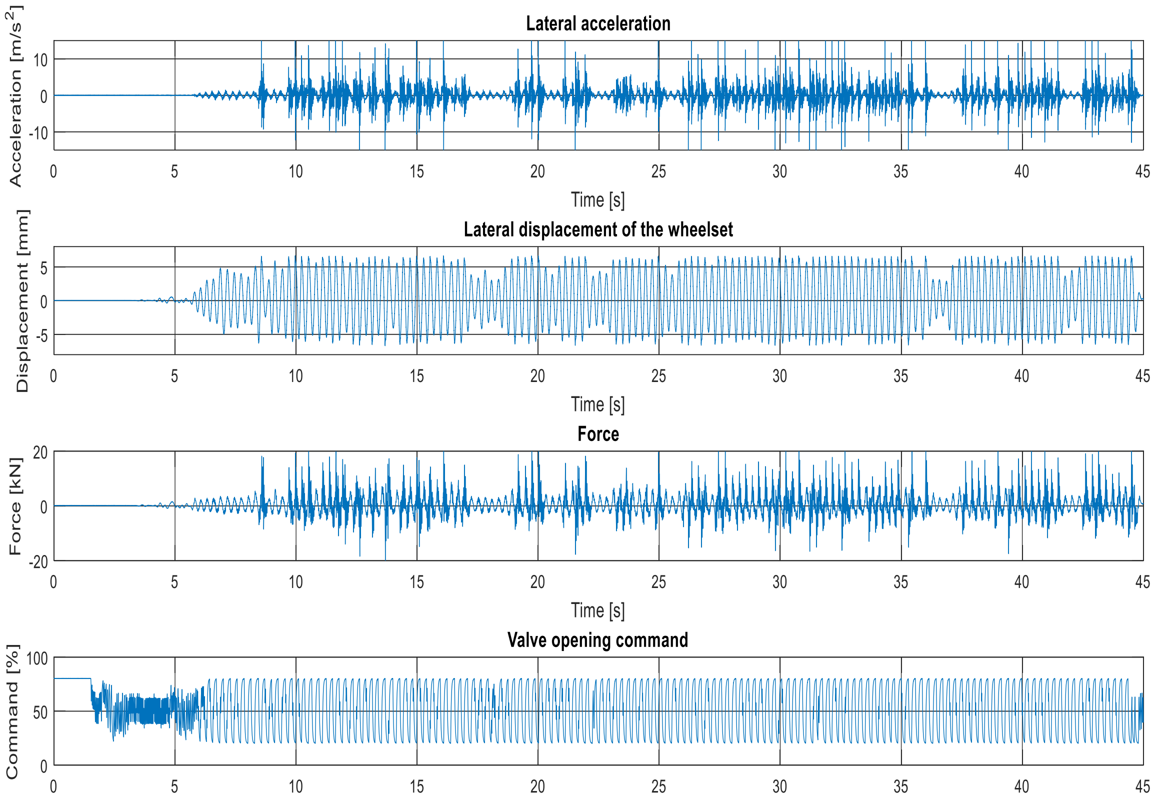

Figure 5.23 Result of HIL test with on/off sky-hook control strategy at 260 km/h.

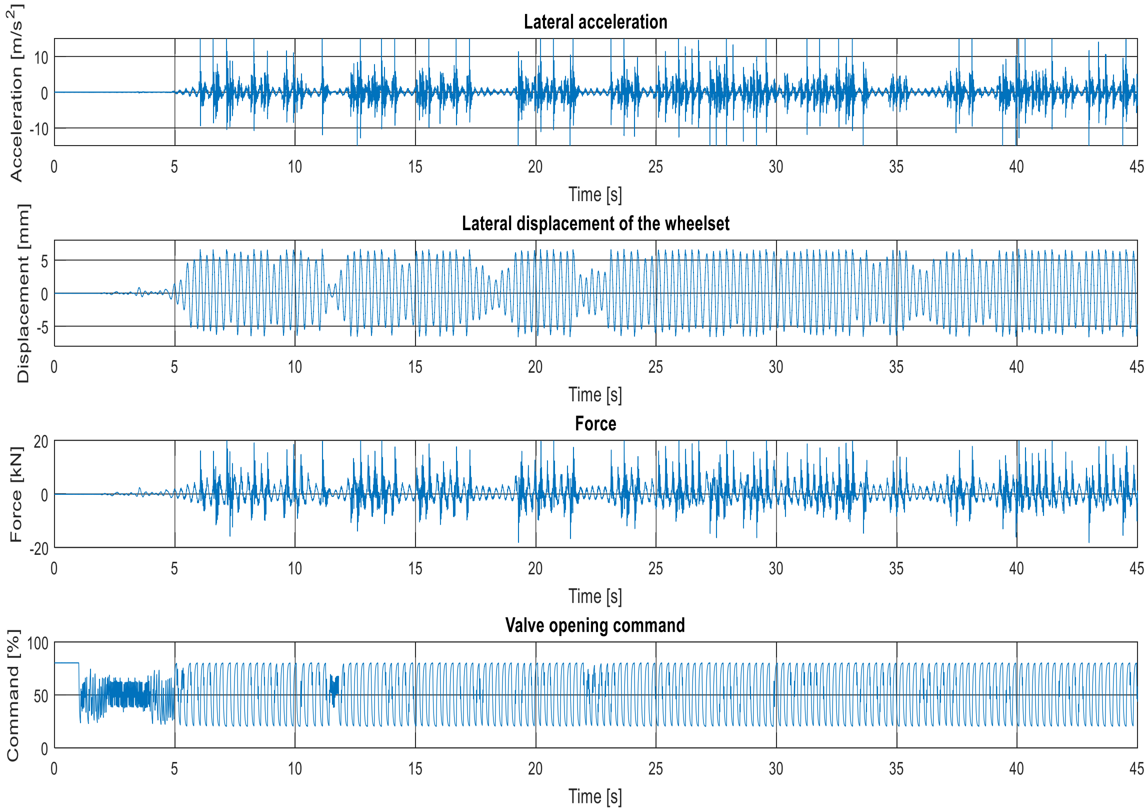

Figure 5.24 Result of HIL test with continuous sky-hook control strategy at 260 km/h.

The main reason for the failure of the sky-hook control logic (in both on/off and continuous versions) is the need to have a very fast dynamics of valve opening and closing. As can be observed from a zoom of the time history of the valve opening command for the on/off sky-hook (Figure 5.25), the measure of the valve command does not switch instantaneously between the maximum and the minimum value as provided by the control algorithm and instead the actual time history of the command shows a sequence of non-oscillatory transients with time constant in the order of 0.1-0.2 seconds, which is a time duration of the same order of magnitude as the period of the hunting oscillation of the bogie.

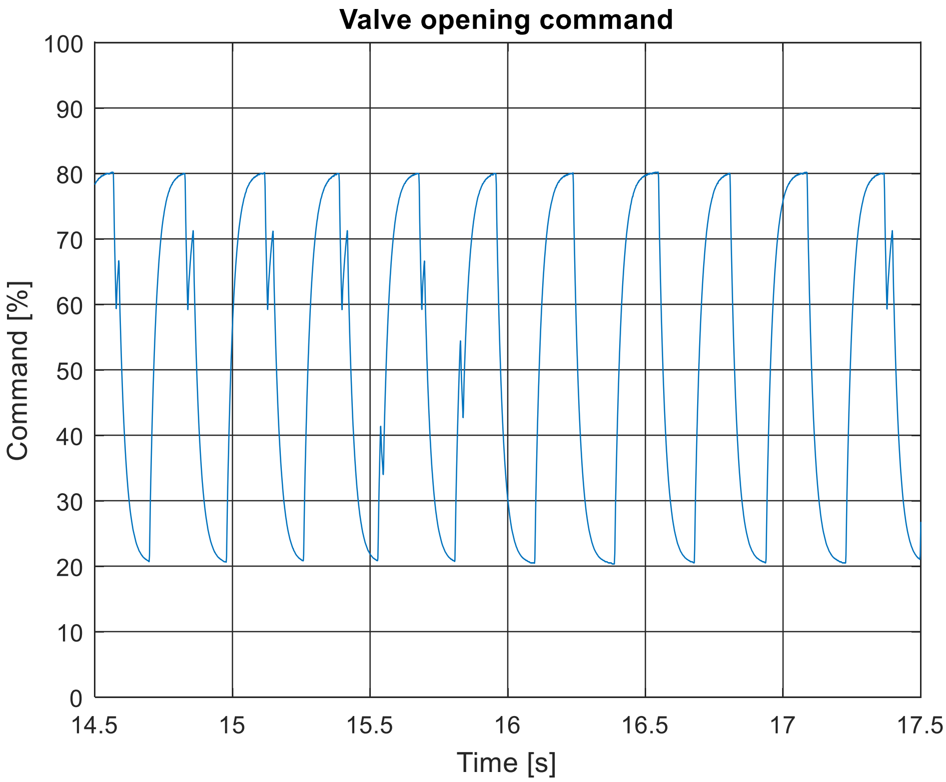

Figure 5.25 Zoom of the valve opening command for on/off sky-hook control strategy

This fact can be better explained considering a single variation between the fully closed to the fully open configuration of the valve. The upper part of Figure 5.26 shows the time history of the input voltage command, whilst the lower subfigure shows the time history of the current fed in the proportional vale. This latter quantity was measured using a current clamp and is the electrical signal available in the test which is more directly related to the opening of the valve. It is possible to observe that the switching of the command in terms of voltage applied to the valve is nearly instantaneous, in fact, the duty cycle immediately changes in correspondence of 43.2 seconds. On the contrary, the current that feed the valve needs 50 ms at least before reaching the steady state condition.

Based on the results presented in this sub-section, it shall be concluded that the proportional valve used in the tested semi-active damper prototype is not fast enough to enable the use of a sky-hook control strategy. This conclusion is different from the one drawn from multi-body simulations about the suitability of the sky-hook strategy for the semi-active damper, but it has to be considered that in the multibody model the assumption was made of using a fast servo-valve (see the considerations about the possibility to neglect the dynamics of the servo-valve reported in Chapter 3) whilst the actual valve used in the prototype damper subjected to the HIL tests clearly has a much more limited pass-band.

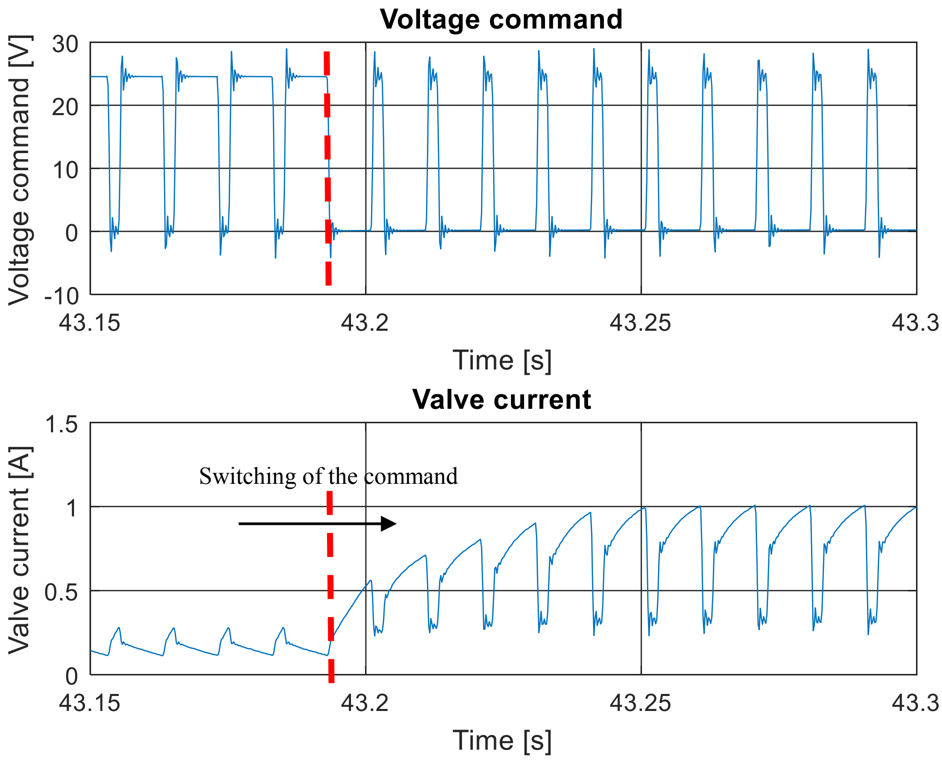

Figure 5.26 Voltage command and valve current variation from fully closed to fully open configuration of the valve.

Chapter 6 Conclusions

In this thesis work, the development and the implementation of full-active and semi-active yaw dampers for improving the running stability of a high-speed train have been investigated. In order to deal with this problem, firstly a general dimensioning of an active and semi-active hydraulic yaw damper was performed. Subsequently, proper control logics for the semi-active and full-active solution were defined and implemented in Simulink environment. The control strategies were then validated through multibody numerical simulations and, for the semi-active solution, also by means of experimental tests based on the HIL concept thanks to a HIL test rig for yaw dampers this is a novel contribution of this thesis. The HIL test rig makes use of a simplified two degrees of freedom model of the railway bogie which is simple enough to enable real-time simulation but was proven in the thesis to be able to reproduce the lateral dynamics of the bogie to the degree of accuracy required by HIL tests.

An assessment of the semi-active and full-active solutions proposed in the thesis was achieved based on the results of multi-body simulations. As could be expected, the performances of the full-active concept are superior compared to the semi-active solution. However, it is worth to notice that the full-active solution is affected by some negative aspects. As a matter of fact, considering a full-active yaw damper means that an on-board pump system with high- and low-pressure circuits has to be considered. Moreover, also the issue related to the damping force could be relevant in case of full-active option. In fact, the forces obtained with the full-active solution are greater than the once obtained with the semi-active solutions, and this means that also the dimensions of the full-active yaw damper have to be greater than the dimensions of the semi-active one. Since the forces of the full-active solution are greater than the semi-active ones, then, probably, transmission of vibration to the carbody has to be considered.

Again, from the results of multi-body simulations it can be concluded that the semi-active is able to significantly improve the critical speed with respect to the passive solution, despite providing a slightly lower critical speed of the vehicle compared to the full-active solution. Moreover, the semi-active solution provides the possibility to adapt the damping force transmitted to the bogie to different running conditions, such as different running speed of the vehicle or different wheel/rail conicity arising from changes in the wheel/rail profiles.

From the control logics point of view, the multibody numerical simulations show that the two control strategies proposed for the semi-active solution have more or less the same impact on increasing the critical speed of the vehicle. The important difference between the two control strategies is how the valve opening command reacts to the bogie lateral displacement. In fact, the MPPT control logic is a relatively slow control logic since it changes the opening of the by-pass control valve at discrete time intervals in the order of one second. On the contrary, the sky-hook solution works with a continuous change of the valve opening using very short time interval. This difference between the two control strategies are underlined especially from the results of the HIL tests. The sky-hook solution with its fast valve opening is significantly affected by the dynamic response of the by-pass valve. In fact, the opening valve does not follow exactly the opening valve command outputting from the control logic algorithm and shows instead an intrinsic delay that eventually leads to a substantial degradation of the performance of this control strategy.

Future extensions of this work might consist of considering different control strategies for the semi-active and/or active damper, e.g. building on the MPPT but improving the capability to reduce the damping force when the vehicle is running well below the critical speed or considering state feedback strategies such as LQG or H_∞. Furthermore, for a full-active solution it would be interesting to add a vibration propagation analysis to the carbody and investigate the effect of failures in the yaw damper on the safe operation of the vehicle.

Bibliography and references

[1] R. Vickerman, High-speed rail in Europe: experience and issues for future development, The annals of regional science, 31 (1997) 21-38.
[2] P. Delfosse, Very-high-speed tests on the french railway track, Vehicle System Dynamics, 20 (1991) 185-206.
[3] M. Taniguchi, High speed rail in Japan: A review and evaluation of the Shinkansen train, (1992).
[4] R. Takagi, High speed railways: the last 10 years, Japan Railway and Transport Review, 40 (2005) 4-7.
[5] L. Zhou, Z. Shen, Progress in high-speed train technology around the world, Journal of Modern Transportation, 19 (2011) 1-6.
[6] W. Zhai, P. Liu, J. Lin, K. Wang, Experimental investigation on vibration behaviour of a CRH train at speed of 350 km/h, International Journal of Rail Transportation, 3 (2015) 1-16.
[7] S. Sone, Comparison of the technologies of the Japanese Shinkansen and Chinese High-speed Railways, in: China's High-Speed Rail Technology, Springer, 2018, pp. 67-87.
[8] K. Knothe, S. Stichel, Rail vehicle dynamics, Springer, 2017.
[9] S. Bruni, A. Collina, G. Diana, P. Vanolo, Lateral dynamics of a railway vehicle in tangent track and curve: tests and simulation, in: THE DYNAMICS OF VEHICLES ON ROADS AND ON TRACKS-SUPPLEMENT TO VEHICLE SYSTEM DYNAMICS, VOLUME 33. PROCEEDINGS OF THE 16TH IAVSD SYMPOSIUM HELD IN PRETORIA, SOUTH AFRICA, AUGUST 30-SEPTEMBER 3, 1999, 2000.
[10] G. Diana, S. Bruni, F. Cheli, F. Resta, Active control of the running behaviour of a railway vehicle: stability and curving performances, Vehicle System Dynamics, 37 (2002) 157-170.
[11] F. Braghin, S. Bruni, F. Resta, Active yaw damper for the improvement of railway vehicle stability and curving performances: simulations and experimental results, Vehicle System Dynamics, 44 (2006) 857-869.
[12] S. Bruni, R. Goodall, T. Mei, H. Tsunashima, Control and monitoring for railway vehicle dynamics, Vehicle System Dynamics, 45 (2007) 743-779.
[13] A. MATSUMOTO, H. Ohno, T. Mizuma, Y. SUDA, Y. MICHITSUJI, M. TANIMOTO, E. MIYAUCHI, Y. SATO, Research on high curving performance trucks-concept and basic characteristics of active-bogie-steering truck, in: THE DYNAMICS OF VEHICLES ON ROADS AND ON TRACKS. PROCEEDINGS OF THE 18TH IAVSD SYMPOSIUM HELD IN KANAGAWA, JAPAN, AUGUST 24-30, 2003, 2004.
[14] S. Simson, C. Cole, Simulation of active steering control for curving under traction in hauling locomotives, Vehicle System Dynamics, 49 (2011) 481-500.
[15] E. 14363, Railway applications–Testing and simulation for the acceptance of running characteristics of railway vehicles–Running Behaviour and stationary tests, in, CEN Brussels, 2016.
[16] S. Iwnicki, Handbook of railway vehicle dynamics, CRC press, 2006.
[17] J. Hedrick, Active Suspension for Ground Transport Vehicles, A state of the Art Review, 21 (1975).
[18] R. Goodall, W. Kortüm, Active controls in ground transportation—A review of the state-of-the-art and future potential, Vehicle System Dynamics, 12 (1983) 225-257.
[19] R. Goodall, Active railway suspensions: Implementation status and technological trends, Vehicle System Dynamics, 28 (1997) 87-117.
[20] I. Ballo, Comparison of the properties of active and semiactive suspension, Vehicle System Dynamics, 45 (2007) 1065-1073.
[21] H. Norinao, Active and semi-active suspensions smooth 300 km/h ride, Railway Gazette International, (1997) 241-242.

[22] K. Tanifuji, S. Koizumi, R.-h. Shimamune, Mechatronics in Japanese rail vehicles: active and semi-active suspensions, Control Engineering Practice, 10 (2002) 999-1004.
[23] R. Goodall, S. Bruni, A. Facchinetti, Active control in railway vehicles, International Journal of Railway Technology, 1 (2012) 57-85.
[24] M. Pollard, N. Simons, Passenger comfort—the role of active suspensions, Proceedings of the Institution of Mechanical Engineers, Part D: Transport Engineering, 198 (1984) 161-175.
[25] P. Gautier, F. Quetin, J. Vincent, Global active suspension system for railway coaches, in: World Congress on Railway Research, Tokyo, 1999.
[26] P. Kjellqvist, C. Sadarangani, S. Ostlund, Design of a permanent magnet synchronous machine for an electromechanical active suspension actuator, in: Electric Machines and Drives Conference, 2001. IEMDC 2001. IEEE International, IEEE, 2001, pp. 534-541.
[27] M. Pollard, Active suspensions enhance ride quality, Railway Gazette International, 139 (1983) 850-853.
[28] R. Goodall, Actuator technologies for secondary active suspensions on railway vehicles, STECH'93, (1993) 377-382.
[29] N. Niksefat, N. Sepehri, Designing robust force control of hydraulic actuators despite system and environmental uncertainties, IEEE Control Systems, 21 (2001) 66-77.
[30] R. Shimamune, K. Tanifuji, Application of oil-hydraulic actuator for active suspension of railway vehicle: experimental study, in: SICE'95. Proceedings of the 34th SICE Annual Conference. International Session Papers, IEEE, 1995, pp. 1335-1340.
[31] K. Sasaki, S. Kamoshita, M. Enomoto, A design and bench test of multi-modal active suspension of railway vehicle, in: Industrial Electronics, Control and Instrumentation, 1994. IECON'94., 20th International Conference on, Vol. 3, IEEE, 1994, pp. 2011-2016.
[32] T. Hirata, S. Koizumi, R. Takahashi, H∞ control of railroad vehicle active suspension, Automatica, 31 (1995) 13-24.
[33] G. Yao, F. Yap, G. Chen, W. Li, S. Yeo, MR damper and its application for semi-active control of vehicle suspension system, Mechatronics, 12 (2002) 963-973.
[34] T. Glad, L. Ljung, Reglerteknik: grundläggande teori, Studentlitteratur, 2006.
[35] D. Karnopp, Active damping in road vehicle suspension systems, Vehicle System Dynamics, 12 (1983) 291-311.
[36] A. STRIBERSKY, A. KIENBERGER, G. WAGNER, H. MÜLLER, Design and evaluation of a semi-active damping system for rail vehicles, Vehicle System Dynamics, 29 (1998) 669-681.
[37] C.R. Sullivan, M.J. Powers, A high-efficiency maximum power point tracker for photovoltaic arrays in a solar-powered race vehicle, in: Proceedings of IEEE Power Electronics Specialist Conference-PESC'93, IEEE, 1993, pp. 574-580.
[38] A. CHIARABAGLIO, A semi-active damper for the secondary suspension of high-speed trains, (2017).
[39] C. Tang, L. Yue, L. Guo, S. Zhou, W. Zhou, Z. Wang, Fuzzy logic control for vehicle suspension systems, in: International Conference on Intelligent Robotics and Applications, Springer, 2008, pp. 197-206.
[40] C. Huang, L. Chen, H. Jiang, C. Yuan, T. Xia, Fuzzy chaos control for vehicle lateral dynamics based on active suspension system, Chinese Journal of Mechanical Engineering, 27 (2014) 793-801.
[41] E. Allam, H.F. Elbab, M.A. Hady, S. Abouel-Seoud, Vibration control of active vehicle suspension system using fuzzy logic algorithm, Fuzzy Information and Engineering, 2 (2010) 361-387.
[42] D. Allen, Active bumpstop hold-off device, in: Proc IMechE Conference Railtech, Vol. 94, 1994.
[43] J.C. Doyle, K. Glover, P.P. Khargonekar, B.A. Francis, State-space solutions to standard H/sub 2/and H/sub infinity/control problems, IEEE Transactions on Automatic control, 34 (1989) 831-847.
[44] H. Kimura, Y. Lu, R. Kawatani, On the structure of H/sup infinity/control systems and related extensions, IEEE Transactions on Automatic control, 36 (1991) 653-667.

[45] A. MORAN, M. NAGAI, Analysis and Design of Active Suspensions by H∽ Robust Control Theory, JSME international journal. Ser. 3, Vibration, control engineering, engineering for industry, 35 (1992) 427-437.
[46] M. Yamashita, K. Fujimori, C. Uhlik, R. Kawatani, H. Kimura, H/sub infinity/control of an automotive active suspension, in: Decision and Control, 1990., Proceedings of the 29th IEEE Conference on, IEEE, 1990, pp. 2244-2250.
[47] L.L.T. Glad, L. Ljung, Reglerteori-Flervariabla och olinjära system, in, Studentlitteratur, Studentlitteratur, Lund, 2003.
[48] I. Pratt, R. Goodall, Control strategies to improve ride quality in railway trains, in: Control, 1994. Control'94. International Conference on, Vol. 1, IET, 1994, pp. 350-355.
[49] I. Pratt, R. Goodall, Controlling the ride quality of the central portion of a high-speed railway vehicle, in: American Control Conference, 1997. Proceedings of the 1997, Vol. 1, IEEE, 1997, pp. 719-723.
[50] M. Tibaldi, E. Zattoni, Robust control of active suspensions for high performance vehicles, in: Industrial Electronics, 1996. ISIE'96., Proceedings of the IEEE International Symposium on, Vol. 1, IEEE, 1996, pp. 242-247.
[51] R. Goodall, R. Williams, A. Lawton, P. Harborough, Railway vehicle active suspensions in theory and practice, Vehicle System Dynamics, 10 (1981) 210-215.
[52] M. Tahara, K. Watanabe, T. Endo, O. Goto, S. Negoro, S. Koizumi, A503 PRACTICAL USE OF AN ACTIVE SUSPENSION SYSTEM FOR RAILWAY VEHILCLES, in: The Proceedings of International Symposium on Seed-up and Service Technology for Railway and Maglev Systems: STECH 2003, The Japan Society of Mechanical Engineers, 2003, pp. 225-228.
[53] Y. Sam, K. Hudha, Modelling and force tracking control of hydraulic actuator for an active suspension system, in: 2006 1st IEEE conference on industrial electronics and applications, IEEE, 2006, pp. 1-6.
[54] W. Kemmetmüller, A. Kugi, Immersion and invariance-based impedance control for electrohydraulic systems, International Journal of Robust and Nonlinear Control: IFAC-Affiliated Journal, 20 (2010) 725-744.
[55] M. Wrang, Instability phenomena of a passenger coach, caused by internal yaw damper flexibility, in: THE DYNAMICS OF VEHICLES ON ROADS AND ON TRACKS-SUPPLEMENT TO VEHICLE SYSTEM DYNAMICS, VOLUME 33. PROCEEDINGS OF THE 16TH IAVSD SYMPOSIUM HELD IN PRETORIA, SOUTH AFRICA, AUGUST 30-SEPTEMBER 3, 1999, 2000.
[56] U. Ferdek, J. Łuczko, Modeling and analysis of a twin-tube hydraulic shock absorber, Journal of theoretical and applied mechanics, 50 (2012) 627-638.
[57] M. Shinozuka, M. Constantinou, R. Ghanem, Passive and active fluid dampers in structural applications, in: Proc. US/China/Japan Workshop on Struct. Control, 1992, pp. 507-516.
[58] M. Ruderman, Full-and reduced-order model of hydraulic cylinder for motion control, in: IECON 2017-43rd Annual Conference of the IEEE Industrial Electronics Society, IEEE, 2017, pp. 7275-7280.
[59] H. Merritt, H.E. Merritt, H.E. Merritt, Hydraulic control systems, John Wiley & Sons, 1967.
[60] R. Stribeck, Die wesentlichen eigenschaften der gleit-und rollenlager, Zeitschrift des Vereines Deutscher Ingenieure, 46 (1902) 1341-1348, 1432-1438, 1463-1470.
[61] A.A. Shabana, K.E. Zaazaa, H. Sugiyama, Railroad vehicle dynamics: a computational approach, CRC press, 2007.
[62] J. Kalker, A fast algorithm for the simplified theory of rolling contact, Vehicle System Dynamics, 11 (1982) 1-13.